THESIS FOR THE DEGREE OF DOCTOR OF PHILOSOPHY

in

Thermo and Fluid Dynamics

Waste Heat Recovery from Combustion Engines based on the Rankine Cycle

GUNNAR LATZ

Department of Applied Mechanics
CHALMERS UNIVERSITY OF TECHNOLOGY
Gothenburg, Sweden, 2016

Waste Heat Recovery from Combustion Engines based on the Rankine Cycle
GUNNAR LATZ
ISBN 978-91-7597-336-4

© GUNNAR LATZ, 2016

Doktorsavhandlingar vid Chalmers tekniska högskola
Ny serie nr 4017
ISSN: 0346-718X

Department of Applied Mechanics
Chalmers University of Technology
SE-412 96 Gothenburg
Sweden
Telephone +46 (0)31 7721000

Chalmers Reproservice
Gothenburg, Sweden 2016

Waste Heat Recovery from Combustion Engines based on the Rankine Cycle

GUNNAR LATZ

latz@chalmers.se
Department of Applied Mechanics
Chalmers University of Technology

Abstract

Most of the energy in the fuel burned in modern automotive internal combustion engines is lost as waste heat without contributing to the vehicle's propulsion. In principle some of this lost energy could be captured and used to increase the vehicle's fuel efficiency by fitting a waste heat recovery system to the engine. This thesis presents investigations into the design and functioning of waste heat recovery systems based on Rankine cycle technology for vehicular applications.

To facilitate the design of such systems, the performance of different working fluids and expansion devices was investigated using a zero-dimensional model of the Rankine cycle. Simulations using this model indicated that water-based fluids should perform well when recovering waste heat from a high temperature source such as a combustion engine's exhaust gas. In addition, evaluations based on similarity parameters indicated that displacement expanders are optimal in systems having low flow rates and high expansion pressure ratios, both of which are to be expected in vehicular systems using water as the working fluid. Organic working fluids allow higher flow rates in the cycle, making the efficient use of turbines possible.

Data from the simulations using the zero-dimensional model were used to guide the design and construction of a demonstrator test bench featuring a Rankine cycle-based recovery system that recovers waste heat from the exhaust gas recirculation system of a heavy duty Diesel engine. The test bench uses water as the working fluid and a piston expander as the expansion device. The Rankine cycle's thermal efficiency was 10%, corresponding to 1-2% of the engine's power output. To find ways of improving the system's performance, one-dimensional models of the expander and the system as a whole were created and then validated by comparing their output to experimental data obtained with the test bench. The expander model suggested that reducing the compression ratio would make it possible to reduce the steam inlet pressure by 30% without affecting the expander's power output. This hypothesis was then confirmed experimentally.

The expander model was used to rank the relative influence of selected steam boundary conditions and expander geometry parameters on the performance of a piston expander. The inlet pressure, steam inlet cut-off timing, expander speed and outlet pressure were found to be the most significant main effects on expander performance. It was also shown that interaction effects between steam conditions and expander geometry had considerable influence on both power output and efficiency.

List of publications

Some of the work in this thesis is based on the following publications (attached to the thesis):

I. **Latz, G.**, Andersson, S., and Munch, K., "Comparison of Working Fluids in Both Subcritical and Supercritical Rankine Cycles for Waste-Heat Recovery Systems in Heavy-Duty Vehicles," SAE Technical Paper 2012-01-1200, 2012, doi:10.4271/2012-01-1200.

II. **Latz, G.**, Andersson, S., and Munch, K., "Selecting an Expansion Machine for Vehicle Waste-Heat Recovery Systems Based on the Rankine Cycle," SAE Technical Paper 2013-01-0552, 2013, doi:10.4271/2013-01-0552.

III. **Latz, G.**, Erlandsson, O., Skåre, T., Contet, A., Andersson, S. and Munch, K., “Water-based Rankine-cycle waste heat recovery systems for engines: challenges and opportunities”, *Proceedings of the 3rd International Seminar on ORC Power System, Brussels*, University of Liège and Ghent University, Brussels:355-364, 2015.

IV. **Latz, G.**, Andersson, S., and Munch, K., "Basic concept comparison of reciprocating expansion machines," manuscript submitted to the journal *Applied Thermal Engineering* in February 2016.

An additional article was submitted based on results presented in this thesis (not attached):

V. **Latz, G.**, Erlandsson, O., Skåre, T., Contet, A., Andersson, S. and Munch, K., “Understanding limitations in a water-based Rankine cycle test rig for heat recovery from a heavy duty Diesel engine”, manuscript submitted to the journal *Applied Energy* in February 2016.

Acknowledgments

The first persons I would like to thank are my supervisors Karin Munch and Sven Andersson. I was able to benefit and learn a lot during my work from their extensive experience. Their enthusiasm and interest in my project created a nice working atmosphere and helped to improve and plan my research activities.

Professor Ingemar Denbratt is acknowledged for giving me the opportunity to work on this interesting PhD project at the division of combustion.

I would also like to thank all members of the waste-heat recovery reference group for the suggestions and discussions about my work. The reference group was a motivating opportunity for me to present the progress of the project frequently to our industrial partners and earning valuable feedback which helped to guide my research activities. Many thanks to Olof Erlandsson from TitanX for the helpful discussions and reflections concerning design questions related to the test bench and the measurement equipment. He and his colleagues Thomas Skåre and Arnaud Contet contributed to our third publication, which was rewarded with the “Best Paper Award” at the ORC Seminar in Brussels 2015 – certainly a highlight in the project!

I am grateful to Jonas Sjöblom for helping me to get a handle on using the Design of Experiments approach for the investigations related to the one-dimensional piston expander model.

The Swedish Energy Agency is acknowledged for funding this project and the industrial partners for supporting us with in-kind contributions.

Experimental work for the validation of the created models played an important role in this project. The first person I would like to acknowledge in this matter is Anders Mattsson. His commitment for the project was simply outstanding. He not only demonstrated his “MacGyver”-skills when building and maintaining the test rig (the word ‘impossible’ did not exist), he was also an essential discussion partner for me when it came to technical modifications of the setup. In this context, I would also like to thank Daniel Härensten, Lars Jernqvist and Robert Buadu for their support related to measurement and control equipment. The success of this project would not have been possible without the great contribution from the guys in the lab!

A big thank you goes also to all my colleagues at Chalmers for making the Division of Combustion a nice place to work. It was an honor for me to share the office with the guy who has the fastest car in the division (Tankai).

In Germany I would like to thank my family for all the support throughout the years. Thanks to my partner Frida for sharing (or was it tolerating?) my passion of being now and then active on the market for nice old cars and even more important: for making life so much more enjoyable for me!

REPORT

Contents

Nomenclature

Abbreviations

1D	one dimensional	IVO	inlet valve opening
°CA	degree crank angle	IR	infrared
ATDC	after top dead center	K	Kelvin
BDC	bottom dead center	LCA	life cycle assessment
ABDC	after bottom dead center	LD	light duty
cyl	cylinder	m	mechanical
CAC	charge air cooler	max	maximum
CAD	computer-aided design	min	minute
CAE	computer-aided engineering	min	minimum
CFD	computational fluid dynamics	NO_x	nitrogen oxide
CFL	Courant-Friedrichs-Lewy	N_2	nitrogen
CO_2	carbon dioxide	O_2	oxygen
CP	critical point	ODP	ozone depletion potential
DoE	design of experiments	ORC	organic Rankine cycle
evap	evaporation	PP	pinch point
ex	exit	ret	retarded
exp	expander	rpm	revolutions per minute
ext	external	RSM	response surface model
ECU	engine control unit	sat	saturation
EES	engineering equation solver	sh	superheated
EGR	exhaust-gas recirculation	teu	twenty-foot equivalent unit
ESC	European stationary cycle	th	thermal
EVC	outlet port closing	TDC	top dead center
EVO	outlet port opening	TEM	thermoelectric material
FMEP	friction mean effective pressure	TFC	trilateral flash cycle
GWP	global warming potential	TM	trademark
H_2	hydrogen	TDC	top dead center
H_2O	water	TEM	thermoelectric material
HD	heavy duty	vap	vaporization
is	isentropic	VLE	vapour liquid equilibrium
IC	internal combustion	WF	working fluid
IVC	inlet valve closing	WHR	waste-heat recovery

Symbols

A	area	n	rotational speed
A_E	effective flow area	N	expander rotational speed
A_R	reference area	N_s	specific expander speed
A_S	surface area	o	overall
β	RSM regression coefficient	p	pressure
c_p	specific heat capacity	q	specific heat
$c_{p,m}$	mean piston speed	Q	heat
C_D	discharge coefficient	Re	Reynolds number
C_f	skin friction coefficient	ρ	density
C_P	pressure loss coefficient	σ	standard deviation
d	diameter	s	specific entropy
dx	length of mass element	S	entropy
D	diameter	Θ	diameter ratio
D_s	specific expander diameter	τ	pressure ratio
ε	compression ratio (expander)	t	time
ε	effectiveness (heat exchanger)	T	temperature
ε	error (RSM model)	u	specific internal energy
e	specific energy	u	velocity
E	expansion factor	v	specific volume
η	efficiency	v	volumetric (efficiency)
h	heat transfer coefficient	V	voltage
h	specifc enthalpy	V	volume
κ	specific heat ratio	VFR	volume flow rate
λ	air-fuel equivalence ratio	w	specific work
μ	dynamic viscosity	W	Work
μ	mean value	x	RSM performance factors
$\dot{m}$	mass flow rate	y	RSM response
M	molar mass	ZT	dimensionless figure of merit

1 Introduction

1.1 Motivation

Modern research and development efforts relating to combustion engines and vehicle design are largely driven by the pressing need to reduce the global consumption of fossil energy carriers and the resulting emissions of the greenhouse gas carbon dioxide.

The limited supply of fossil fuels is one of the most important factors underpinning these efforts. Oil and natural gas are currently the most important energy carriers used in transportation, with oil accounting for 93% of the energy used in this sector in 2013 [1]. At current rates of production, the world's proven oil reserves will expire in approximately 52 years, while the prognosis for natural gas is 54 years [2]. However, an even more important factor is that as production rates start to decline, the limited supply of fossil fuels will become increasingly problematic. Global oil production is expected to peak before 2030 and may do so before 2020 [3].

A second, possibly even more important, factor underpinning the desire to develop energy-efficient vehicles relates to emissions of greenhouse gases. The combustion of fossil fuels generates CO_2 emissions, which absorb re-radiated heat from the earth's surface and thereby contribute to global warming. This anthropogenic greenhouse effect alters natural marine and terrestrial carbon cycles, reducing the environment's capacity for CO_2 storage [4]. In the year 2005, the transport sector was responsible for slightly more than 23% of the world's CO_2 emissions, with road transport accounting for 17%. The largest share of the globe's CO_2 emissions (45%) originated from fossil fuels burned for energy generation. Overall CO_2 emissions have increased by 80% since 1970 (and those from the transportation sector have increased by more than 100%), contributing to an average atmospheric temperature increase of around 0.8 °C over the same period [5]. While this may sound small in absolute terms, the long term effects of this trend are predicted to be devastating for life on earth [6].

The need to reduce emissions and minimize the consumption of fossil fuel reserves thus necessitates a strong focus on environmental sustainability in vehicle and engine development. This need is exacerbated by the rapid growth in vehicle density seen in highly populated countries such as China and India. Conservative estimates suggest that vehicle ownership in China will increase by around 500% between the present day and 2050 [7]. A range of alternative propulsion concepts that could potentially be used in vehicles in the future have been evaluated. However, it has become clear that neither electric vehicles nor the internal combustion engine will by themselves be capable of meeting future transportation needs in a sustainable fashion [7, 8-10]. Moreover, life cycle assessments (LCA) have shown that pure electric vehicles and vehicles that run on electricity generated in H_2 fuel cells only have favourable life cycle CO_2 emissions if they run on energy generated from renewable sources [8,10]. Unfortunately, the growing energy requirements of the transportation sector are too great to be met by renewable sources alone [8]. It is therefore likely that hybrid powertrains that incorporate both a combustion engine and an electric motor will become increasingly popular in the future, with the exact contribution of the two systems varying depending on the vehicle's intended application [7-9]. Moreover, the fossil fuels used in combustion engines will be blended with (and possibly even replaced by) biofuels, which offer lower overall CO_2 emissions. However, there are numerous issues relating to trade and sustainable development that will have to be overcome in order to enable a major breakthrough in biofuel usage [11].

All propulsion concepts involving combustion engines, from heavy duty engines running on biodiesel to small gasoline engines in hybrid powertrains, have one thing in common: the majority of the energy in the fuel they burn is lost and doesn't contribute to vehicle propulsion. Modern heavy duty Diesel engines are the most efficient combustion engines used for road transportation; they can achieve fuel efficiencies in excess of 42% under optimal operating conditions [12].

As a result, a lot of research and development work has been devoted to increasing combustion engine efficiency by reducing these losses. This can be done in various ways, including reducing losses due to mechanical friction, optimizing the engine to increase the efficiency of the combustion process, and creating superior gas exchange paths.

Despite these efforts, a relatively large proportion of the energy in the fuel will inevitably be lost from the engine as heat. This is largely due to energy lost via the hot exhaust gas, the coolant that is used to control the engine's temperature, and the hot recirculated exhaust gas that is used to reduce engine-out emissions but must be cooled before being returned to the cylinder. Systems that can recover some of the energy lost in this way are therefore important for achieving higher propulsion efficiencies. Heat recovery systems that are generally considered suitable for this purpose include turbocompound systems, thermoelectric converters and setups based on the Rankine cycle. Turbocompound systems are based on a power turbine, which is integrated into the exhaust system. Thermoelectric converters rely on the Seebeck effect, which means they generate electrical power directly from the temperature difference between a heat source and the environment. In the Rankine cycle, gases carrying waste heat are passed through a heat exchanger and used to evaporate a pressurized working fluid. Power is then produced by the expansion of the vaporized fluid. The cycle is closed by the condensation of the working fluid, which is then pumped back up to the evaporation pressure.

1.2 Scope of the thesis

This thesis focuses on the Rankine cycle as the most promising existing technology for engine waste heat recovery in terms of recuperation efficiency. While it is a comparatively mature technology and is widely used in power generation, its use in vehicles presents new challenges in system design. These stem from environmental and packaging issues, as well as difficulties relating to the quality and quantity of the available heat and its transient availability.

It is not yet clear which working fluid and expansion device are optimal for use in a Rankine cycle-based system for vehicular applications. However, previous studies have indicated that these components are among the most important factors for the system's performance [12-14]. Therefore, investigations were conducted to identify a suitable working fluid (attached ***Paper I***) and expansion device (attached ***Paper II***) for a vehicular Rankine cycle heat-recovery system.

The models and findings from the theoretical part of the project were used to guide the design and construction of a demonstrator test-rig for a Rankine cycle-based heat recovery system. The test rig consists of a full-scale system recovering heat from the exhaust gas recirculation (EGR) of a 12.8 liter heavy duty Diesel engine. The objective of the experimental work was to create a versatile validation platform for both system and component models of the heat recovery system. Previously unrecognized challenges arising from the use of such systems with water-based working fluids were identified and some new opportunities were revealed (attached ***Paper III***), confirming the importance of experiments as a supplement to the predominantly theoretical work in this field.

A reciprocating piston expander was used as the expansion device in the demonstrator test-rig. This expansion concept offers practical advantages over turbomachinery due to its robustness and low speed of rotation. A one dimensional model of the expander was developed, validated, and used to identify the most significant boundary conditions and design parameters affecting the performance of this expansion concept (attached ***Paper IV***).

2 Background

2.1 Energy balance in combustion engines

This chapter discusses energy balances in Diesel engines for heavy duty vehicles and gasoline engines for light duty passenger cars. Because these engine types have very different applications, discussing them together makes it possible to clearly show how fuel energy is lost in different types of vehicle. In both cases, the engines are assumed to be operating under conditions that produce near-maximal brake-power efficiency.

2.1.1 Heavy duty Diesel engine

Figure 2-1 shows the energy balance for a 12.8 liter heavy duty Diesel engine, which was derived based on a validated simulation model for this engine. The engine has 6 cylinders, is turbo-charged to increase performance, and uses a short-route EGR system. This means that a controlled amount of exhaust gas is taken directly from the exhaust manifold and mixed with fresh air on the inlet side. The purpose of the EGR system is to reduce engine-out NOx emissions, which happens because the combustion temperature decreases as the proportion of recirculated exhaust gas in the cylinder increases. The recirculated exhaust gas must be cooled to maximize the efficiency of this process and avoid a negative impact on the engine's volumetric efficiency.

Potential waste heat sources in the heavy-duty engine are the charge air cooler (CAC) on the inlet side, the cooler for the EGR system, the post-turbine exhaust gas, and heat lost to the surroundings via the coolant and radiation.

The analysis in this case focuses on the engine's B75 operating point, which corresponds to an intermediate engine speed and 75% of the engine's maximum torque at this speed. Under these conditions, the engine operates at around its maximum brake-power efficiency of 42%. However, even under these optimal conditions, heat losses account for more than half of the energy in the fuel that is burned. The majority of this energy is lost from the coolant and by radiation. The radiative losses would be very difficult to reclaim using a system based on the Rankine cycle and are therefore not considered further in this work. Heat losses via the exhaust gas account for 15% of the fuel energy, while losses from the post-compressor charge air and the exhaust gas entering the EGR cooler account for 11% each.

The quality of the available waste heat from a given source is arguably more important than the source's contribution to the total waste heat when designing heat recovery systems. It can be assessed by considering the Carnot efficiency η_{Carnot}, which represents the maximum achievable efficiency for a heat engine operating under reversible conditions driven by a heat source at temperature T_{source} and a heat sink at temperature T_{sink}, ***eq. (2.1)***.

$$\eta_{Carnot} = 1 - \frac{T_{Sink}}{T_{Source}} \tag{2.1}$$

If the heat sink is assumed to be the ambient air and to have a constant temperature, the heat source temperature is the only variable that determines the potential efficiency of a system for recovering waste heat from the source. Given the heat source temperatures for the heavy duty engine listed in ***Figure 2-1***, it is clear that the EGR system provides the highest waste heat quality due to its temperature of 470 °C, followed by the post-turbine exhaust gas at 250 °C. The temperature of the coolant is rather low, making it less suitable for efficient heat recovery. The compressed charge air, which is cooled in the CAC, accounts for roughly the same proportion of the total fuel energy as the EGR, but at 200 °C, its temperature is less than half that of the exhaust gas entering the EGR cooler.

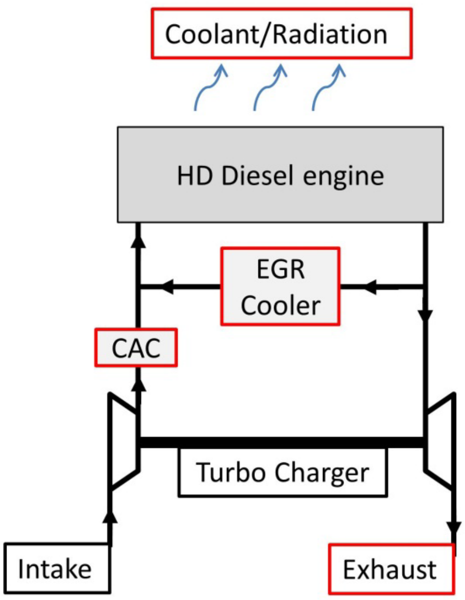

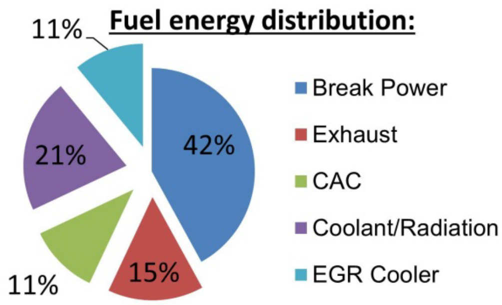

Heat Source	Source temperature
Exhaust	250°C
EGR Cooler	470°C
CAC	200°C
Coolant	100°C

Figure 2-1: Energy balance for a 12.8 litre heavy duty Diesel engine at the B75 operating point (simulation results)

2.1.2 Gasoline engine (Light duty)

A typical energy balance for a light-duty gasoline engine is shown in ***Figure 2-2***. The underlying data were obtained from driving experiments using a Volvo XC 60 under motorway driving conditions. The vehicle was propelled by a 2.0 litre, turbo-charged 4-cylinder engine.

The motorway driving cycle was conducted at an average velocity of 110 km/h, under which conditions the engine operates close to its maximum brake-power efficiency, implying that 35% of the fuel energy was used to propel the vehicle. The hot exhaust gases downstream of the turbine accounted for 33% of the total fuel energy, while coolant and radiator losses accounted for 31% of the total fuel energy. Energy losses via the CAC accounted for only 1% of the total fuel energy, making this waste heat source much less important than in the heavy duty case. This is partly because of the driving conditions considered: when driving on the motorway at near-constant speed, the charge air pressure (and therefore the temperature of the charge air) would only be elevated during infrequent load peaks, for instance when driving uphill or accelerating to overtake another vehicle.

In the light duty case, the waste heat source with the greatest potential for energy recovery is the post-turbine exhaust gas, which has a temperature of around 820 °C. Both the coolant and the charge air are much cooler and therefore offer much lower Carnot efficiencies.

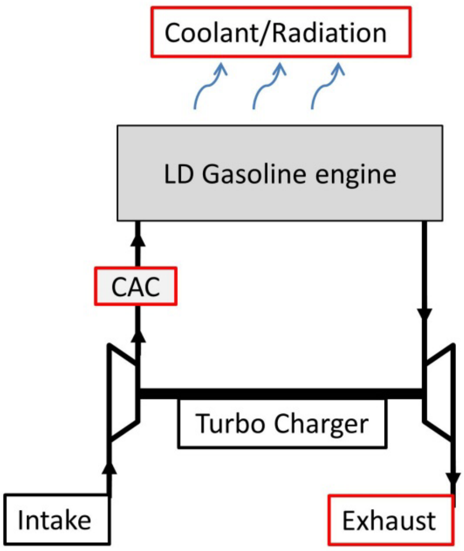

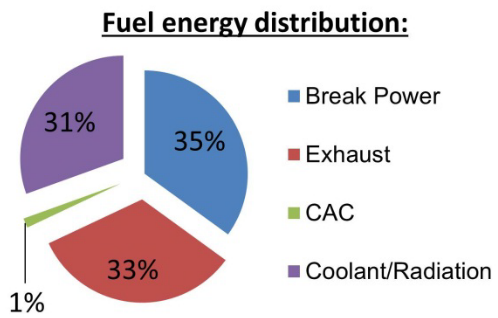

Heat Source	Source temperature
Exhaust	820°C
CAC	50°C
Coolant	100°C

Figure 2-2: Energy balance for a 2.0 litre turbocharged gasoline engine under motorway driving conditions

2.2 Heat recovery technologies

This chapter describes the three heat recovery technologies that are most commonly seen as viable options for combustion engines: turbocompound systems, thermoelectric converters, and Rankine cycle systems.

2.2.1 Turbocompound systems

The turbocompound system is a technology that recovers energy from the exhaust gas by using an additional turbine in the exhaust system, which is typically located downstream of the turbocharger turbine. The expansion of the exhaust gas in the turbine reduces the enthalpy of the exhaust gas. When multiplied by the turbine's efficiency, this enthalpy decrease represents the maximum work that can be obtained from the device. In contrast to turbochargers, where the recovered energy is used to power a compressor, the turbocompound system's output is used to directly augment the vehicle's propulsion or to drive a generator that produces electricity for the vehicle. As such, there are two types of turbocompound systems: mechanical and electrical. ***Figure 2-3*** shows one possible configuration for a combustion engine with a mechanical turbocompound system. In mechanical turbocompound systems, it is necessary to use gears to reduce the turbine's output speed such that it matches the engine's crankshaft speed. In addition, a fluid coupling must be used to separate the compound turbine from torsional crankshaft vibrations and thereby prevent damage to the turbine and the high-speed gear set [15-16]. Electrical turbocompound systems have the advantage of not being connected to the vehicle's propulsion system. Their speed can thus be controlled independently of the engine's speed, which avoids the risk of having to operate the turbine inefficiently under off-design conditions [16].

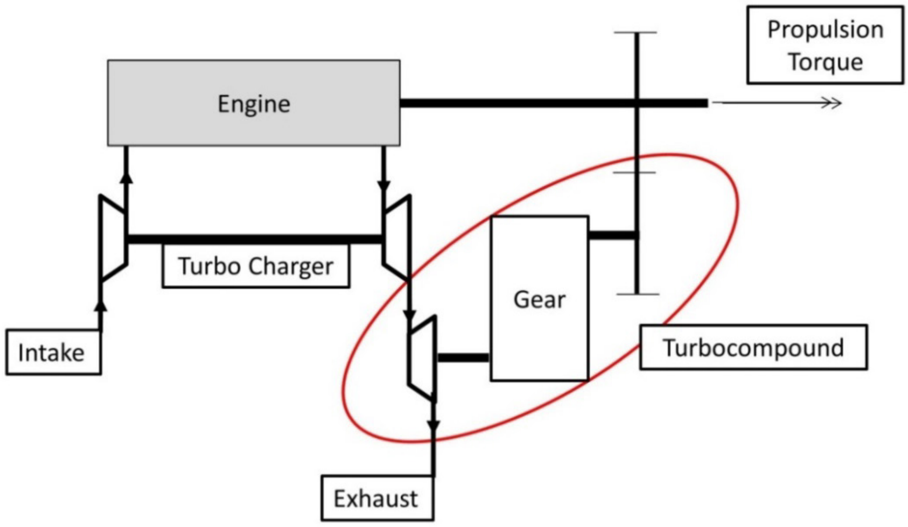

Figure 2-3: Configuration of a mechanical turbocompound system in a combustion engine

At present, turbocompound systems are most widely used in aircraft and heavy duty engines, where they typically reduce fuel consumption by 3 to 5% [15-16]. However, such reductions are not achieved under all operating conditions; under low engine loads, the turbocompound system may even cause a slight increase in fuel consumption [16]. This occurs because the turbine increases the exhaust backpressure, which causes increased pumping losses during gas exchange in the combustion engine. On the other hand, the increased exhaust back pressure makes it easier to achieve high EGR rates when using a short route EGR system because it increases the difference in pressure between the intake and the exhaust manifold [16].

Several companies currently produce or are developing engines featuring a turbocompound system for the heavy duty and off-road sectors, including Volvo, Scania, Cummins, Caterpillar, Iveco and Detroit Diesel [16]. Research on these engines typically focuses on understanding how the configuration of the turbine in the exhaust system affects performance, improving part-load performance, and developing hybrid engines with electric turbocompound systems.

2.2.2 Thermoelectric converters

Thermoelectric materials rely on the Seebeck effect, i.e. the generation of an electrical potential when a temperature gradient is applied across the junctions of two dissimilar conductors [17]. This phenomenon was named after Thomas Johann Seebeck, who discovered it in 1823.

Figure 2-4 shows how thermoelectric materials (TEM) can be used for exhaust heat recovery in passenger cars. TEM devices for power generation usually employ p- and n-type semiconductor elements as the dissimilar conductors because this increases the device's potential output [18]. In heat recovery systems for combustion engines, the temperature gradient applied across the junction of the device originates from the difference between the temperature of the hot exhaust gas (T_{source}) and that of a cooling fluid (T_{sink}). At equilibrium, the temperature of the hot side of the TEM is T_{hot} and that of the cold side is T_{cold}.

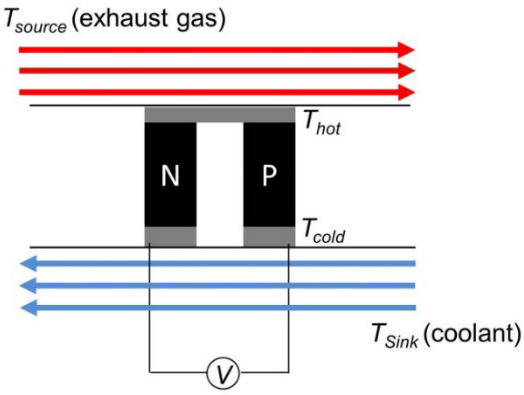

Figure 2-4: A thermoelectric generator for recovering waste heat from exhaust gases

TEMs are usually employed in exhaust heat exchangers (thermoelectric converters), in which the exhaust gas and cooling fluid flow in opposing directions and in separate channels [18-20]. The TEM devices are located between these channels, isolated by a non-conducting paste to prevent electrical contact between the TEM and the heat-exchanger [18].

The heat recovery efficiency η_{TEM} of the TEM is given by ***eq. (2.2)***. It is a function of T_{cold}, T_{hot} and the mean value of these temperatures (T). The factor ZT is known as the dimensionless figure of merit and is a characteristic constant for the two conducting materials used in the TEM. Together with the heat source and sink temperature, it is one of the major determinants of TEM performance [17-18]. It can be seen that the efficiency of the TEM is determined by a factor that includes the figure of merit and another factor that corresponds to the Carnot efficiency η_{Carnot}, i.e. the maximum achievable heat recovery efficiency.

$$\eta_{TEM} = \left[\frac{\sqrt{1 + Z \cdot T} - 1}{\sqrt{1 + Z \cdot T} + \left(\frac{T_{cold}}{T_{hot}}\right)}\right] \cdot \underbrace{\left(1 - \frac{T_{cold}}{T_{hot}}\right)}_{\eta_{Carnot}} \tag{2.2}$$

Modern commercial TEMs cannot achieve ZT factors above 1, giving a maximum realistic efficiency of around 5% for the conversion of exhaust gas waste heat in automotive applications [18,20]. A study conducted by the Ford Motor Company in 2009 examined the potential of thermoelectric heat recovery systems in gas-electric hybrid vehicles. It was found that for a city cycle, 2.4% of the waste energy in the exhaust gas could be recovered. This value rose to 5.7%

for the highway cycle, due to the higher loads and exhaust gas temperatures that occur under these driving conditions [20]. A study published in 2009 by Honda concluded that the use of a thermoelectric converter in a 2.0 litre gasoline engine would reduce overall fuel consumption by less than 1% [19], while a publication by Stobart et al. in 2010 predicted yearly fuel-saving potentials of 3.9% to 4.7% for a passenger car and up to 7.4% for a transit bus [18].

The major drawbacks of modern TEM systems are their low conversion efficiencies and the high costs of the devices [18,19-21]. The potential reductions in fuel consumption increase with the number and performance of the system's TEM elements. However, increasing the number of TEM elements also increases the system's cost and payback time. It is therefore desirable to develop exhaust heat exchangers that produce the greatest possible power with the lowest possible number of TEM devices [20]. This will necessitate the creation of systems with high heat transfer rates that do not increase the backpressure in the exhaust system to the point that the resulting increase in fuel consumption outweighs the contribution of the heat recovery system.

Despite the need to address these challenges, heat recovery systems based on thermoelectric generators are the best of the current heat recovery technologies in terms of their ease of integration into existing vehicles and the sophistication of their control systems [19]. In addition, they produce electrical energy directly without requiring any prior conversion of mechanical energy. This is useful if the recovered energy will be used to power the vehicle's electrical systems.

2.2.3 The Rankine cycle

The Rankine cycle is a model of an ideal steam-power cycle and was first described by the Scottish engineer William Rankine in 1859 [22], although the idea of using steam to generate power had been proposed long before then. The cycle involves using a heat source to vaporize a pressurized working fluid (usually water in power plants), which is then allowed to expand in a steam turbine. The power output of the turbine is used to drive a generator, producing electricity [23]. Rankine cycles of this type are used in the majority of modern power plants.

In heat recovery systems based on the Rankine cycle, the heat source is the waste heat produced by some primary process. In the case of a combustion engine, the relevant waste-heat sources are those listed in chapter ***2.1***. Individual heat sources can be exploited separately or in tandem if the situation permits, and the power that is generated can either be used to augment the vehicle's propulsion system or to drive a generator that produces electricity for the vehicle's electrical systems as was discussed in the chapter on turbocompound systems.

Figure 2-5 shows the key processes involving the working fluid in the Rankine cycle. The process steps in the pump and in the expander are assumed to be isentropic:

- An isentropic fluid pump does pump work, $w_{01,is}$, on the liquid working fluid (specific volume v). Its pressure is raised from the condensation pressure p_0 to the desired evaporation pressure p_1 (Stage 0→1):

$$w_{01,is} = v \cdot (p_1 - p_o) \tag{2.3}$$

- The pressurized working fluid is preheated, evaporated, and superheated to a certain extent utilizing the heat q_{12} in the heat exchanger (Stage 1→2). In this process, the specific fluid enthalpy is raised from h_1 to h_2:

$$q_{12} = h_2 - h_1 \tag{2.4}$$

- The superheated fluid vapour expands from the evaporation pressure p_2 to the condensation pressure p_3, implying a change in specific fluid enthalpy from h_2 to h_3. The isentropic work of expansion is denoted by $w_{23,is}$ (Stage 2→3):

$$w_{23,is} = h_3 - h_2 \tag{2.5}$$

- Finally, the working fluid is condensed back into the liquid phase in a condenser. Its heat of condensation, q_{30}, is rejected to a heat sink (Stage 3→0):

$$q_{30} = h_0 - h_3 \tag{2.6}$$

While this theoretical Rankine cycle is based on a sequence of reversible processes, real world systems involve irreversible changes of state in the pump and the expansion device. The corresponding isentropic efficiency η_{is} for these devices is defined according to ***eq. (2.7)-(2.8)***. Their effect of irreversibility on the pumping and expansion processes is indicated in ***Figure 2-5.***

$$\eta_{is,pump} = \frac{w_{01,is}}{w_{01}} \tag{2.7}$$

$$\eta_{is,exp} = \frac{w_{23}}{w_{23,is}} \tag{2.8}$$

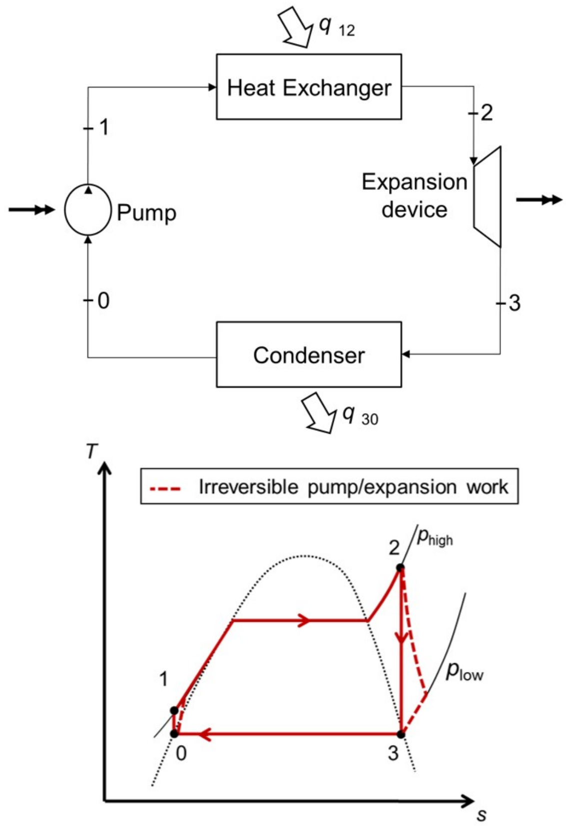

Figure 2-5: Layout of an illustrative Rankine cycle-based heat recovery system (top) and a temperature-entropy (T-s) diagram showing the different stages of the cycle (bottom)

The thermal efficiency η_{th} of a Rankine cycle can be calculated by considering its net work output w_{net} and the heat input q_{12}, ***eq. (2.9)***. The net work output is given by the difference between the mechanical output of the expansion device w_{23} and the pumping work done on the fluid, w_{01}. When calculating the thermal efficiency of the reversible process $\eta_{th,rev}$, the isentropic values for the pump and expansion work should be used.

$$\eta_{th} = \frac{w_{net}}{q_{12}} = \frac{|w_{23}| - |w_{01}|}{q_{12}} \tag{2.9}$$

Waste heat recovery systems based on the Rankine cycle are already used in stationary installations for recovering energy from industrial waste heat or off-grid power generators. They have also been adopted in marine engines. Notably, Opcon has developed a heat-recovery system for ships that promises fuel savings of 5 – 10%. The first system of this type has been in operation since 2012 [24]. In addition, Wärtsila and Turboden are collaborating to develop a similar heat recovery system for large vessels that promises to reduce fuel consumption by up to 12% [25]. If used in an 8000 teu (twenty-foot equivalent unit) container ship with a fuel consumption of 220 tons crude oil per 24 hours at normal speeds, this would correspond to a fuel saving of 25 tons per day, demonstrating the importance and potential of heat recovery systems in marine transport applications [26]. The heat-recovery systems that have been developed for ships use a so-called organic Rankine cycle (ORC), i.e. a Rankine cycle that uses an organic working fluid instead of water. This improves the efficiency of power generation from low temperature waste heat sources.

No commercial heat-recovery systems based on the Rankine cycle are currently used in on-road vehicles. However, there are several systems in development.

For heavy-duty trucks, studies published by AVL [27], Behr [28], Bosch [29], Voith [30], Ricardo and Volvo [31], and Cummins [32] have shown that Rankine cycle-based systems can reduce fuel consumption by 3 to 6%. All of these authors consider the EGR and exhaust gases to be the most viable waste-heat sources in vehicle engines. The achievable fuel consumption benefits depend strongly on the driving conditions considered. Lower engine loads mean lower exhaust temperatures and mass flows, which decreases the thermal efficiency of the heat-recovery system. Thus, one of the challenges in developing systems for vehicle-based applications is the transient nature of different operating modes. In contrast, heat recovery systems for stationary installations can be designed against a single specific set of operating conditions.

For light-duty passenger cars, Honda [33] and BMW [34] have reported that fuel savings of up to 10% can be achieved by recovering exhaust heat. However, there has been relatively little published work describing heat-recovery systems based on the Rankine cycle for passenger cars. This could be due to one of the notable drawbacks of this technology: Rankine cycle systems take up considerable amounts of space and are heavier than alternative heat recovery solutions. These problems are significant even when working with heavy-duty vehicles, and can be extremely restrictive when designing systems for passenger cars. Nevertheless, BMW have demonstrated that these issues can be worked around with sufficiently well-optimized designs by creating a Rankine cycle heat recovery system that weighs only 10 - 15 kg and can be integrated into the underbody of a car to save space.

3 Considerations in the design of Rankine cycles

The basic Rankine cycle setup presented in ***Figure 2-5*** can be adapted to the boundary conditions of its intended working environment by tuning some fundamental design parameters. The following chapters provide an overview of these parameters, with particular emphasis on the case of an engine waste heat recovery system.

3.1 Working fluid

The working fluid employed in the Rankine cycle is among the most important and thus most frequently discussed components of heat recovery systems relying on that technology. Its choice is a basis for the subsequent design process of the system, affecting beside the performance also the choice of the physical cycle components. A detailed working fluid assessment, including the evaluation of safety and environmental aspects, is provided in ***Paper I***. The aim of this chapter is to highlight the most important properties of a working fluid and to explain how they affect the operation and design of a Rankine cycle.

The thermophysical differences between different working fluids can be explained by considering three representative fluids that are commonly proposed for use in vehicle waste heat recovery systems [35]:

- ***water*** – The traditional working fluid of the steam Rankine cycle used in power generation. It has been considered by numerous investigators for IC engine heat recovery (*e.g.* [28,35,36,37,38])
- ***ethanol*** – An organic fluid (alcohol) that is frequently mentioned as a suitable alternative to water for vehicular applications (*e.g.* [28,29,39]). It solves the freezing problem encountered when using pure water in mobile applications but has the drawbacks of being flammable and less thermally stable.
- ***R245fa*** – An organic fluid (hydrofluorocarbon) that is one of the most popular fluids for ORC applications (e.g. [35,41]). It offers low flammability but its use will be restricted by legislation in the near future because of its high global warming potential. A replacement fluid addressing the latter issue has been introduced [42].

T-s diagram ***(Figure 3-1)***

The *T-s* diagram clearly shows that the saturation curves for the three fluids (water, ethanol, R245fa) differ considerably in size and shape. The saturated vapour line for water has a negative slope. An isentropic expansion starting from the saturated vapour state will thus always end up in the two-phase region, so water is referred to as a “wet” fluid. Conversely, the saturated vapour line for R245fa has a positive slope, so a comparable expansion brings the system into the superheated vapour state, making R245fa a “dry” fluid. Ethanol is classified as an “isentropic” fluid because its saturated vapour curve has a near-vertical inclination. The fluid’s expansion behaviour has practical implications when selecting an expander because turbine expanders are known to suffer from erosion when droplets are present at the end of the expansion, i.e. when the expansion ends in the two-phase region [14,43]. This can occur if a wet fluid is used with inadequate superheating and/or the superheating is insufficiently stable and the expansion pressure ratio is high. Rapid variation in the waste heat rate (as occurs in vehicle exhausts) together with the dynamics of the Rankine cycle itself can make it difficult to maintain a given level of superheating, creating a significant control challenge [44].

For a reversible isothermal heat transfer process, the change in entropy ΔS can be expressed as a function of system temperature T_0 and heat transfer Q [45]. If considering the isothermal vaporization (*vap*) of a fluid at its saturation temperature T_{sat}, the relation can be rewritten as shown in ***eq. (3.1)***.

$$\Delta S = \frac{Q}{T_0} \overset{vap}{\Longrightarrow} \Delta S_{vap} = \dot{m} \cdot (s_g - s_l) = \frac{Q}{T_{sat}} \tag{3.1}$$

Assuming constant Q and T_{sat}, this equation indicates that the greater the vaporization entropy of the Rankine cycle’s working fluid, the lower the expected fluid mass flow $\dot{m}$. This is why the pump power required when using water is typically considerably lower than that required for organic working fluids in similar applications [35]. Reducing the pump power is beneficial for the net power output of the Rankine cycle.

The *T-s* diagram features two scatter bands representing the boundary conditions of the process in terms of the Carnot efficiency:

- T_{source}, representing typical IC engine EGR/exhaust temperatures (see also chapter ***2.1***)
- T_{sink}, representing available heat sink conditions (ambient air/engine coolant)

At a first glance, one might conclude that a water-based Rankine cycle would best match the temperature boundaries of the IC engine case because water evaporates and condenses at temperatures close to T_{source} and T_{sink}, respectively, which would be expected to yield a promising thermal efficiency (compare ***eq. (2.1)***). However, in real applications the heat source and sink are sensible heat sources, which means their temperature is affected by the heat transfer to the working fluid. Under such conditions, a fluid like water with a large latent heat and a high boiling temperature can be impractical. When attempting heat recovery from the exhaust or EGR of an IC engine operating under low load, the mass flow rates of a water-based Rankine cycle can be very low and the heat utilization becomes very poor due to the low temperature and flow rate of the exhaust gases. This issue is discussed at greater length in chapter ***3.2*** and the results section of ***Paper III***. An issue with organic fluids such as ethanol and R245fa is that their thermal stability limit is considerably lower than that of water [46]. The decomposition temperature depends on the fluid type, but for most organic fluids it is expected to be lower than the heat source temperature for IC engine exhausts in ***Figure 3-1*** [40,47]. Thus, the risk of thermal decomposition is always present when recovering heat from the exhaust of an IC engine with these fluids. It will be important to investigate how thermal decomposition is affected by system design and thermal cycling, and to assess the consequences of thermal degradation of the working fluid in future studies.

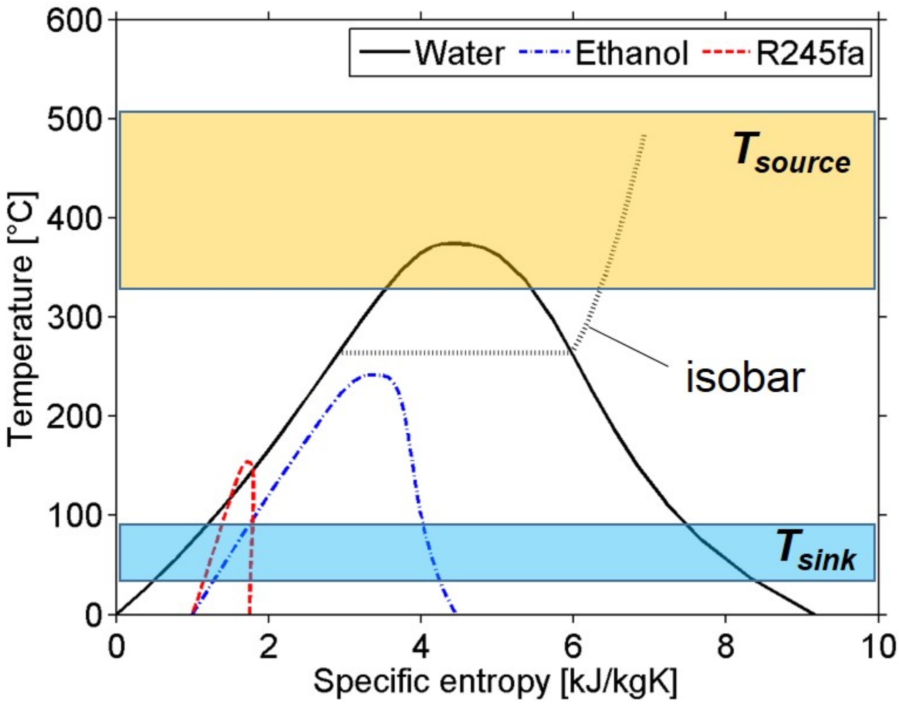

Figure 3-1: T-s diagram for three representative working fluids

<u>P-v diagram and volume flow rate (VFR)</u> ***(Figure 3-2)***

A high specific volume of the working fluid vapour is often said to necessitate the use of large components (particularly heat exchangers) and to lead to high pressure losses due to a high volume flow rate (*VFR*) on the vapour side of the Rankine cycle [35,43,48,49,50]. These factors are problematic in vehicular applications because of their packaging implications. Ethanol and R245fa seem to be superior to water as working fluids in terms of their vapour specific volume (***Figure 3-2***, left). However, because the mass flow rates in the cycle can differ substantially depending on the fluid type, such a conclusion cannot be drawn based on specific volumes alone. The right-hand side plot in ***Figure 3-2*** shows the *VFR*s for ethanol and R245fa in a basic Rankine cycle with an assumed fixed heat input, normalized against the *VFR* of water under the same conditions, at a range of expansion pressure ratios (p_2/p_3) with p_3 corresponding to the saturated vapour state at 100 °C in all cases. Water has the highest *VFR* in all cases, both before and after expansion, so ranking the fluids on the basis of their vapour specific volumes does not change their order in terms of required system volume. However, the difference in *VFR* between water and the two organic fluids is smaller than one might expect from looking at the *P-v* diagram. Under the considered conditions, the mass flow rates for ethanol and R245fa are up to 3 and 12 times greater, respectively, than those of water. Therefore, when attempting to determine how different working fluids will affect the volume of a Rankine cycle system, it is necessary to consider the mass flow rate as well as the specific vapour volume.

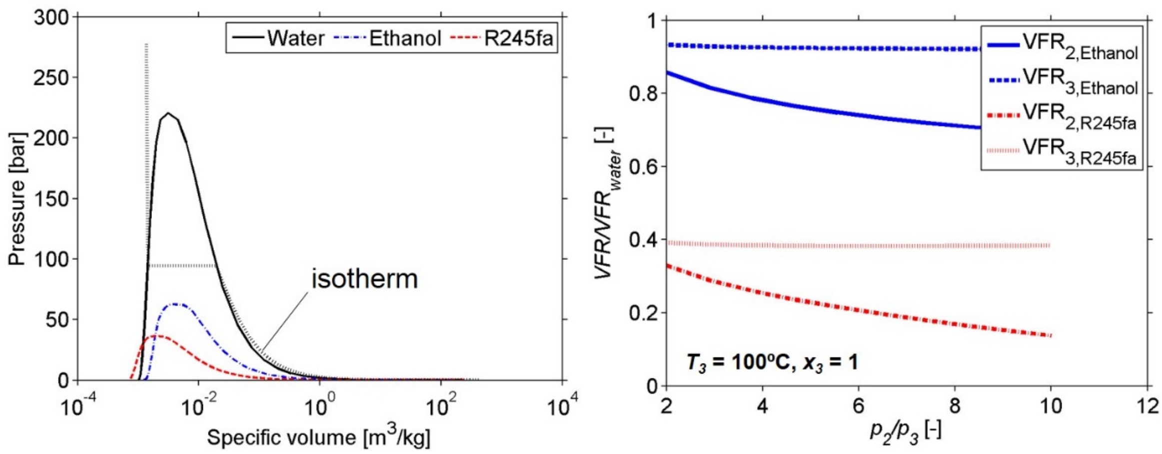

Figure 3-2: P-v diagram for three representative working fluids (left) and volume flow rates (VFR) of ethanol and R245 in relation to water (right)

Vaporization (latent) heat, molecular mass and boiling point (***Figure 3-3***)

This figure shows the heat of vaporization, Δh_{vap}, (also known as the latent heat) for the three considered fluids. According to Panesar et al. [35] and Chen et al. [51], given fixed heat source and sink temperatures, the fluid with the highest latent heat will give the highest Rankine cycle work output per unit mass. Based on this hypothesis, water should be preferable to ethanol or R245fa. However, as mentioned earlier in this chapter, the waste heat sources in an IC engine (e.g. the exhaust gas) are sensible, so their temperature decreases during heat transfer to the Rankine cycle. Under these conditions, a large latent heat is not necessarily an advantage since an organic fluid with a lower latent heat might provide a better match to the temperature profile of the heat source, reducing the irreversibility of the heat transfer [49]. It is therefore impossible to determine the optimal latent heat for the working fluid of a given Rankine cycle without first considering the cycle's boundary conditions.

The tabulated data in ***Figure 3-3*** shows that organic fluids have lower boiling points and higher molecular masses than water. A low boiling point can be an advantage when using low temperature heat sources such as the engine coolant or the CAC, but creates problems on the heat sink side of the Rankine cycle in vehicular applications. For example, if one were to use engine coolant at 90 °C as the heat sink, the condensation pressure required for R245fa would be above 10 bar, reducing the viable expansion pressure ratio and thus the work output. Low heat sink temperatures (ambient or low temperature coolant) can thus be regarded as a prerequisite for using organic fluids in a Rankine cycle. These trends can also be seen in the T-s diagram (***Figure 3-1***). A viable modified cycle for fluids with low boiling points and critical pressures is the supercritical cycle, which is introduced in chapter ***3.3***.

The molecular mass of the working fluid is described in the literature as an indicator of the fluid's vapour specific volume, specific heat of vaporization Δh_{vap}, specific expansion enthalpy drop and mass flow rate. When compared to fluids of lower molecular mass, fluids with high molecular masses such as R245fa typically have:

- A lower vapour specific volume [52].
- A lower Δh_{vap} [35].
- A lower specific enthalpy drop during expansion [35,43].
- A higher mass flow rate (which increases the pump power) [43].

The latter two properties are known to be favourable for an efficient single stage expansion in a turbine expander [35,43].

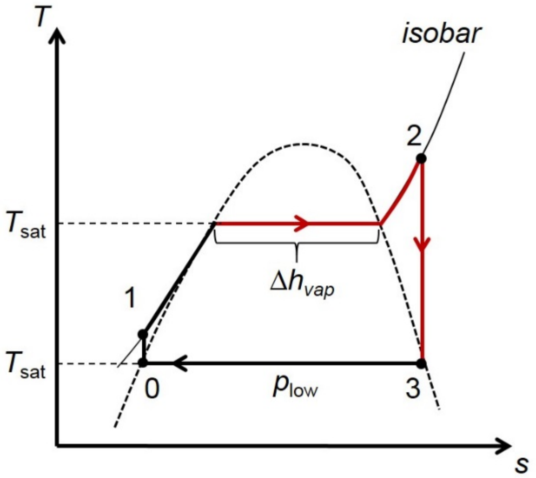

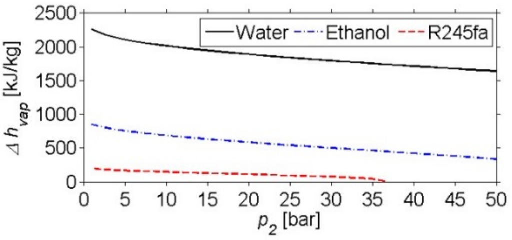

	Water	Ethanol	R245fa
$T_{sat,1\ bar}$ [°C]	99.6	78.1	14.86
$T_{sat,10\ bar}$ [°C]	179.9	150.1	89.6
$T_{sat,30\ bar}$ [°C]	233.9	200.1	143.5
M [g/mol]	18.015	46.068	134.05

Figure 3-3: Thermophysical properties for the three representative working fluids

3.2 Operating parameters

The traditional Rankine cycle can be described in terms of the following operating parameters:

- Pressures and temperatures in process stages *0 - 3* (***Figure 2-5*** and ***Figure 3-3***).
- The mass flow rate of working fluid.
- The working fluid's properties.

This chapter discusses the major correlations among these parameters as well as their impact on the expectable performance (efficiency and power output) of the cycle.

Fluid properties, mass flow rates and boiling pressure

The heat exchange process between the IC engine source (e.g. the EGR) and the fluid in the Rankine cycle can be described in a simple but clear way by applying the first law of thermodynamics, ***eq. (3.2)***. Heat losses to the surroundings are neglected.

$$Q_{12} = \dot{m}_{WF} \cdot (h_2 - h_1) = \dot{m}_{EGR} \cdot c_{p,EGR} \cdot \Delta T_{EGR} \tag{3.2}$$

This equation contains all of the available information about the correlation between the flow rates of the working fluid ($\dot{m}_{WF}$) and the EGR ($\dot{m}_{EGR}$), as well as the enthalpy changes for the working fluid (h_2-h_1) and EGR ($c_{p,EGR} \cdot \Delta T_{EGR}$). The exhaust gas in the EGR loop can be assumed to be an ideal gas [54].

Figure 3-4 provides a graphical interpretation of ***eq. (3.2)***. It also shows the so-called pinch point, i.e. the point at which the temperature difference between the working fluid and the heat source is minimized during the heat exchange process. This typically occurs at the onset of evaporation of the working fluid. The pinch point temperature difference is typically a consequence of the design trade-off between the size and efficiency of the heat exchanger [55]. Large heat exchangers allow smaller pinch point temperature differences and vice versa. Two major statements can be made, assuming a constant pinch point temperature difference, EGR inlet temperature and flow rate, and heat exchanger size:

i. A higher working fluid boiling point implies a flatter EGR temperature profile due to the pinch point, which means that ΔT_{EGR} decreases and so less waste heat is utilized. The flow rate $\dot{m}_{WF}$ of the working fluid must thus be reduced to maintain superheating at point 2. This phenomenon was confirmed during the experiments conducted within this project and is known from previous studies [37,56,57].
ii. The use of a working fluid with a high latent heat has been claimed to be beneficial for the cycle's work output (chapter ***3.1***). However, fluids with low latent heats can be advantageous in terms of heat recovery from a sensible heat source [58,59,60] because a higher share of the overall heat is transferred during the pre-heating of the fluid, allowing the heat source to be cooled down to a lower temperature and consequently more heat to be utilized.

Both observations apply to the Rankine cycle in heat recovery applications and contradict the general trend for the thermal Rankine cycle efficiency to increase with higher boiling pressures (at a fixed condensation pressure) and with the latent heat of the working fluid [61]. However, as the temperature and energy content of the waste heat source increase, the optimal configuration is shifted back towards the 'conventional' position, favouring fluids with higher boiling points and larger latent heats.

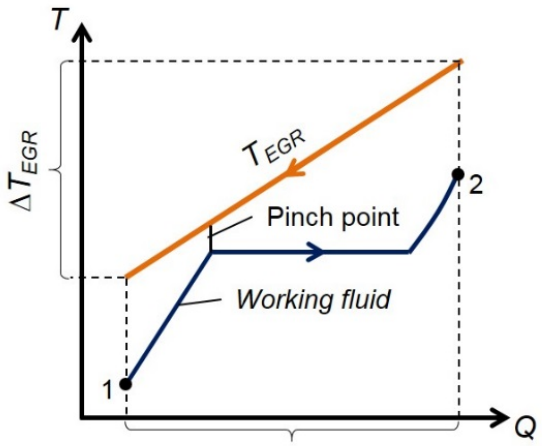

$$Q_{12} = \dot{m}_{WF} \cdot (h_2 - h_1) = \dot{m}_{EGR} \cdot c_{p,EGR} \cdot \Delta T_{EGR}$$

Figure 3-4: Schematic temperature profiles for the EGR and working fluid

Figure 3-5 presents the simulated performance of the three representative working fluids (water, ethanol and R245fa) in EGR heat recovery for a heavy duty Diesel engine (T_{EGR} = 400 °C). Unless otherwise specified, the condensation temperature was fixed at 100 °C while the boiling pressure p_2 was varied. The level of superheating was chosen so that the fluid was always maintained in at least the saturated vapour state throughout the expansion process. The observed thermal efficiencies and cycle power outputs confirm the statements made in the preceding sections in that the thermal cycle efficiency tends to increase with the heat of vaporization (water>ethanol>R245fa) and maximum cycle pressure. Because the high condensation pressure of R245fa at 100 °C permits the use of a relatively low expansion pressure ratio, an additional case assuming condensation at 50 °C is presented for this fluid. Under these conditions, its performance becomes competitive with ethanol. Looking at the isentropic expansion power, the cycle using water as a fluid shows a weak maximum at low values of p_2 because the EGR heat utilization declines at higher boiling pressures. The organic fluids are not affected by this limitation due to their lower boiling points and latent heats; the power output of the corresponding cycles therefore increases with p_2. A study based on similar assumptions that confirms these findings has been reported by Panesar et al. [35]. Higher EGR inlet temperatures would further increase the optimum boiling pressures for water, allowing it to outperform the organic fluids.

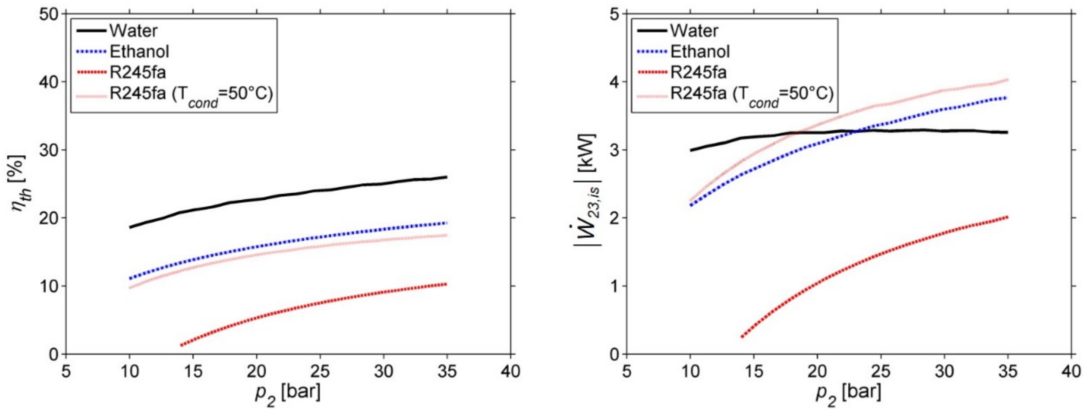

Figure 3-5: Thermal efficiency and isentropic expansion power as functions of the boiling pressure p_2

Given the data presented above, it is clear that the operating parameters of the Rankine cycle must be optimized on the basis of the properties of the waste-heat source to be utilized. It is important to consider not just the thermal efficiency of the Rankine cycle but also the amount of heat from the source (i.e. the IC engine in our case) that is utilized and the actual power output of the heat recovery system. Since neither the temperature nor the flow of the EGR and exhaust gas are stable over the operating range of a typical vehicle, the optimal operating parameters and fluid for the cycle are strongly dependent on achieving a good match with the boundary conditions defined by their variation. On the condensation side, low pressures and temperatures are always beneficial, both for thermal cycle efficiency and power output. A low condensation pressure increases the Rankine cycle's thermal efficiency but the scope for reducing the condensation pressure is often restricted by the available heat sink temperatures in vehicular applications and the increase in the specific volume of the working fluid at low vapour pressures (which necessitates the use of large condensers). In addition, various authors have noted that sub-atmospheric condensation pressures should be avoided due to the risk of air infiltration [14,43,52,62].

Superheating of the working fluid

From a practical point of view, superheating of the working fluid is necessary to avoid expansion into the two-phase region when using a wet fluid (see ***Figure 3-6***, left). This is not usually a problem with dry fluids because their saturated vapour lines have positive slopes (see ***Figure 3-6***, right): after expanding from the saturated vapour state, these fluids typically remain in the superheated state.

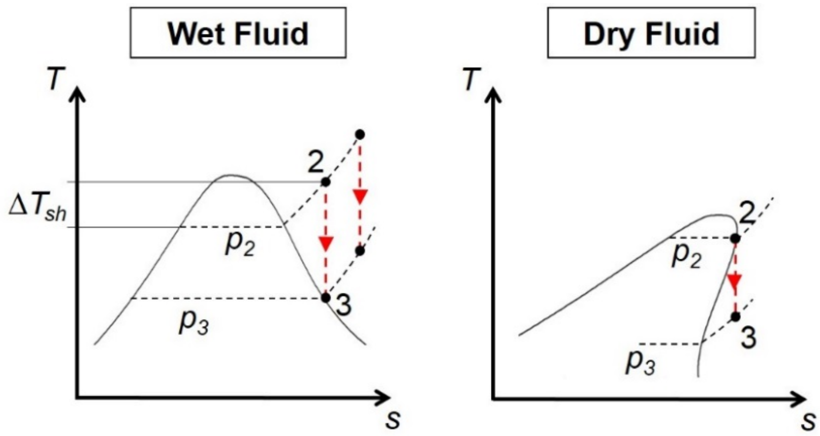

Figure 3-6: Role of superheating for a wet fluid (left) and a dry fluid (right)

A question that remains to be answered is whether higher levels of superheating than necessary for dry expansion are beneficial for the performance of the Rankine cycle in a heat recovery system. This question can be addressed by considering an enthalpy-entropy diagram for water and R245fa as representative wet and dry fluids, respectively (see ***Figure 3-7***). Isobars corresponding to fluid pressures of 1 bar, 10 bar and 20 bar are included in the diagrams for both fluids.

For water (***Figure 3-7***, left), the isobars diverge in the superheated region, which is considered to be a characteristic trait of wet fluids [35]. This means that higher levels of superheating at similar expansion pressure ratios yield higher isentropic expansion work. In principle, superheating should therefore have a positive effect on the power output of a water-based Rankine cycle. To assess the effect of superheating on thermal efficiency, it is necessary to compare the additional heat required for superheating to the resulting surplus power output. For wet fluids, the efficiency is expected to increase [51].

For R245fa (***Figure 3-7***, right), the isobars don't diverge in the superheated region, so no additional power output can be expected despite the additional heat required for superheating. Superheating thus tends to reduce thermal efficiency. Such behaviour is claimed to be characteristic of dry fluids [35,51]. From a practical point of view, superheating dry fluids before expansion is counterproductive because it increases the superheating level of the fluid after expansion even further. This would increase the size of the condenser required under a given set of boundary conditions without increasing the cycle's power output [35,58].

In the context of waste heat recovery applications, superheating beyond the level necessary for a dry expansion cannot be recommended, especially in cases where the overall size of the system is an important parameter. Heat transfer coefficients in the gas phase of the working fluid are lower than in the two-phase state or liquid phase, requiring a larger heat exchange area per unit heat transferred [35]. With a larger share of the heat transfer occurring in the pre-heating phase, the heat source can be cooled down more efficiently and thus more heat can be recovered. In heat recovery applications, the mass flow of working fluid must typically be reduced to reach higher levels of superheating under otherwise similar system operating conditions (compare ***eq. (3.2)***). Thus, less vapour is expanded per unit time, with a negative effect on expander power output.

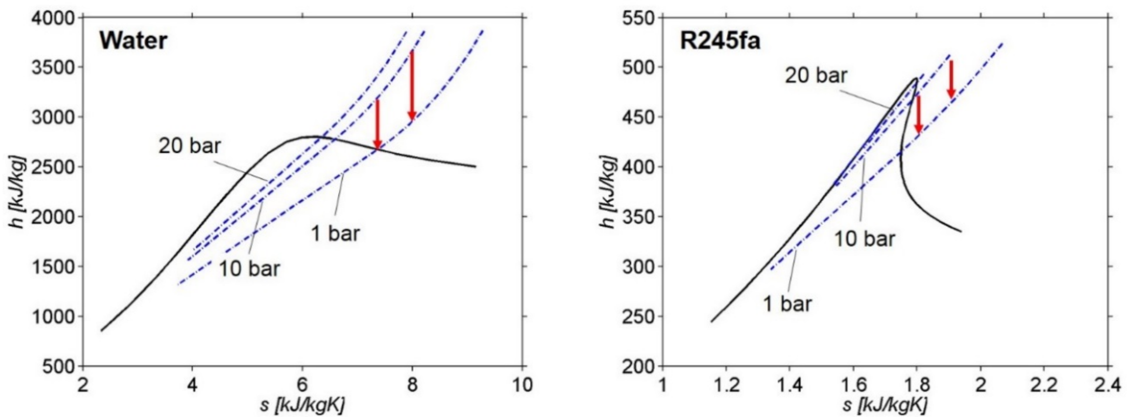

Figure 3-7: h-s diagrams for water (left) and R245fa (right), including isobars for 1, 10 and 20 bar

3.3 Cycle configurations and modifications

This chapter briefly reviews a selection of published modifications to the traditional Rankine cycle. Some of them have not yet been implemented in a way that would be practical for vehicular applications, but the ideas behind them may be valuable to consider when seeking to improve the performance of the Rankine cycle and associated heat recovery systems. With the exception of the regenerative Rankine cycle, there is no experimental validation of the predicted system-level efficiency trends for any of the reviewed technologies. Most of the modifications aim to improve the temperature profile match between the working fluid and heat source during heat transfer. This would increase the cycle's thermal efficiency but reducing the temperature difference (driving force) between source and fluid means that a larger area is needed to transfer the same amount of heat, which is an important factor to bear in mind when thinking about practical applications.

Regenerative Rankine cycle

The regenerative Rankine cycle is intended to offer a superior thermal efficiency to the conventional Rankine cycle, particularly in cases involving a dry working fluid (***Figure 3-8***). This cycle differs from the conventional one in that it includes an additional internal heat exchanger to transfer residual heat from the expanded vapour (process stage ***3***) to the pre-heating phase (***1*** → ***1'***). This is possible because when using dry fluids the expander output is typically still superheated, so it is possible to reduce the amount of heat supplied to the Rankine cycle without greatly reducing its power output. In the case of most waste heat recovery applications, this criteria is not that significant since the heat supplied is anyway for free and the outlet temperature of the waste heat source is usually not constrained. The regenerative Rankine cycle would require and additional heat exchanger without a benefit for the objective of the application [58,63,64]. However, the regenerative cycle's ability to improve thermal efficiencies is sometimes advantageous, such as when there is a lower limit on the outlet temperature of the heat source. This may be necessary in some cases to avoid the condensation of corrosive acids out of the waste heat flow

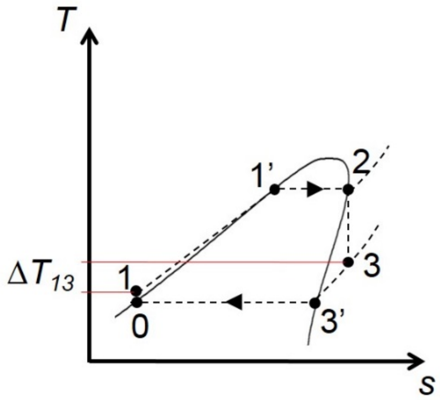

Figure 3-8: T-s diagram for a Rankine cycle with a dry fluid

<u>*Supercritical Rankine cycle*</u>

The purpose of the supercritical Rankine cycle (also referred to as the transcritical Rankine cycle) is to avoid entering the two-phase region during heat transfer from the waste heat source (see ***Figure 3-9***). This can be achieved by pumping the fluid to a pressure above the fluid's critical point (CP) (***0 → 1)***. The objective of doing this is to improve the match between the temperatures of the heat source and fluid by avoiding isothermal evaporation. In theory, this can shift the thermal efficiency closer to the Carnot efficiency [65,66]. Avoiding the fluid's two-phase region during heat transfer allows the usage of a simpler and cheaper heat exchanger [66,67]. The drawbacks of supercritical operation are higher pressures and expected issues relating to the thermal stability of organic fluids [58].

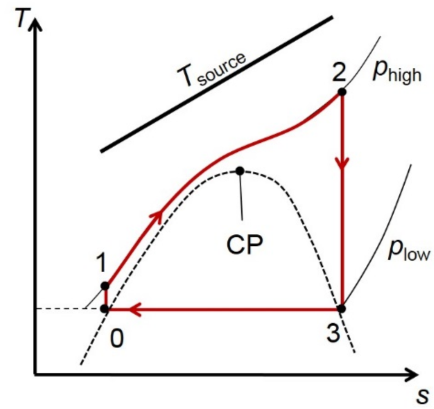

Figure 3-9: T-s diagram of a supercritical Rankine cycle

The supercritical cycle is impractical for heat recovery systems that use water as the working fluid because of its high critical temperature and pressure (220.6 bar, 374 ºC), especially since

p_{high} for the cycle should exceed the critical pressure by 20% for stability reasons [68]. Organic fluids such as ethanol (62.68 bar/241.6 ºC) or R245fa (36.51 bar/154 ºC) generally have lower critical parameters, making the supercritical concept a viable option for the ORC. It has mainly been studied using theoretical methods, focusing on heat recovery from low-temperature heat sources (<200 ºC) in stationary systems (e.g. geothermal power plants). The thermal efficiencies of supercritical ORCs in such applications were predicted to be 10-30% higher than those of subcritical ORCs [64,66]. Supercritical cycles were also considered in ***Paper I***, which focuses on IC engine waste heat sources; in such cases, they did not offer superior efficiencies to subcritical cycles. Similar conclusions were presented by Panesar et al. [58] based on a study of supercritical cycles under EGR boundary conditions.

Rankine cycle with mixture working fluids

One motivation for using working fluid mixtures is to avoid or weaken undesirable properties of the pure fluids. Mixing water with alcohol (e.g. ethanol or methanol) can reduce the flammability risk of pure alcohol and eliminates the freezing problem encountered when using pure water in vehicular applications (see also ***Paper I***). In addition to practical considerations, basic thermodynamic factors suggest that binary working fluid mixtures can have beneficial properties. So called zeotropic mixtures exhibit non-isothermal vaporization and condensation over their entire composition range as shown in ***Figure 3-10*** (left), in which the mole fraction of the symbolic mixture component A is plotted on the abscissa [66]. When using such a mixture in the Rankine cycle, a temperature drift can be achieved during evaporation and condensation, ***Figure 3-10*** (right). This may be advantageous for the same reason as the supercritical cycle: the improved match between working fluid and heat source temperature should increase cycle efficiency. Theoretical studies predict potential increases in thermal efficiency of 4-15% compared to a conventional Rankine cycle [69,70].

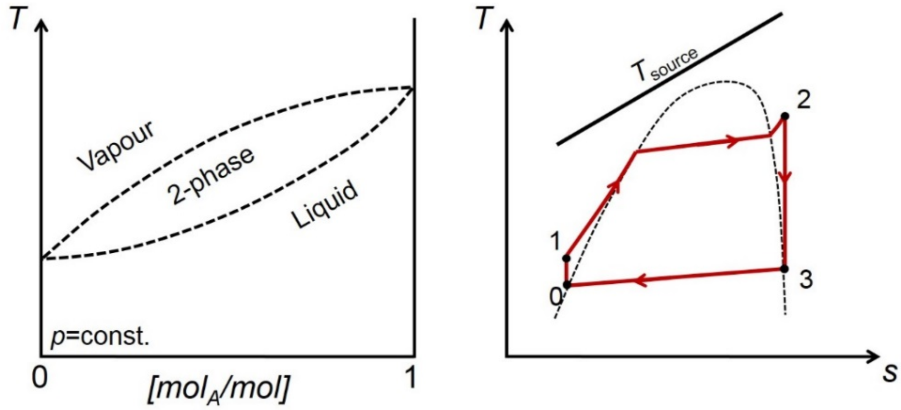

Figure 3-10: Vapour liquid equilibrium (VLE) for a binary zeotropic mixture (left) and T-s diagram of a Rankine cycle with a zeotropic mixture fluid (right)

<u>*Trilateral flash cycle (TFC)*</u>

Unlike in the Rankine cycle, the working fluid in the TFC is only heated to the saturated liquid state, after which it undergoes a wet expansion (***Figure 3-11***). This cycle is compatible with wet, isentropic or dry fluids. Consequently, the state of the fluid after expansion (state *3*) may lie in the superheated vapour region, for example if a dry working fluid is used. The motivation for using this cycle is that it offers a good match between the fluid and heat source temperatures and also requires no evaporator, which reduces the system's cost and size [71]. The need to design an expander capable of accommodating wet expansion is considered to be the most challenging element of implementing such a cycle. The TFC is predicted to provide better efficiencies than the conventional Rankine cycle, although very little research has been done so far on this concept [70,71,72]. There is some evidence that its efficiency advantage declines as the waste heat source temperature rises above 200 °C [72] because the increasing temperature difference between heat source and fluid under such conditions diminishes the advantage of the improved temperature match during heat transfer.

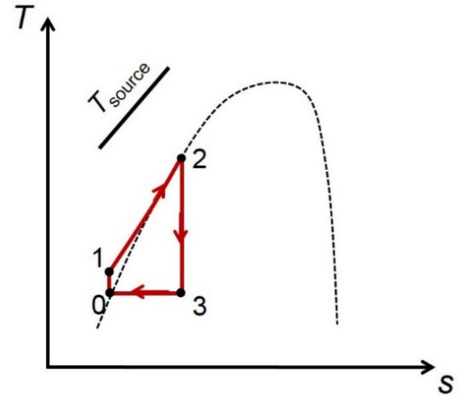

Figure 3-11: T-s diagram of trilateral flash cycle (TFC)

4 Methodology

The following chapters summarize the techniques, assumptions and methodology used to derive the original results presented in this thesis and the appended publications.

4.1 Fluid properties

Both the theoretical modelling and the calculations based on the experimental data require accurate information on the properties of the studied fluids. This chapter introduces the approaches and assumptions used to estimate the fluids' properties in this work.

<u>*Exhaust gas*</u>

A heavy duty Diesel engine (Volvo D13 US10) was used as the heat source for the heat recovery system examined in this project. In keeping with the literature, the exhaust gas of this engine was assumed to be an ideal gas [54]. Its composition was estimated based on the stoichiometric equation for the combustion of Diesel fuel in air, ***eq. (4.1)***. This equation is expressed as a function of λ, which represents the air-fuel equivalence ratio. The 'average' formula of diesel is taken to be $C_{12}H_{23}$ [73].

$$C_{12}H_{23} + \lambda \cdot 17.75 \cdot 4.762 \cdot (0.21 \cdot O_2 + 0.79 \cdot N_2) \tag{4.1}$$

$$\rightarrow 12 \cdot CO_2 + 11.5 \cdot H_2O + \lambda \cdot 17.75 \cdot 3.762 \cdot N_2 + 17.75 \cdot (\lambda - 1) \cdot O_2$$

Data on the properties of the combustion products were obtained from the REFPROP database [74]. Using the expression for the exhaust composition as a function of λ, it was possible to compute the specific heat ratio κ and the specific heat capacity c_p for various exhaust temperature levels (see ***Figure 4-1***). Reliable data for the experimental engine's air-fuel equivalence ratio were not available, but a GT-Power model indicated it to have global λ values between 1.5 and 2 depending on the engine's operating point. Within this range, the influence of λ on κ and c_p is considerably weaker than the effect of the gas temperature. It was therefore assumed that the exhaust gas had a constant λ value of 1.7 and that its properties were temperature-dependent.

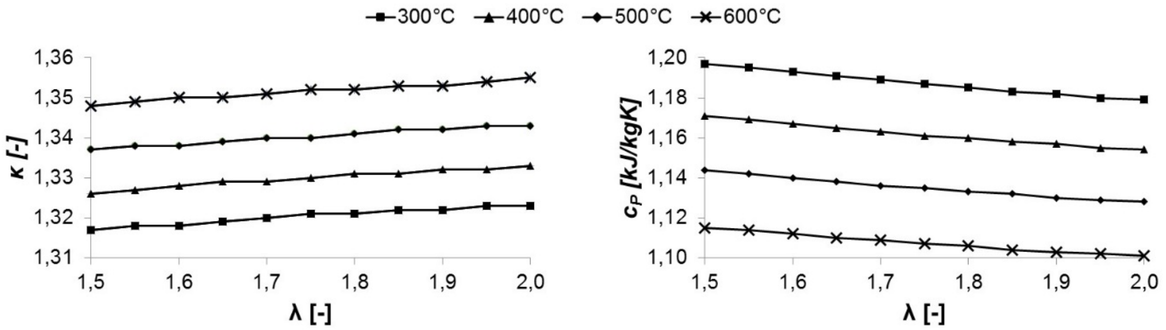

Figure 4-1: The specific heat ratio (left) and specific heat capacity c_p (right) of Diesel exhaust as functions of λ

<u>Rankine cycle working fluid</u>

All property data for the working fluids used in the Rankine cycle in all of the states considered in this work were obtained directly from the corresponding equations of state included in the REFPROP database [74].

4.2 Simulation models

The work performed in the first half of this PhD project was purely theoretical and based on zero- and one-dimensional modelling approaches. The results obtained using the system and component models created during the first half of the project were then used to guide the design of the demonstrator test bench. Experiments conducted using the test bench were used to validate the theoretical models, and the experimental results were used in conjunction with the models to suggest design optimizations for the test rig.

4.2.1 The zero-dimensional system model

A zero-dimensional model of the Rankine cycle was created using <u>E</u>ngineering <u>E</u>quation <u>S</u>olver (EES), which is a general equation solving program with a thermodynamic property database [75]. The modelling of the cycle was based on the following assumptions:

- No pressure losses occur during the cycle.
- All cycle components are assumed to be adiabatic.
- The exhaust gas can be treated as an ideal gas.
- Constant isentropic efficiencies are assumed for the pump and expander.
- The condensation pressure is greater than the atmospheric pressure (to minimize the risk of air infiltration).

- The vapour is saturated after expansion (this requirement defines the level of superheating).

When the project was initiated, no experimental hardware or calibration data were available. The objective of the zero-dimensional modelling work was thus to pave the way to the design of a demonstrator test rig. In particular, the models were intended to facilitate:

- Comparisons of different working fluids' performance under various heat source conditions.
- The selection of an expansion device concept based on selected cycle operating parameters.

A detailed description of the applied methodology can be found in the related publications at the end of this thesis. A summary is given in the following sections.

Comparison of working fluid candidates (***Paper I***)

A range of potential working fluids were considered including water, ammonia and organic fluids such as alcohols and refrigerants. The safety of the candidate fluids was evaluated in terms of their flammability and toxicity. Pure alcohols and some refrigerants are highly flammable, and some refrigerants produce toxic gases when they burn. The environmental factors considered when evaluating the potential working fluids were their Global Warming Potential (GWP) and Ozone Depletion Potential (ODP). To comply with future environmental legislation relating to vehicles, only fluids whose GWP values are at most 150 times greater than that of CO_2 were considered suitable for mobile heat-recovery systems [76]. All fluids with non-zero ODP values will be banned in 2030, and laws have been passed requiring a 90% reduction in the production of such fluids by 2015 [77,78].

The basic stages of the Rankine cycle as described by ***eq. (2.3)-(2.9)*** and illustrated in ***Figure 2-5*** were implemented in EES. The temperatures of the heat sources (i.e. the EGR, exhaust and CAC) were obtained from a GT-Power model for a Volvo D13 heavy duty engine. Both the thermal efficiency η_{th} (***eq. (2.9)***) and the exergy efficiency η_{II} (***eq. (4.2)***) were computed for the various fluids. The temperature of the heat sink is denoted by T_0.

$$\eta_{II} = \frac{|w_{23}| - |w_{01}|}{q_{12} \cdot \left(1 - \frac{T_0}{T_{\text{Source}}}\right)} = \frac{\eta_{th}}{\left(1 - \frac{T_0}{T_{\text{Source}}}\right)} \tag{4.2}$$

The exergy efficiency relates the thermal cycle efficiency to the Carnot efficiency and thus contains information on the cycle performance in relation to the quality (temperature) of the heat source.

<u>*Selection of a suitable expansion concept*</u> (***Paper II***)

The expander has a significant effect on the performance of the heat recovery system and must be chosen carefully. There are two types of expansion device in common use: displacement expanders (e.g. piston expanders, scroll expanders, screw expanders, and others) and turbine expanders (e.g. radial and axial turbines). Some practical considerations relevant to these expander concepts are discussed in ***Paper II.***

The isentropic efficiency $\eta_{is,exp}$ of an expansion device can be estimated based on an approach known as the similarity concept [79,80] that requires only two input parameters:

- The isentropic enthalpy drop over expansion $\Delta h_{is,23}$.
- The volume flow rate VFR of the fluid at the expander outlet.

These parameters are used to calculate two characteristic similarity numbers: the specific speed, N_s (***eq. (4.3)***), and the specific diameter, D_s (***eq.(4.4)***).

$$N_S = N \cdot \frac{VFR_{ex}^{1/2}}{\Delta h_{is}^{3/4}} \tag{4.3}$$

$$D_S = D \cdot \frac{VFR_{ex}^{1/2}}{\Delta h_{is}^{3/4}} \tag{4.4}$$

By considering an evaluation chart (an N_sD_s turbine chart) drawn up using these numbers, the expansion device with the best performance potential for the application at hand can be identified. Moreover, the device's isentropic efficiency can be estimated by examining the diagram's isolines. ***Figure 4-2*** shows an N_sD_s chart based on imperial units [81]. Favourable operating regimes for displacement and turbine expander concepts are highlighted.

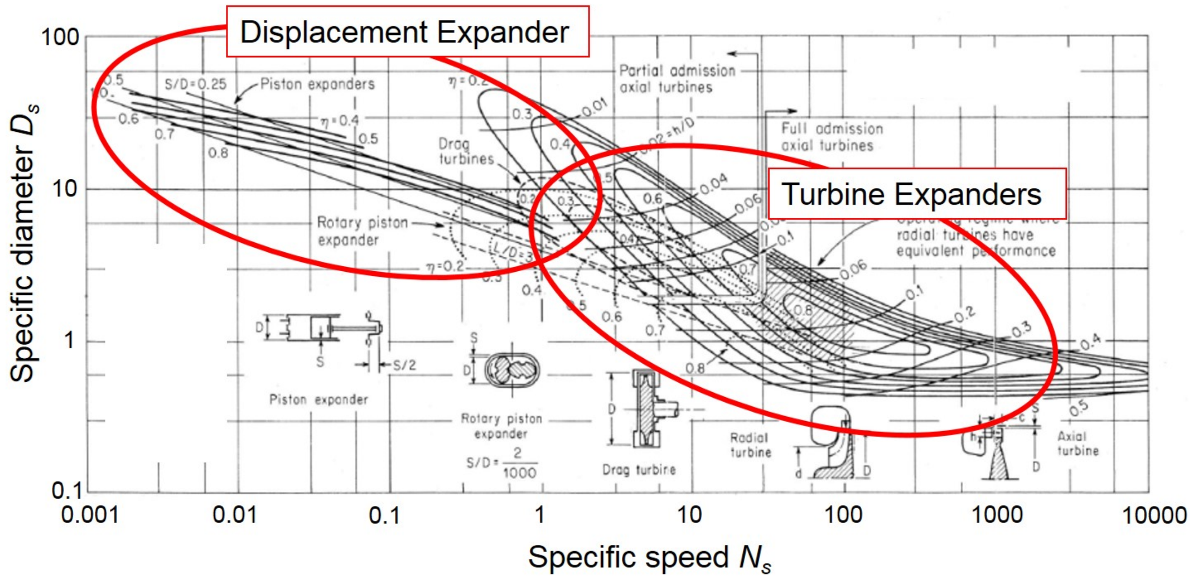

Figure 4-2: N_sD_s turbine chart (imperial units) [81], axis labels traced for better readability

The data for the N_sD_s chart is based on loss analysis and test data. More information regarding the theoretical background of these charts is provided in Baljé's publication introducing the similarity concept [79]. A downside of the approach is that the diagram hasn't been updated since 1962. It therefore does not account for subsequent improvements in turbine design and manufacturing or loss analysis. In addition, a recently published work questioned the accuracy of this method for organic working fluids because of the way their thermophysical properties differ from those of steam [82].

Despite these downsides, the similarity approach based on N_sD_s charts was considered to be adequate for use in the zero-dimensional modelling work because its main aim was to identify a suitable expansion concept based on the operating parameters of the Rankine cycle rather than to accurately determine isentropic efficiencies. Quantitative accuracy is not required during the early stages in the design of a heat recovery system when no validation data are available.

To compute the input parameters for the similarity approach, it was necessary to combine the zero-dimensional Rankine cycle model presented in *Paper I* with estimates of the flow rate of the working fluid. These estimates were obtained by applying the pinch point approach and considering the energy balance for the heat source side (***Figure 4-3***). The pinch point temperature difference ΔT_{PP} correlates negatively with the required size of the heat exchanger [55]. By setting a minimum value for ΔT_{PP} of 20 °C, which is a reasonable number for the considered application according to the literature [37], it was possible to derive the flow rates and the heat source outlet temperature. This was achieved by using the energy balances presented in ***eq. (3.2)*** for the preheating (***phase I***) and vaporization/superheating (***phase II***) phases. In addition, the influence of the working fluids' latent heat and boiling temperature on the utilization of heat from the heat source could be estimated.

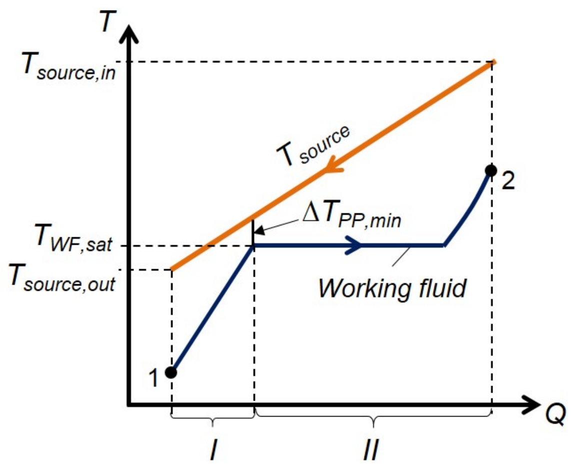

Figure 4-3: Energy balance between a heat source and a working fluid (phase I – preheating; phase II - vaporization/superheating)

4.2.2 Expander efficiency terminology

Three measures of efficiency are considered in connection with the expansion device in this thesis. To avoid confusion, these efficiencies are briefly defined and it is explained how they differ.

The isentropic efficiency η_{is} (***eq. (4.5)***) describes the actual expansion work w_{exp} done by the fluid on the piston (in a reciprocating expander) or rotor (in a turbine expander) in relation to the theoretical maximum work $w_{exp,is}$ done by the fluid in an isentropic expansion. Kinetic and potential energy effects are neglected in this thesis, so $w_{exp,is}$ can also be expressed as the isentropic fluid enthalpy drop over expansion Δh_{is}.

$$\eta_{is} = \frac{w_{exp}}{w_{exp,is}} = \frac{w_{exp}}{\Delta h_{is}} \tag{4.5}$$

The mechanical efficiency η_m relates the work available at the expander output shaft $w_{exp,shaft}$ to the actual expansion work w_{exp} of the fluid, ***eq. (4.6)***. As the name implies, the mechanical efficiency describes the mechanical (friction) losses in the expander

$$\eta_m = \frac{w_{exp,shaft}}{w_{exp}} \tag{4.6}$$

The overall expander efficiency η_o is a product of the isentropic and mechanical efficiencies, ***eq. (4.7)***. It directly relates the expander shaft work to the maximum available expansion work (or the fluid enthalpy drop Δh_{is}).

$$\eta_o = \eta_m \cdot \eta_{is} = \frac{w_{exp,shaft}}{w_{exp,is}} = \frac{w_{exp,shaft}}{\Delta h_{is}} \tag{4.7}$$

4.2.3 The one-dimensional system model

The one-dimensional modelling in this project was performed using the commercial CAE tool GT-SUITE. A system model of the Rankine cycle was implemented in GT-SUITE as a complement to the experimental test rig and the zero-dimensional model, motivated by the following main objectives:

- Reproduction and prediction of 1D fluid dynamic effects in the Rankine cycle.
- Creation of a validated development and simulation tool to facilitate improvement of the test rig.

This section outlines the approach adopted when using GT-SUITE as a CAE tool for flow simulations and then introduces the Rankine cycle system model.

GT-SUITE – Flow modelling theory and spatial discretization

The flow systems modelled with GT-SUITE are discretized into many subvolumes, ***Figure 4-4***. A set of conservation laws based on the Navier-Stokes equations is implemented in each subvolume:

- Conservation of mass, ***eq. (4.8)***.
- Conservation of energy, ***eq. (4.9)***.
- Conservation of enthalpy, ***eq. (4.10)***.
- Conservation of momentum, ***eq. (4.11)***.

These equations are resolved in the flow direction by the software (corresponding to a 1D approach), averaging the physical values over the flow cross section [83].

$$\frac{dm}{dt} = \sum_{boundaries} \dot{m} \tag{4.8}$$

$$\frac{d(me)}{dt} = -p\frac{dV}{dt} + \sum_{boundaries} (\dot{m}H) - hA_s(T_{fluid} - T_{wall}) \tag{4.9}$$

$$\frac{d(\rho HV)}{dt} = V\frac{dp}{dt} + \sum_{boundaries} (\dot{m}H) - hA_s(T_{fluid} - T_{wall}) \tag{4.10}$$

$$\frac{d\dot{m}}{dt} = \frac{dpA + \sum_{boundaries}(\dot{m}u) - 4C_f \frac{\rho u|u|}{2}\frac{dxA}{D} - C_p\left(\frac{1}{2}\rho u|u|\right)A}{dx} \tag{4.11}$$

The spatial discretization approach used in GT-SUITE is the so called staggered grid, which means that scalar variables such as the pressure, energy, density and temperature are calculated in the centre of each subvolume and assumed to be uniform over the subvolume. Conversely, vector variables such as the flow velocity and mass-flow rate are calculated at the boundaries between adjacent subvolumes. The motivation for this approach is to prevent the persistence of spurious pressure oscillations between the subvolumes, which can occur when vector and scalar variables are computed at the same grid points (which is known as the collocated approach) [84]. The origin of these oscillations can be understood by looking at ***Figure 4-4***. Suppose that the pressure at adjacent scalar variable grid points initially alternates between 1 and 5 bar (i.e. the pressure at the first grid point is 1 bar, that at the second is 5 bar, that at the third is 1 bar, and so on). The staggered grid approach would take these pressure differences into account when solving the momentum equation (***eq. (4.11)***) which is used when evaluating the vector variables. This would cause the alternating pressures to be dampened out after a number of time steps. In contrast, when using the collocated grid approach, the momentum equation only 'sees' the two adjacent pressure values, disregarding the pressure value at the grid point where the vector variable is to be calculated. It cannot discover the alternating pressures because it only sees the identical pressures on either side, so there is no dampening out of the alternation.

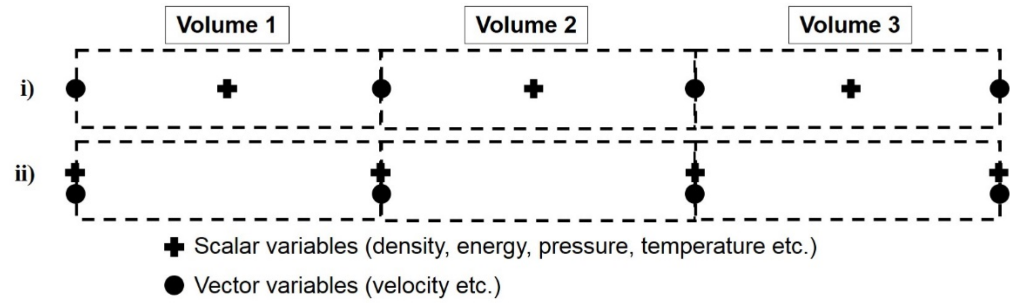

Figure 4-4: Staggered (i) and collocated (ii) grid approaches for spatial discretization

Rankine system model - Overview

The GT-SUITE system model for the Rankine cycle is shown in ***Figure 4-5***. The model's layout, component specifications, and dimensions correspond to those of the test rig, which will be introduced in chapter ***4.3.*** Calibration data from the experiments were used to validate the model. EGR boundary conditions for a Volvo D13 heavy duty Diesel engine were chosen as the sole heat source, mainly because the EGR's high temperature makes it highly suitable for heat recovery. The decision not to include more heat sources such as exhaust or CAC was motivated by a desire to minimize complexity, particularly that of the experimental system that was used to calibrate the system model. The Rankine cycle in the model is not closed; a boundary condition called "Tank" is imposed downstream of the condenser and upstream of the pump. These positions correspond to the location of the atmospheric pressure working fluid tank in the test rig. The fluid tank collects the condensed fluid and serves as a reservoir for the pump. Its volume (10.2 litres) is large compared to the system (7.8 litres) with the system operating at flow rates below 1 litre/min. The flow of coolant to the condenser is controlled so as to ensure that the temperature of the working fluid entering the tank is constant. These factors justify the assumption of constant boundary conditions at the "Tank" positions in the GT-SUITE model. Data on the properties of the studied working fluids (in the liquid, two phase and superheated states) were obtained directly from REFPROP [73]. The coolant is treated as an ideal liquid and the exhaust is approximated as an ideal gas.

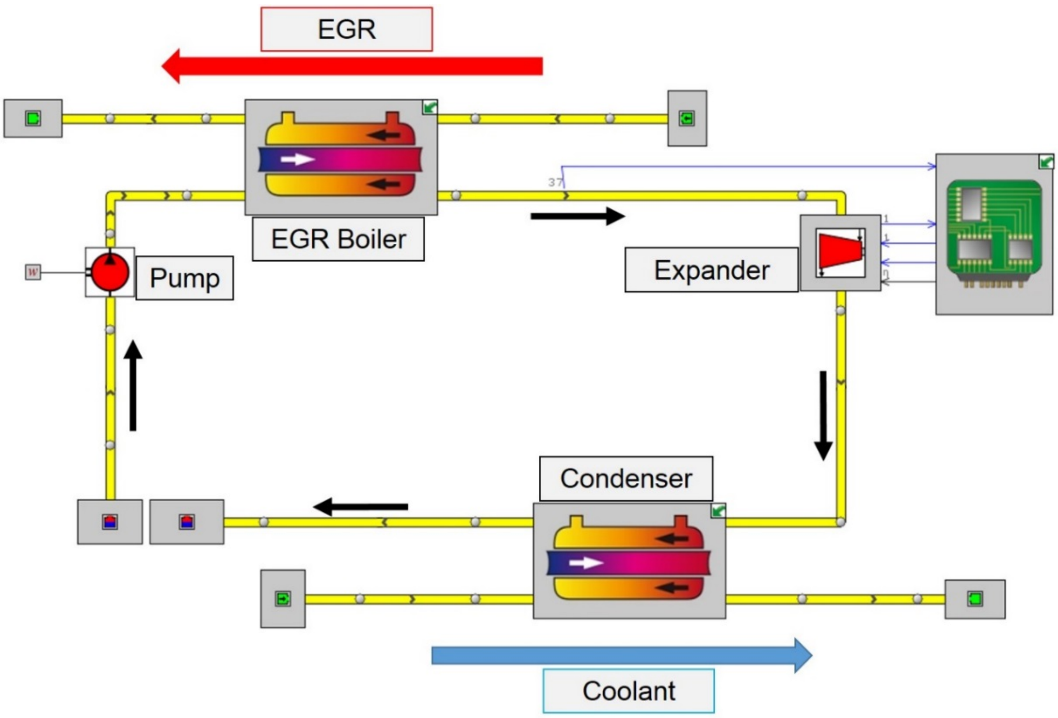

Figure 4-5: Schematic depiction of the GT-SUITE Rankine cycle system model

An implicit solver **is** used for the time discretization of the conservation laws **used in the model** (***eq. (4.8)-(4.11)***). At the start of each time step, all of the quantities featured in these equations are simultaneously evaluated by iteration in all subvolumes. The primary solution variables are the mass flow, enthalpy and the pressure. The implicit solver was chosen because of its ability to accommodate large time steps, which makes it suitable for use in long-run simulations [83,84]. The use of large time steps has the drawback that certain effects (e.g. high frequency pressure pulsations) cannot be observed, but this was considered less important than the ability to perform long-run simulations in a time-efficient manner.

Rankine system model – Components and assumptions

An overview of the Rankine cycle components and their modelling is provided in ***Table 4-1***.

The test rig's piping is discretized as a succession of subvolumes (see ***Figure 4-4***) for which the introduced conservation laws were solved. The pump was modelled as a positive displacement device having constant isentropic and volumetric efficiencies, and two outputs: a volume flow rate *VFR* and an enthalpy drop Δh. Heat losses to the surroundings as well as kinetic energy and pressure effects were neglected in the pump model. This assumption proved to be reasonable for the axial piston pump used in the experiments. The volumetric efficiency includes the flow losses during the inlet phase. The product of the volumetric and isentropic efficiencies varied only marginally over the pressure range applied in the system, being higher than 90% in most cases. The expander in the Rankine system model was approximated by a map-based device. Implementation of a detailed expander model in the Rankine system model would have complicated the setup considerably, with negative effects on numerical stability and computation time. The detailed expander model (which is introduced in the next chapter) provides map data for the volumetric and overall expander efficiencies as a function of the expander inlet pressure, outlet pressure and geometry settings. Unlike in the pump model, both heat and friction losses are considered. Thus the product of the overall expander efficiency $\eta_{\mathrm{o,exp}}$ and the isentropic enthalpy drop Δh_{is} over the expander yields the expander shaft work output. This value can then be directly compared to the measured shaft power output of the expander on the test rig. The heat exchangers in the system model are represented by generic templates, calculating the heat transfer rate Q to and from the working fluid based on the effectiveness ε of the device. The values for the heat exchangers' effectiveness were calibrated against experimental data.

Table 4-1: Specifications of the components used in the GT-SUITE Rankine system model

Component	**Part display**	**Modelling approach**
Piping		Discretized into subvolumes, ***eqs* (4.8)-(4.11)**
Pump	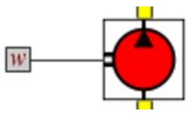	$VFR = n \cdot \eta_v \cdot V_D$ $\Delta h = \dfrac{\Delta h_{is}}{\eta_{is,pump}}$
Heat exchangers (EGR boiler and condenser)	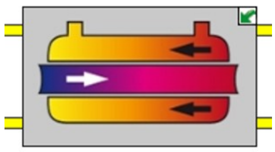	$Q = \varepsilon \cdot \min(Q_1, Q_2)$ $Q_1 = \dot{m}_{WF} \cdot (h_{wf,in} - h_{wf,T_{ext,in}})$ $Q_2 = \dot{m}_{ext} \cdot (h_{ext,in} - h_{ext,T_{WF,in}})$
Expander	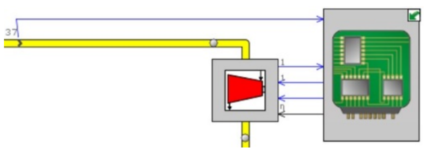	$\dot{m} = \rho \cdot n \cdot \eta_v \cdot V_D$ $w = \Delta h_{is} \cdot \eta_{0,exp}$
Boundary	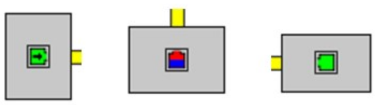	Specified boundary conditions for • mass flow (EGR/coolant inlet) • pressure (EGR/coolant outlet and working fluid tank) • temperature (all)

As an alternative to the effectiveness-based heat-exchanger models, detailed geometry models for plate heat exchangers were also considered. These models use a Nusselt correlation on the external fluid side (EGR/coolant) and a combination of single and two-phase correlations from the literature on the working fluid side. The Nusselt correlation is approximated via a regression analysis based on experimental data. The simpler effectiveness-based heat exchanger models were ultimately used in the system model because of their superior numerical robustness and faster computation times. Geometry-based models may be preferable in cases where the temperature profiles in the heat exchangers or quantities such as the spatial movement of the evaporation front are of interest.

4.2.4 The one-dimensional expander model

For the experiments performed in this project, a prototype reciprocating piston expander was used as the expansion device in the Rankine cycle. The expander was not customized in any way for use with the test rig. It was considered essential to create and validate a separate one-dimensional GT-SUITE model of the expander in order to properly understand its functioning within the system and the limitations on its performance. The resulting validated model was subsequently used to suggest design modifications to the expander used in the experiments (***Paper III***).

After proving the applicability of the 1D modelling approach for the reciprocating piston expander, the model was used to compare a range of different reciprocating expansion concepts with the following objectives (***Paper IV***):

- To compare the performance of uniflow and counterflow expander gas exchange systems.
- To evaluate the influence of selected factors (the expander geometry and steam boundary conditions) and determine which of them significantly affect the expander's isentropic efficiency and power output.
- To rank the main and interaction effects associated with the expander geometry and steam boundary conditions in terms of their influence on expander performance.

<u>*Time discretization*</u>

In contrast to the Rankine system model introduced in chapter ***4.2.3***, the 1D expander model relies on an explicit flow solver. This means that when integrating ***eq. (4.8) - (4.11)*** over time, the scalar variables on the right hand side of the equations always use the results from the previous time step. Thus, in contrast to the implicit method, no iterative solution of the equation system is necessary. The stability condition applied in the explicit solver is based on the

Courant-Friedrichs-Lewy (CFL) condition [84]. This implies that the discretized time step Δt must be small enough to ensure that even at its maximum velocity, $u_{flow,max}$, the flow does not travel further than the spatial discretization length Δx, ***eq. (4.12)***:

$$\frac{\Delta x}{\Delta t} \cdot \left|u_{flow,max}\right| < 1 \tag{4.12}$$

At each time step, the solver starts by directly calculating the scalar variables energy and mass in the subvolume by integrating ***eq. (4.8)*** and ***(4.9)***. With this information, the density in the specified subvolume can be computed. Using the density and energy, the pressure and temperature can be obtained from the fluid property tables. Finally, integration of the momentum equation ***eq. (4.11)*** provides the vector variables at the subvolume boundaries. The explicit solver is better able to capture high frequency pressure oscillations in the flow system than the explicit solver, which is important for flow systems containing a reciprocating piston device [83].

Reciprocating piston expander model - Experimental hardware

The hardware used in this work, which served as a template for the 1D expander model, was a reciprocating piston expander with two cylinders (see ***Figure 4-6***) that operates according to the uniflow concept. The superheated working fluid enters the expansion cylinder through poppet valves close to the piston top dead centre (TDC), while the expanded vapour is exhausted through ports in the cylinder wall close to the piston bottom dead centre (BDC).

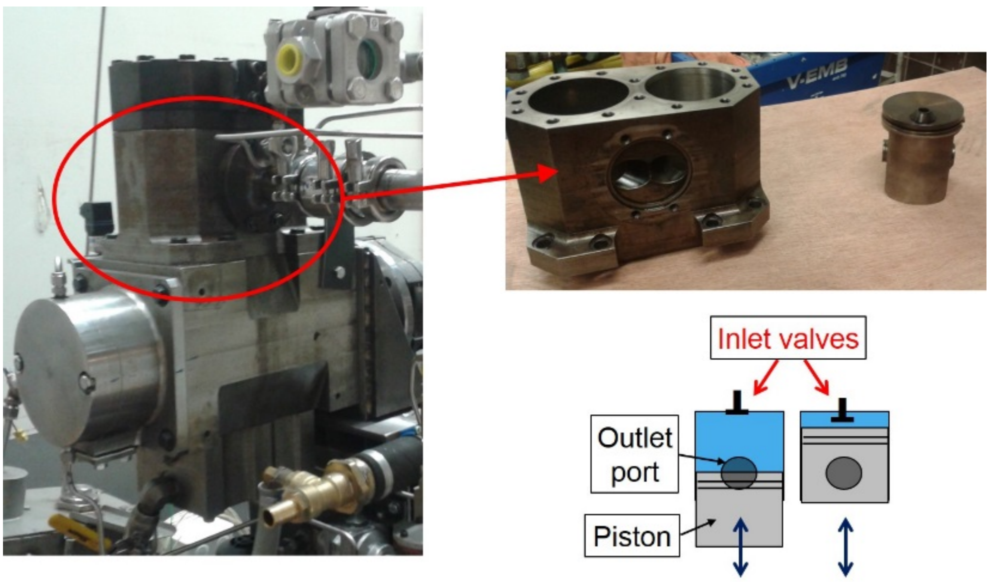

Figure 4-6: Reciprocating piston expander (left), cylinder housing and piston (upper right) and a schematic representation of the expander's operating mechanism (lower right)

The geometric data for the expander and the valve timings used in the experimental work are provided in ***Table 4-2***. The geometric compression ratio is the quotient of the BDC to the TDC cylinder volume. The expansion ratio (or effective compression ratio) relates the cylinder volume at outlet port closing/opening to the TDC volume. These data were used as input when implementing the expander model in GT-SUITE. The circular outlet port is half opened when the piston reaches the BDC position.

Table 4-2: Geometric data for the reciprocating piston expander

Number of expansion cylinders	2
Cylinder bore	90 mm
Cylinder stroke	60 mm
Inlet valve opening (IVO)	-17 °CA ATDC
Inlet valve closing (IVC)	34 °CA ATDC
Inlet valve diameter	23mm
Inlet valve max. lift	3.1 mm
Outlet port opening (EVO)	110 °CA ATDC
Outlet port closing (EVC)	-110 °CA ATDC
Outlet port diameter (1 per cylinder)	32 mm
Compression ratio (geometric)	21
Expansion ratio (TDC → EVO)	15.67
TDC clearance	3 mm

Reciprocating piston expander – GT-SUITE model

A preliminary GT-SUITE model of the expander was constructed on the basis of the available geometric data (see ***Figure 4-7***). The model's boundary conditions are the pressure and temperature of the expander's inlet and outlet environments. A bypass to the expansion cylinders was added to the model to simulate blow-by losses passing the piston rings. The gap size is represented by an orifice with a fixed diameter of 1.2 mm, which was calibrated based on experimental results.

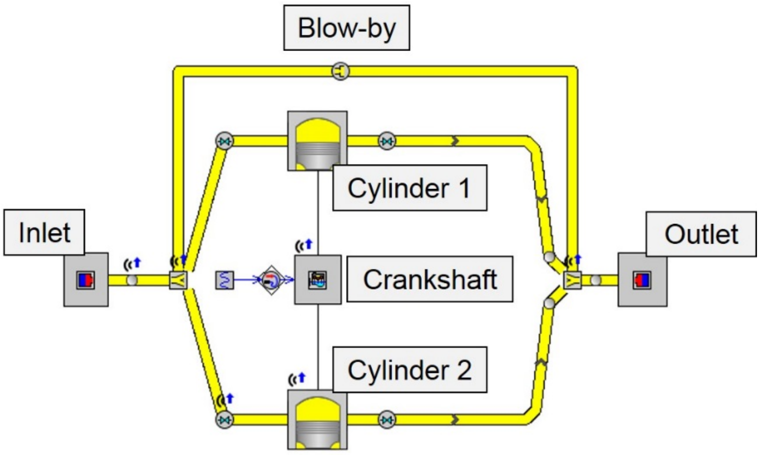

Figure 4-7: 1D GT-SUITE model of the piston expander

The *cylinder* modules in the model represent each a subvolume of variable size. The volume and the mass of the cylinder charge (and hence its density) are known at every time step. The values of the in-cylinder pressure and temperature are initialized for the first simulation time step. The energy in the cylinder at a given point in time is determined by the enthalpy of the inflowing gas, the heat transfer to the cylinder wall and the piston work (***eq.(4.9)***). The remaining properties for the time step, such as the cylinder pressure and temperature, are calculated from the energy and the density. The cylinder mass is determined by the pressure ratio between the cylinder and the adjacent volumes as well as the discharge coefficient and the timing of the inlet valve and exhaust port.

The *crankshaft* component contains the friction model for the expander. In keeping with expander studies from other research groups [85,86], this component was described using the empirical regression model of Chen-Flynn [87]. It was initially developed for a compression ignition engine and provides the friction mean effective pressure (FMEP) for the device based on the mean piston speed $c_{p,m}$ and the cylinder peak pressure $p_{cyl,max}$ [88].

$$FMEP = FMEP_{constant} + A \cdot p_{cyl,max} + B \cdot c_{p,m} + C \cdot c_{p,m}^2 \tag{4.13}$$

A, B and C are constants that were calibrated based on friction measurements obtained for the experimental device.

The discharge coefficient C_D for the *inlet valves* and the *outlet ports* is defined as the ratio of the effective flow area A_E through a constriction in relation to a reference area A_R [54], ***eq. (4.14)***. It is assumed that the flow velocity and density are similar in both areas.

$$C_D = \frac{\dot{m}}{\dot{m}_{theor}} = \frac{A_E}{A_R} \tag{4.14}$$

In the case of the poppet valves, A_R was taken to be the curtain area and the port opening area was used as the reference area for the outlet ports. Discharge coefficients were not measured for the expander during this project because of technical limitations. It was therefore necessary to estimate these coefficients using reasonable assumptions based on previous works that used comparable valve arrangements. There is little published data on reciprocating piston expanders, so the IC engine literature was consulted because 2-stroke IC engines have similar valve arrangements to that in the uniflow piston expander. The following values were selected for the discharge coefficients C_D based on a literature search:

- Outlet ports: 0.8 [89].
- Inlet poppet valves: 0.6 [54,90].

Blair et al. [89] pointed out that the values of discharge coefficients should actually be obtained as functions of the valve lift and pressure ratio. However, developing such functions would be beyond the scope of this work.

<u>Heat losses</u> caused by convective heat transfer from the steam to the wall were identified as a major component of the overall losses from reciprocating piston expanders [91] in early studies. However, Ferrara et al. [90] found that the expander's performance was not very sensitive to the heat transfer coefficient during expansion, and that the associated heat release had only a minor impact. A detailed summary of the modelling approaches used by other research groups to estimate the in-cylinder heat transfer is provided in ***Paper IV.*** Some investigators assumed that a fixed proportion of the cycle work was lost in this way [85,92] while others relied on empirical heat transfer correlations [86,93]. The latter approach was adopted in this work by implementing the so-called "flow" heat transfer model suggested by Morel and Keribar [94] for bowl-in piston combustion engines.

<u>*Reciprocating piston expander model – Concept comparison and optimization (**Paper IV**)*</u>

While the expander employed in the experiments uses the uniflow expansion concept described above, an alternative design for the valve arrangement of the reciprocating expander is possible: the counterflow concept (see ***Table 4-3***). In this concept, the expanded steam is exhausted through an outlet valve in the cylinder head area. This allows the outlet timing to be independent of the piston position.

A set of geometric factors and steam boundary conditions that could influence the performance of expanders using both concepts were identified (***Table 4-3***). A study was then conducted to determine the relative influence of the individual factors and their interactions on two responses - the expander power output and expander isentropic efficiency – in expanders based on the uniflow and counterflow concepts. The results provided new insights into the parameters that have the greatest influence on expander performance and the overall design of the cycle. Such information is valuable when implementing a given piston expander concept in a Rankine cycle. The ranges considered for the performance factors were chosen based on reasonable assumptions (see ***Paper IV***).

Table 4-3: Uniflow and counterflow expander concepts

	Uniflow	**Counterflow**
Concept	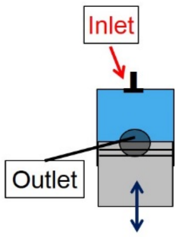	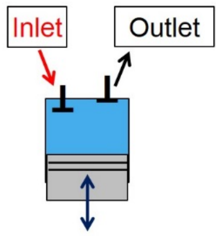
Performance factors	1. Inlet pressure 2. Inlet superheat 3. Outlet pressure 4. Expander speed 5. Inlet valve opening 6. Inlet valve diameter 7. Inlet valve dwell at max. lift 8. Compression ratio 9. Outlet opening timing 10. Outlet flow area 11. Outlet closing (counterflow)	
Responses	1. Brake power 2. Isentropic efficiency	

The one-dimensional GT-SUITE model of the piston expander, which was introduced in the beginning of section ***4.2.4*** was validated against experimental data. On the basis of this validation work, the expander model (***Figure 4-7***) was simplified by removing one expansion cylinder and the blow-by path. These modifications reduced the model's complexity and computation time without affecting the results of qualitative comparisons of different concepts.

The Design of Experiments (DoE) approach was used to specify the settings of the performance factors in the GT-SUITE model. Ten factors needed to be varied for the uniflow concept, while the counterflow concept had 11 degrees of freedom because of the flexible closing time of the outlet valve.

A response surface model (RSM) of the form shown in ***eq. (4.15)*** was fitted to the result matrix from the GT-SUITE simulations for each response y based on the performance factors x. The model's characteristic parameters are the regression coefficients β and the model error ε. The model consists of a constant term, and terms representing main effects with linear factor dependence, quadratic effects, and interaction effects between two factors.

$$y = \beta_0 + \sum_{j=1}^{k} \beta_j x_j + \sum_{i} \sum_{< j} \beta_{ij} x_i x_j + \sum_{j=1}^{k} \beta_{jj} x_j^2 + \varepsilon \tag{4.15}$$

Figure 4-8 summarizes the process used to construct the RSM model, starting from the selection of significant design factors for the expander (geometry and steam boundary conditions) and concluding with the fitting of the RSM model. This model was then used to identify optimal factor settings for a response of interest (e.g. power output or isentropic efficiency).

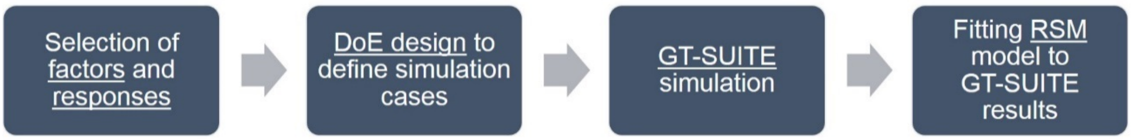

Figure 4-8: Process which was followed to obtain the RSM model

Three different DoE designs for varying the performance factors were compared:

- A full factorial design (three levels).
- A Box-Behnken design.
- A D-Optimal design.

The structures of the three design types are shown in ***Table 4-4*** for a system with three factors x_1,x_2 and x_3.

In the full factorial design, each factor is varied over three levels (low, medium and high) and every possible combination of level and factor is tested. This provides the greatest possible coverage of the design space. The use of three levels per factor is necessary to be able to estimate quadratic effects for individual factors. A drawback is the large number of required simulations and the resulting computational effort when the design is scaled up to 10 factors (3^{10} cases) for the uniflow case or 11 factors (3^{11} cases) for the counterflow case.

More efficient in terms of computational effort is the Box-Behnken design [95]. It leaves out the corners of the design cube, so extreme factor combinations are excluded. This is justified because such extreme combinations are typically subject to physical constraints or simply provide unsatisfactory performance. A downside of this approach is that it reduces the quality of the resulting information on interaction effects to some extent.

The D-Optimal design is generated by an algorithm that aims to minimize the variance of the RSM regression coefficients [96]. It requires a low number of runs, even for a large amount of factors.

Table 4-4: Comparison of DoE design types for the piston expander model

	Full factorial (3 level)	Box-Behnken	D-Optimal
Design cube example (3 factors x_1,x_2,x_3)	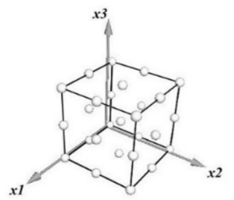	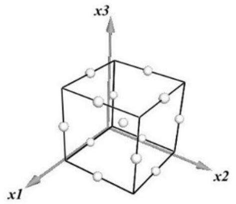	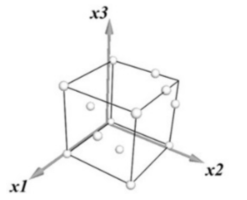
# of cases in GT-SUITE (uniflow/counterflow)	59049/177147	161/177	150

4.3 Experimental setup

One intention when designing and building the experimental test rig was to create a resource for the validation of the presented 1D models. An additional and potentially more important goal was to improve the understanding of the heat recovery system's behaviour during "real world" operation. Most published studies on heat recovery systems for vehicle engines have relied on simulations or component tests; there is a general lack of experimental studies that could reveal the challenges and limitations encountered when using such systems on a full-scale test rig. The system examined in this project was designed to recover heat from the EGR line of a Volvo D13 US10 heavy duty Diesel engine (***Figure 4-9***). All of the major components installed in the system (pump, piston expander, EGR boiler and condenser) were prototypes.

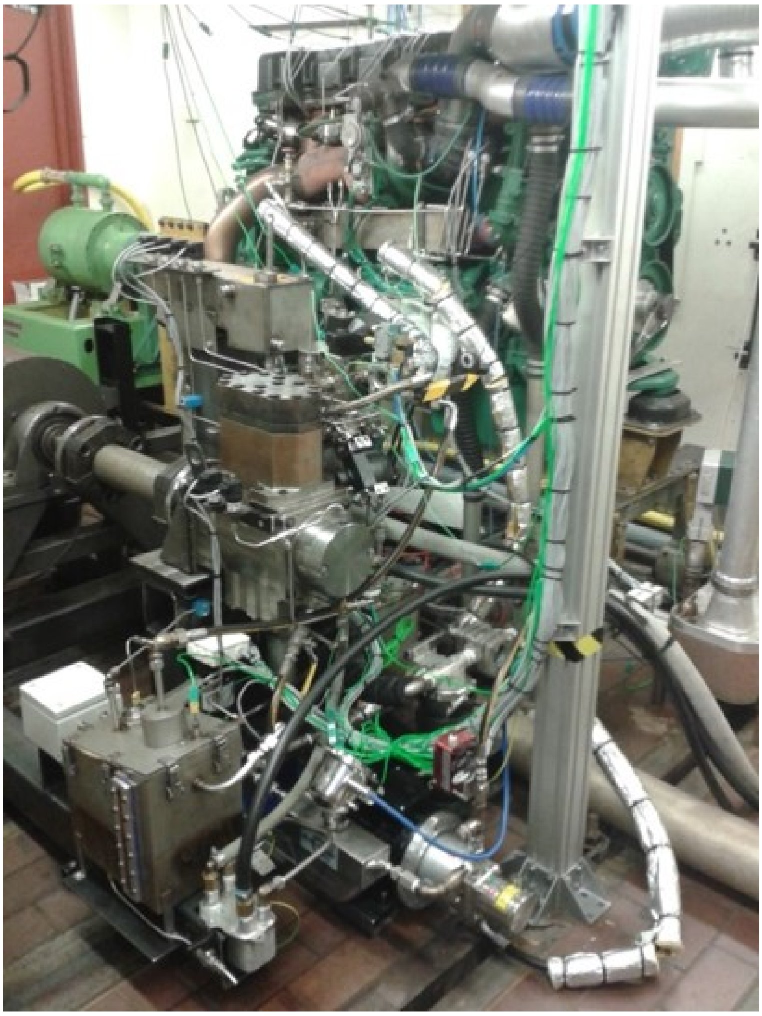

Figure 4-9: Experimental setup of the heat recovery system in the engine test cell

The working fluid used in the system was water. Results obtained using the model of the system (chapter ***4.2.1***) indicated that water would be a competitive working fluid for EGR heat recovery, particularly in combination with a displacement expander device. An important reason for using water as a fluid is that it is much less potentially harmful than flammable fluids such as alcohol or potentially toxic fluids such as refrigerants. Deionised water was used to avoid the formation of deposits and scale in the boiler.

A schematic layout of the test rig's flow system is shown in ***Figure 4-10***. The fluid coming from the fluid receiver is filtered and then pumped into the EGR boiler. The pump bypass can be opened to further reduce the flow to the boiler if the minimum allowable pump speed is reached. Downstream of the boiler, the superheated steam flows into the expander to do mechanical work. During start-up and under certain operating conditions (e.g. when the steam pressure is low or the steam is wet, or during boiler testing), the expander path can be closed and bypassed. A pressure relief valve protects the boiler from pressures exceeding the permitted limit of 30 bar. The condenser turns the expanded steam back to a liquid before it enters the fluid receiver, closing the Rankine cycle. The fluid receiver is connected to an atmospheric expansion tank, which means that the condensation pressure in the system is kept around 1 bar absolute pressure. A sight glass was installed downstream of the EGR boiler for live monitoring of the vapour quality during operation. A second sight glass was installed at the pump inlet to check the pump head and to enable detection of fluid contamination.

More detailed descriptions of the components and subsystems as well as the measurement equipment are provided in chapters ***4.3.1*** and ***4.3.2***, respectively.

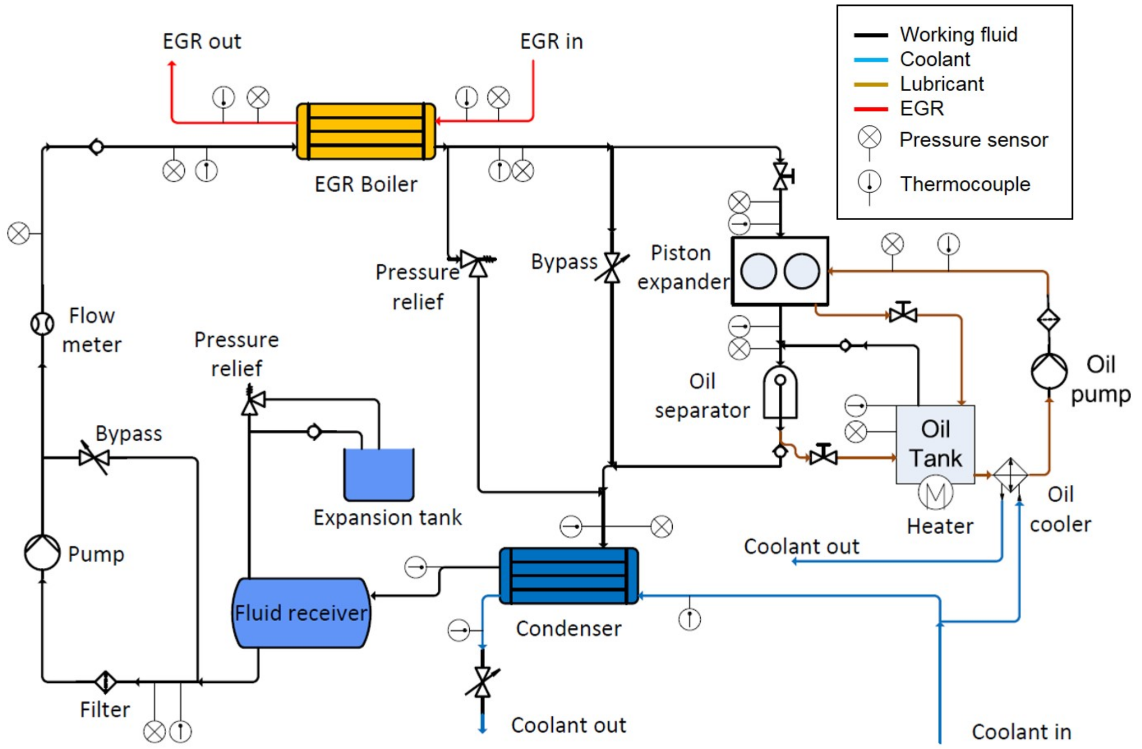

Figure 4-10: Schematic layout of the heat recovery system

4.3.1 Components and subsystems

<u>EGR boiler</u>

The EGR boiler was designed and supplied by TitanX, one of the industrial partners in the project. Factors considered during its design included the EGR flow and temperature for the test rig, as well as predicted mass flow rates for the Rankine cycle derived from simulations performed with the zero- and one-dimensional models. The boiler replaces the original EGR cooler supplied with the engine, so its outer dimensions were constrained by the engine's design. It features a plate-type heat exchanger in a counterflow configuration (***Figure 4-11***). As a special feature, the plates are oriented vertically, both for packaging reasons and to investigate the influence of gravity effects on boiling. The prototype used in the experiments has 22 channels on the fluid side and 21 channels on the gas side. Offset strip fins are used on the fluid and gas sides to enhance heat transfer.

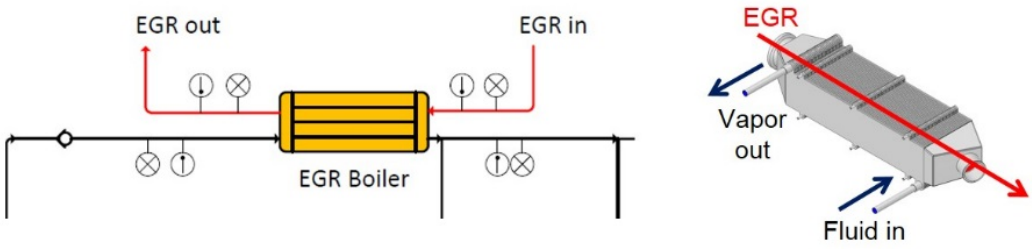

Figure 4-11: The EGR boiler in the system layout (left) and as a CAD drawing (right)

Expander subsystem

The expander used for this project was introduced in chapter ***4.2.4***. It was initially designed for a system recovering heat from both EGR and exhaust of a heavy duty Diesel engine using ethanol as the working fluid. The experimental setup in this project was water-based and only recovered heat from the EGR, so the expander was used under off-design conditions. The tests thus provided new information on the device's performance under these conditions.

The layout of the expander subsystem downstream of the EGR boiler is shown in ***Figure 4-12***. The expander bypass was used under special operating conditions (i.e. during startup and when the steam quality was low) and to test the performance of the EGR boiler at various EGR rates and boiling pressures. The boiling pressure can be precisely controlled by varying the orifice diameter of the bypass valve. Engaging the expander during the boiler tests would have added complexity, introduced the risk of oil contamination of the working fluid, and made the pressure control less precise, thereby reducing the repeatability of the boiler performance tests. The piston expander is engaged by closing the bypass valve and opening the expander inlet valve. The expander output shaft is connected to a speed-controlled eddy current brake.

The expander lubrication system supplies the hydrodynamic crankshaft bearings. A crucial factor to consider is the dilution of the lubricating oil with water due to blow-by and condensation on the cylinder liners. The external oil tank was thus heated to 120 ºC to allow immediate evaporation of the water from the recirculated oil. These high oil temperatures damaged the gaskets of the pump and reduced the oil viscosity, so an oil cooler was installed in the supply line of the oil pump. The initial idea was to feed the evaporated water back downstream of the expander to maintain a closed system, but this caused high oil contamination of the working fluid. Therefore, in the final design, the evaporated water was directed into an external drain. The oil used was a steam engine oil with a kinematic viscosity of 290 mm^2/s (40 ºC, DIN 51562-1).

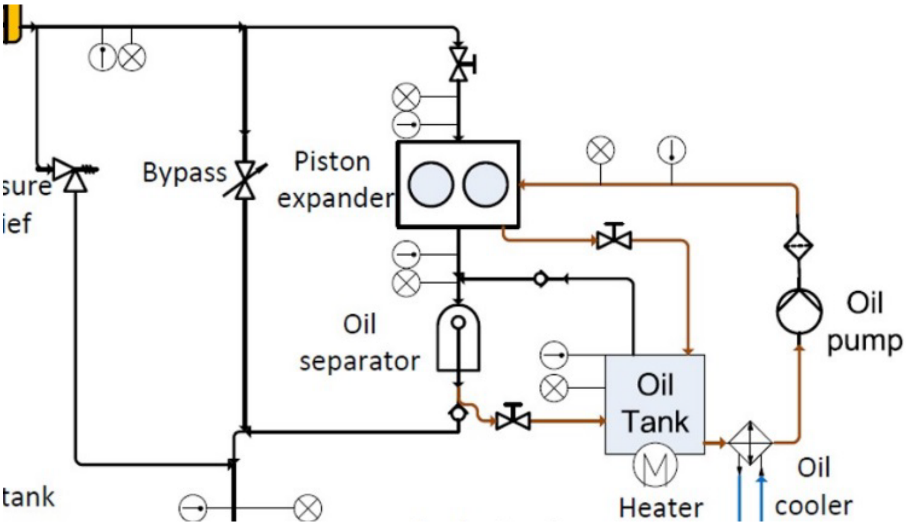

Figure 4-12: Expander subsystem

<u>*Condenser and pump subsystem*</u>

The subsystem containing the condenser and the pump is shown in ***Figure 4-13***.

A plate-type heat exchanger was installed to condense the expanded steam. Cold tap water was used as a heat sink. The coolant flow rate can be controlled by a throttling valve to achieve the desired level of subcooling before the working fluid enters the fluid receiver. An atmospheric expansion tank for the working fluid is required to compensate for the variation of liquid fraction in the system.

An axial piston pump (swash plate) with the following specification was used:

- Displacement: 2 cm^3.
- 9 axial pistons (oil free).
- Volumetric/Mechanical efficiency: 43.9/72.5% at 1500 rpm and 120 bar.
- Pump speed range: 1000-3000 rpm.
- Max. fluid temperature: 90 °C.

A valuable advantage of a reciprocating pump with a fixed displacement per revolution is the fact that the discharge pressure is independent of pump speed and flow. At the maximum pressures in the Rankine cycle for the present system layout (< 30 bar), the volumetric pump efficiency increases to values of around 90%. The speed range is limited to maximize the pump's lifetime; friction increases at the lower end of the range and cavitation risk becomes problematic at the higher end. Given the expected water mass flow rates of < 20 g/s, the pump was over-dimensioned for the current heat recovery system. The mass flow rate to the EGR boiler was therefore controlled by adjusting the pump bypass, with the surplus mass flow being recirculated to the pump inlet. The specification of the pump allows for future extensions or modifications of the system that may require higher flow rates. The filter upstream of the pump was chosen according to the pump manufacturer's requirement for a filter rating of 10 microns and a beta value below 5000.

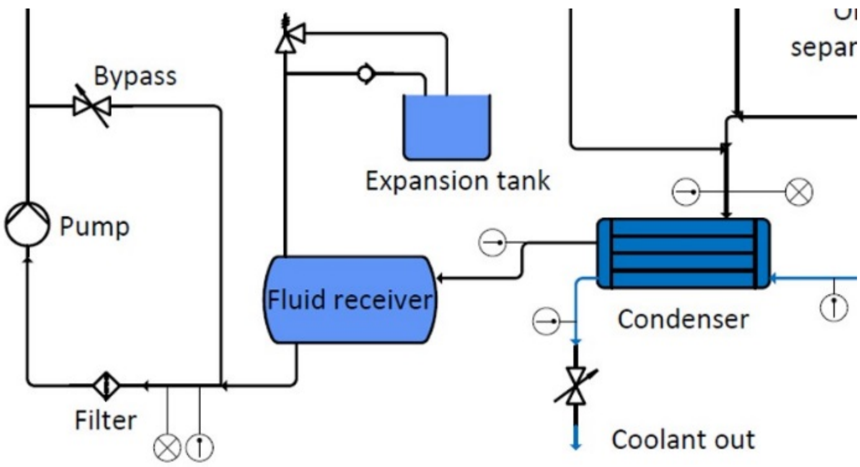

Figure 4-13: Condenser and pump subsystem

4.3.2 Measurement equipment

The LabVIEW^{TM} platform was used to control the Rankine cycle test bench and for data acquisition. The positions of the various sensors in the flow scheme of the heat recovery system are shown in ***Figure 4-10***. The sensors' operating principles, ranges, and accuracies are listed in ***Table 4-5***.

Table 4-5: Sensor equipment installed on the test rig

Variable	Sensor principle	Range	Accuracy
Flow-rate (working fluid)	Coriolis	0-2.72 kg/h	0.2% of reading
Flow-rate (coolant)	Turbine flowmeter	0.8-80 liter/minute	2% of reading
Temperature	Thermocouple (K-type)	-40-1100 °C	< 2.4 °C @ max. 600 °C
Pressure	Piezoresistive	0-10 bar, 0-60 bar	0.25% of range

The Venturi tube located in the standard EGR line of the IC engine was used to measure the EGR flow (***Figure 4-14***), which is needed to determine the EGR boiler's energy balance. The pipe was equipped with a differential pressure sensor, which provides an analogue voltage signal to the engine control unit (ECU). This signal could be utilized for data logging; the pressure sensor is claimed to be accurate to within 2% of its reading. As shown in the figure, the Venturi tube is installed directly downstream of the EGR boiler after an elbow piece.

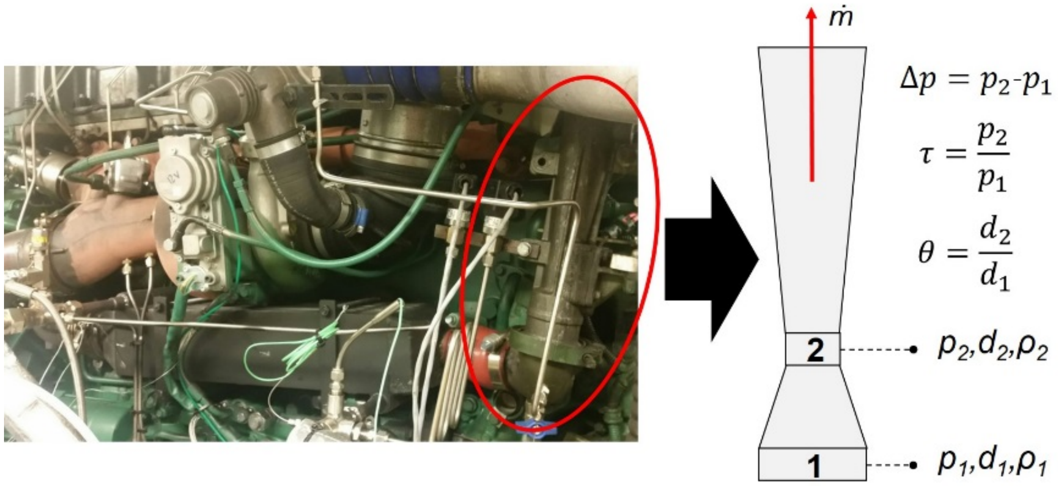

Figure 4-14: EGR line with Venturi tube (left) and nomenclature for the Venturi pipe (right)

After replacing the standard EGR cooler with the boiler, the discharge coefficient C_D (see ***eq. (4.14)***) of the Venturi tube in the EGR line arrangement was determined by measuring the air flow through the pipe using a calibrated turbine flow meter. The calibration air was introduced upstream of the mounted EGR boiler and released into the engine's intake manifold at the EGR outlet. This preserved the working setup of the system, which is needed to achieve a meaningful calibration of the Venturi tube [97]. Pressure and temperature sensors were installed at the entrance to the Venturi tube so that the gas density could be calculated.

Based on Bernoulli's equation for a compressible fluid, the theoretical mass flow rate $\dot{m}_{theor}$ in a Venturi tube can be calculated based on its geometry and pressure data, ***eq. (4.16)***.

$$\dot{m}_{theor} = \frac{E}{\sqrt{1 - \Theta^4}} \cdot \frac{\pi}{4} \cdot d_2^2 \cdot \sqrt{2\rho_1 \Delta p} \tag{4.16}$$

To account for the compressibility of the gaseous media, the expansion factor E in the equation assumes an isentropic expansion from measurement points 1 to 2 in the device, ***eq. (4.17)***.

$$E = \sqrt{\left(\frac{\kappa\tau^{\frac{2}{\kappa}}}{\kappa - 1}\right)\left(\frac{1 - \Theta^4}{1 - \Theta^4\tau^{\frac{2}{\kappa}}}\right)\left(\frac{1 - \tau^{\frac{\kappa-1}{\kappa}}}{1 - \tau}\right)} \tag{4.17}$$

The procedure was that the theoretical mass flow rate $\dot{m}_{theor}$ was first calculated for various air flow rates. After comparison to the measured flow rate $\dot{m}_{meas}$, the discharge coefficient C_D for the Venturi tube could be calculated and expressed as a function of the Reynolds number Re at the pipe inlet. The Reynolds number for a fluid of dynamic viscosity μ travelling at a velocity u can be computed with ***eq. (4.18)***. It is a dimensionless similarity parameter that characterizes flow regimes in similar geometries, so it can be used to link the C_D of the EGR and the air flow in the Venturi tube.

$$Re = \frac{\rho \cdot u \cdot D}{\mu} \tag{4.18}$$

The C_D chart obtained from the calibration with air (***Figure 4-15***) could then be used to determine the actual EGR mass flow based on the exhaust Re number and the calculated theoretical EGR flow rate (***eq. (4.16)***). The viscosity of the exhaust gas was approximated by assuming it to be equal to that of air at the EGR pressure and temperature.

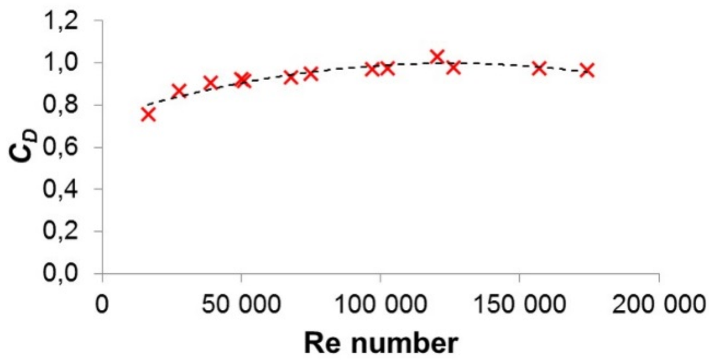

Figure 4-15: Discharge coefficient for the EGR Venture pipe

4.3.3 Engine operating points

The tests with the heat recovery system focused on steady state operating points that were chosen based on the European Stationary Cycle (ESC). The ESC includes a selection of engine operating points at three different speed (A, B, C) and load levels (25, 50, 75, 100), illustrated in ***Figure 4-16*** for the speed range of the Volvo D13 US10 engine.

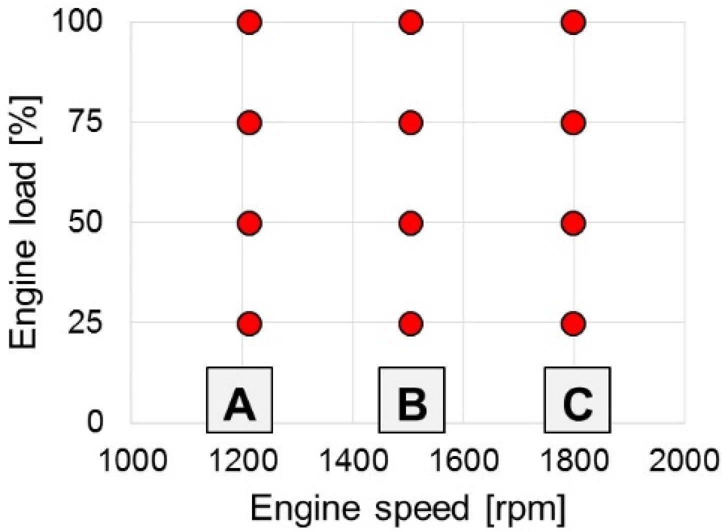

Figure 4-16: Operating points of the ESC cycle

5 Results and discussion

This chapter presents the results obtained from the simulations and the experimental work conducted within this project. The major findings of the attached papers are briefly summarized; more detailed discussions of the results can be found in the papers themselves.

5.1 Zero dimensional system model (*Paper I & II*)

The results obtained using the zero-dimensional model are discussed extensively in the first two attached publications arising from this project. The objectives of these studies were to:

- **Identify** suitable working fluids given representative constraints in terms of Rankine cycle operating parameters and vehicle applicability.
- **Compare** expander concepts based on relevant heat source boundary conditions, operating parameters and working fluids.

Working fluids

From a practical, safety and environmental point of view, a system employing water as a working fluid clearly poses fewer concerns than one based on an organic fluid. However, freezing is a significant problem in water-based systems for vehicular applications. One way to address this drawback would be to instead use an 80:20 blend of water and alcohol such as ethanol or methanol. Such mixtures are still classified as non-flammable but remain liquid at temperatures as low as -25 °C. Pure alcohols suffer from flammability issues, while most of the typical refrigerants used in heat recovery systems (e.g. R245fa) don't comply with incoming regulations that require the fluids used in vehicles to have a global warming potential (GWP) of less than 150. This problem has been addressed in recent years and suitable replacement refrigerants with low GWP values have been announced [42].

Figure 5-1 shows the results obtained for the thermal efficiency of a Rankine cycle using suitable candidate fluids at three different maximal cycle temperatures, reflecting heat recovery from an IC engine's coolant, exhaust, and EGR. A minimum fluid pressure of 1 bar and a minimum fluid temperature of 50 °C were required on the condensation side, representing realistic conditions for a vehicle using air cooling or a low temperature coolant cycle as the heat sink. The expansion pressure ratio was limited to 10 and, in order to be conservative, it was specified that the vapour conditions after expansion should be near-saturated. The aim was to identify a working fluid that would be compatible with an efficient and compact expansion concept under these conditions.

When high Rankine cycle temperatures were allowed, the water-based fluids showed the highest thermal efficiencies, followed by pure alcohols. This order did not change when a cycle temperature limit of 250 °C was imposed. For low temperature heat recovery, corresponding to a cycle temperature limit of 150 °C, alcohols showed the highest thermal efficiencies followed by HCFC-123, which is a low-GWP refrigerant that has an ozone depletion potential of 0.02 and whose manufacture will therefore be banned by 2030.

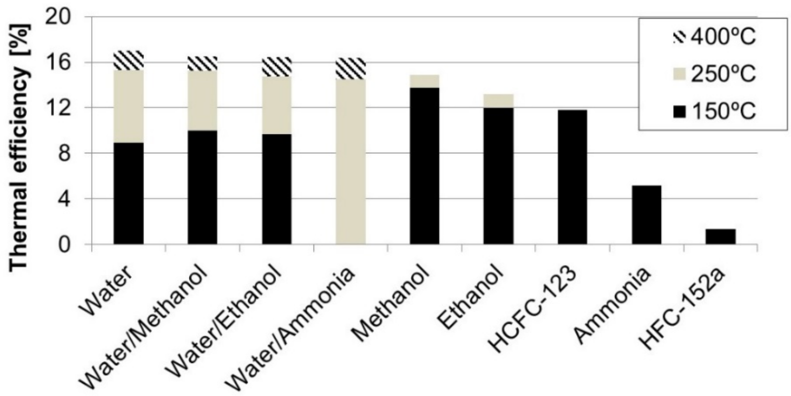

Figure 5-1: Thermal efficiencies of selected candidate working fluids at three different maximum cycle temperatures

The main results of this study can be summarized as follows:

- High/medium cycle temperatures: Water-based fluids show the highest thermal efficiency.
- Low cycle temperatures: Alcohols and refrigerants with lower boiling points than water offer the best efficiencies.
- Safety and environmental considerations are a concern for alcohols and many refrigerant working fluids.

A weakness of this study was that no direct heat source boundary conditions relating to variable such as flow rates or temperature profiles were imposed. It was therefore not possible to say how the different working fluids affected the cycle power output, which is considered more important than thermal cycle efficiency for heat recovery applications because the recoverable heat is already a loss for the IC engine**.**

<u>*Expander concepts*</u>

To compare the performance achievable with the different expander concepts (i.e. displacement and turbine expanders), the Rankine cycle model was extended with heat source boundary conditions that were applied to the cycle using the pinch point method. Two IC engine types were investigated for heat recovery: a heavy duty (HD) Diesel engine with exhaust and/or EGR as the potential heat sources and a light duty (LD) gasoline engine with exhaust gas as the sole heat source.

The similarity concept was introduced in chapter ***4.2.1*** as an approach for evaluating Rankine cycle operating conditions with respect to the applicability of certain expansion concepts.

Some often mentioned practical advantages and drawbacks of displacement and turbine expanders are listed in ***Table 5-1***.

Table 5-1: Frequently mentioned practical pros and cons of displacement and turbine expanders

	Displacement expander	Turbine expander
+	• Low speed operation [12,92,98] • High expansion ratio [98,99,100]	• No need for internal lubrication [34,101]
–	• Typically bulkier than turbines, particularly reciprocating piston expanders [14,98]	• Sensitive to droplets in vapour [14,43] • High speed operation [102]

Returning to the N_sD_s diagram (***Figure 5-2***), which is used in conjunction with the similarity concept (chapter ***4.2.1***), the most favourable expander concept can be identified by considering the specific speed N_s as a function of various parameters. These are the volume flow at the expander exit (VFR_{ex}) and the isentropic enthalpy drop Δh_{is} over expansion. The rotational speed N for the expander was assumed to be < 4000 rpm [30,92,93] for displacement expanders and 50000 – 120000 rpm [34,57,92] in case of small-scale turbine expanders. The findings concerning the interconnections between working fluid properties, cycle operating parameters, and heat source conditions under various conditions are summarized in ***Figure 5-2***. The area of the diagram corresponding to the reference case (Ref) contains the simulated heat recovery cases from the engine exhaust and/or EGR of the HD engine exhaust at various load points and heat source configurations (sole, serial and parallel):

Ref: The simulated working fluid in the reference case was a water/alcohol mixture with a water mass fraction of 80%. This mixture has a high heat of evaporation and boiling point, yielding a low flow rate of the working fluid. The expansion pressure ratio was optimized for maximum cycle power output under the specified heat source conditions. These settings yielded specific speeds N_s in the range suitable for displacement expanders due to the high isentropic enthalpy drop Δh_{is} and the low flow rates obtained when using fluids with high water contents. The importance of EGR as a heat source in the HD case was clear because it permitted the use of working fluids with high boiling temperatures resulting in higher thermal cycle efficiency. A near-constant ratio of the Rankine cycle power output to the engine power was achieved under these conditions for various engine load points.

Starting from the reference (Ref) case for HD engine heat recovery, an iterative optimization process was performed for the LD engine boundary conditions with the aim of achieving higher specific speeds and thus more favourable conditions for the efficient usage of turbine expanders. The cases considered were:

A. The initial LD operating case with water/alcohol as the working fluid and an optimized expansion pressure ratio in terms of cycle power output.
B. The expansion pressure ratio was limited to 2 in order to reduce the enthalpy drop and slightly increase the mass flow rates in the cycle by allowing more heat to be utilized. This yielded poor thermal cycle efficiencies, causing the Rankine cycle power output to drop by at least 50% compared to case A.
C. The water/alcohol working fluid was replaced with pure alcohol at the same expansion pressure ratio, giving a lower enthalpy drop and similar volume flow rates at the expander exit and thus higher specific speeds.
D. Alcohol was replaced with a refrigerant (R123), yielding an enthalpy drop that was around 70% lower while only slightly reducing the fluid's VFR_{ex} at a similar power output.

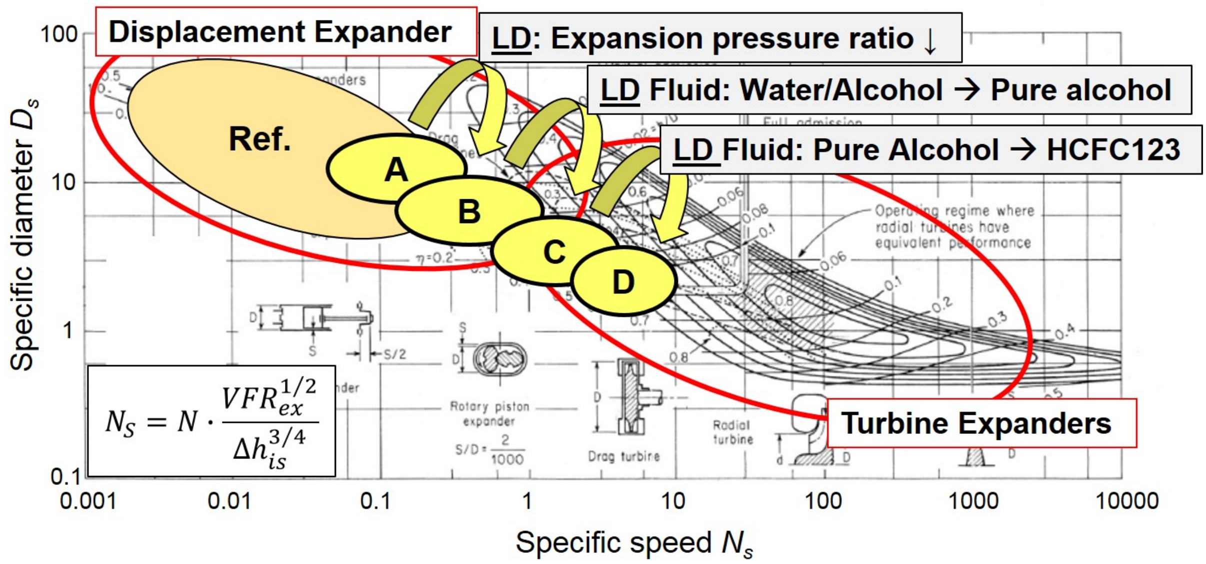

Figure 5-2: N_sD_s turbine chart (imperial units)

Based on the similarity concept, the use of turbine expander cannot be recommended when using fluids with high water contents. In such cases, displacement expanders were predicted to achieve higher efficiencies. The flow rates in the water-based system were too low and the high expansion enthalpy drop was suboptimal for a single stage turbine. Organic fluids with high molecular masses typically exhibited lower expansion enthalpy drops and higher mass flow rates under comparable heat source conditions, and were thus more likely to yield efficient expansion processes in a turbine.

One factor that renders the applicability of the N_sD_s chart somewhat uncertain is that it is based on data that have not been updated since its first publication in 1962 [79]. Rahbar et al. [82] recently suggested that loss models have been improved since then, shifting the regime of turbomachinery to lower specific speeds. A new correlation was proposed for computing the efficiencies of radial turbines when used with a set of four organic fluids typically employed in ORCs. The result was that the efficiency maximum for a radial turbine was shifted to around half the specific speed suggested by the traditional N_sD_s charts, with a weak dependency on the fluid choice. Organic fluids in particular were predicted to exhibit pronounced deviations from the traditional N_sD_s chart due to the usually high expansion pressure ratios in ORCs, leading to high Mach numbers in the turbine. Mach number effects are neglected in the efficiency predictions for similar turbines in the traditional N_sD_s concept [79].

Accounting for these potential error sources would be unlikely to appreciably alter the general outcome and findings of the present work. If anything, it would strengthen the case for using the modified cycle operating parameters and alternative fluid selections that were identified as favouring the use of turbines. Even halving the specific speeds of the turbines' operating regimes while using a high expansion pressure ratio and a water-based working fluid would not make turbine expanders competitive with displacement-type expanders under the investigated boundary conditions.

5.2 Experiments

The expander was bypassed in the initial experiments on the heat recovery system (see ***Figure 4-10***). This reduced the system's complexity and facilitated testing of the loop comprising the fluid pump, EGR boiler and condenser. After test data had been acquired for these components at the ESC operating points, the whole system including the expander was engaged.

5.2.1 Bypassed system (Paper III)

Detailed results **for** the experiments with the bypassed system were presented in ***Paper III***. A major discovery of these tests was that the heat recovery system did not cause strong EGR cooling, yielding post-boiler EGR temperatures of around 200 °C compared to approximately 80 °C with the original EGR cooler. ***Figure 5-3*** shows the *T-s* diagram for the EGR boiler and its measured heat transfer values at various boiling pressures and engine operating points. All tests were run in steady state mode with a stabilized system and superheated vapour conditions, yielding standard deviations of less than 1 kW for the heat rates presented in ***Figure 5-3***.

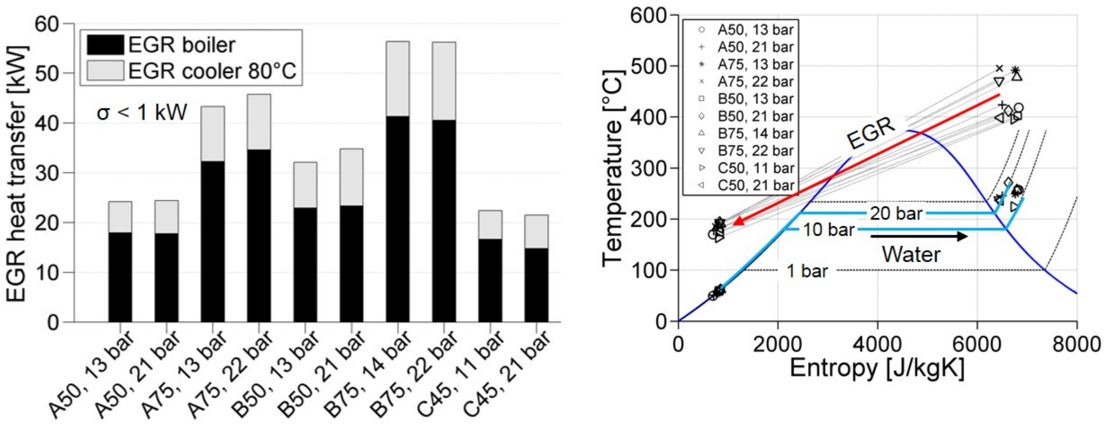

Figure 5-3: EGR boiler heat transfer (left) and T-s diagram (right) at various ESC operating points and boiling pressures

The high EGR temperatures at the boiler outlet meant that only 60-70% of the heat originally rejected in the EGR boiler could be utilized by the heat recovery system. Two phenomena that contribute to this problem have been identified:

- The high boiling temperature and large heat of vaporization for water, which produce a pinch point at the onset of evaporation in the boiler (see chapter ***3.2***)
- The internal circulation of a steam "bubble" in the boiler, which reduced both its heat transfer area and internal temperature difference

The latter point was discovered and confirmed by TitanX based on IR camera images recorded during the tests and CFD simulations performed with Ansys^{TM}. ***Figure 5-4*** shows one such IR image (in which the boiler is viewed side-on), with the EGR entering from the left and the fluid entering in the lower right corner. Since the engine is mounted at a slight tilt in the test rig, the fluid turned to the left after entering the boiler and gradually evaporated on the way down. Some of the vapour started circulating clockwise in the boiler after entering the centre region, causing the formation of the steam "bubble".

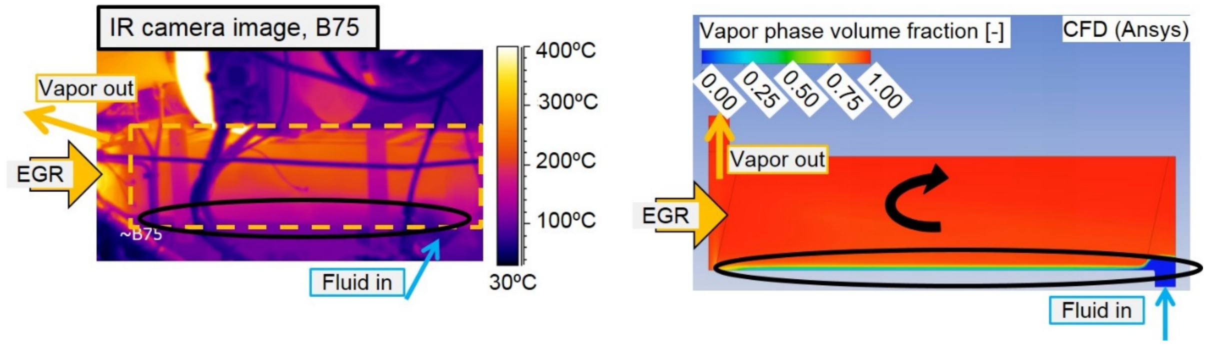

Figure 5-4: IR image (left) and CFD result (right) provided by TitanX for the EGR boiler

The high post-boiler EGR temperatures make the EGR system less effective at reducing engine emissions, which was the initial motivation for introducing EGR systems, and adversely affect engine efficiency. In addition, the ECU closed the EGR valve to protect the engine after having operated with high EGR temperatures for some time. To obtain comparable EGR cooling to that achieved with the production EGR cooler, it was necessary to design an aftercooler and install it in the EGR route downstream of the EGR boiler.

A simple aftercooler was tested initially: a stainless steel pipe with a water jacket was used to replace a suitable section of the original EGR route right above the engine's valve cover (***Figure 5-5***). The cooling of the pipe wall by the water jacket was not sufficient to reduce the EGR temperatures after the boiler to the target level (around 100 °C), so a helical copper coil was installed inside the pipe. The endings of the coil extended through the pipe's walls so that cooling water could be supplied. These passages were soldered air-tight to avoid slippage of the EGR. It was expected that the thermal expansion of the copper would be compensated for by the windings of the coil. Cooling water from a tap (20 °C) was initially passed through the water jacket and then through the copper coil. This construction had the advantage of causing insignificant pressure losses, so it did not greatly affect the EGR route but afforded cooled EGR temperatures comparable to those for the original engine setup.

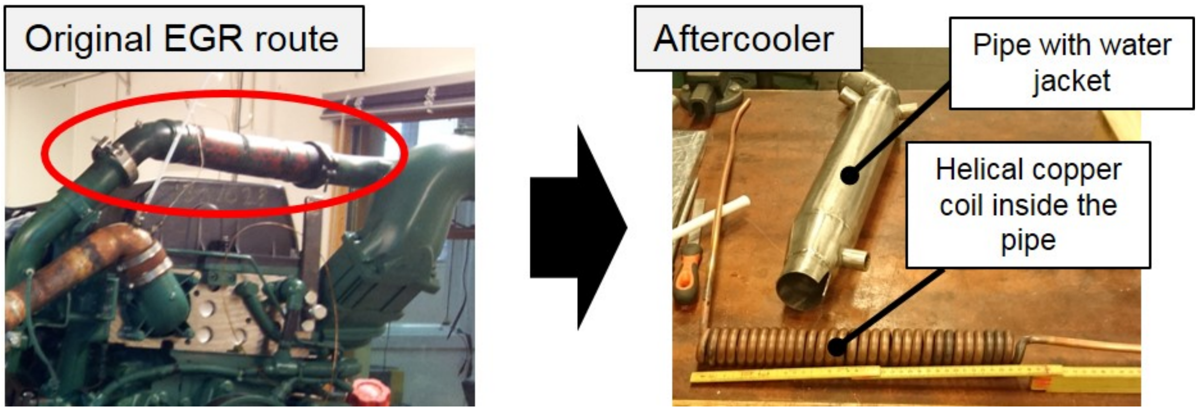

Figure 5-5: Original EGR route (left) and components of the EGR aftercooler (right)

After 5 hours of operation with this setup, the copper coil in the aftercooler cracked at the point where it was soldered to the pipe wall. The suspected causes were a combination of thermal stress and vibrations since the coil inside the EGR pipe had some clearance from the pipe walls. The aftercooler was then replaced with the engine's original EGR cooler, which was regarded as a more robust alternative with more than sufficient cooling capability. However, this increased the pressure drop on the EGR side by up to 0.06 bar. The flow of cooling water through the heat exchanger was controlled to achieve EGR temperatures of 100 °C at all operating points before being mixed with the air in the inlet manifold.

<u>*Simulations (one-dimensional expander model) – Implications for expander performance*</u>

Preliminary tests of the piston expander in the test rig yielded poor performance and barely any power output when the steam pressure was below 20 bar. Therefore, simulations using the one-dimensional expander model were performed before performing further experimental tests with the expanders (chapter ***4.2.4***). The model's results for the expander power output with the original compression ratio (ε=21) confirmed the initial observations from the test rig, as shown in ***Figure 5-6*** (left). The expander maps displayed in this chapter were computed with the validated model, so the data deviate to some extent from the maps presented in ***Paper III***. However, the qualitative conclusions do not differ.

The reason for the poor device power output at pressures of 20 bar and lower was the over-compression of the residual steam in the cylinder. The risk of over-compression is particularly pronounced when using uniflow expanders (see ***Figure 4-6***), in which the outlet ports in the cylinder wall typically close quite early in the compression stroke. If the final compression pressure exceeds the pressure of the steam supplied to the expander, the pressures will equalize after the inlet valve has opened. This will cause a direct loss of excess compression work as well as a reduction of the available time for steam admission. Re-compression of the residual cylinder charge in steam engines is generally a positive feature because the supplied live steam is not dissipated to compress the cylinder's dead volume [82]. However, the risk of over-compression increases when the expander is not operated at the pressure boundary conditions it was designed for. This was the case for the device used in this project at its original compression ratio.

Therefore, the effect of reducing the compression ratio from 21 to 13 to suppress re-compression was investigated. This approach could easily be implemented with the current expander design, allowing the model's predictions to be validated against experimental data. Aside from the compression ratio, none of the geometric parameters were changed (see ***Figure 5-6***). The results obtained show that the isolines for the expander power output were shifted to the left, i.e. towards lower inlet pressure levels. The maximum power output also became slightly more dependent on the expander speed, particularly for speeds above 600 rpm. This can be attributed to the higher pressure difference over the inlet valve when re-compression is suppressed, which reduces the resistance to the entry of the working steam into the cylinder.

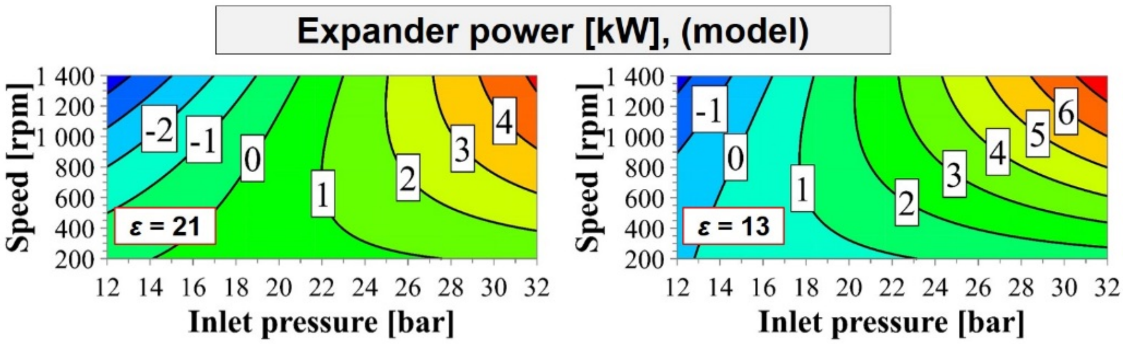

Figure 5-6: Simulated expander power as a function of the inlet steam pressure and rotational speed for the original (left) and reduced (right) compression ratios

As might be expected, increasing the dead volume of the device has some negative consequences. For example, it is necessary to increase the flow rate of steam from the EGR boiler at a given inlet pressure and expander speed (***Figure 5-7***). At high EGR flow rates and temperatures such as those corresponding to the A75, A100, B75, and B100 engine operating points, superheated steam flow rates of around 10 g/s could be supplied by the boiler. Peak expander power outputs of 2-3 kW should thus be achievable at both compression ratios, with the inlet pressure being up to 30% lower in the low compression ratio case.

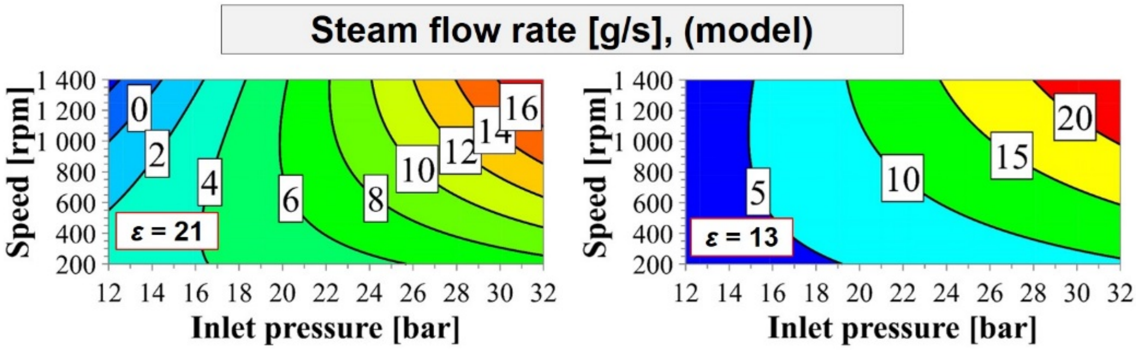

Figure 5-7: Simulated steam flow rate as a function of the inlet steam pressure and rotational speed for the original (left) and reduced (right) compression ratios

The effect of reducing the compression ratio on the isentropic efficiency of the expander design used in this work is shown in ***Figure 5-8***. According to the definition presented in chapter ***4.2.2***, the isentropic efficiency relates the expander power (minus friction) to the product of the steam flow rate and the isentropic enthalpy drop. These parameters are computed by the model and are discussed above. As shown in the figure, reducing the compression ratio shifts the expander's most efficient operating regime to lower inlet pressures. The decreased re-compression pressure combined with the larger dead volume allowed more live steam to enter the cylinder in the investigated operating range, and the gain in expansion work outweighed the increase in steam mass per cycle at the lower compression ratio. This was particularly true for live steam pressures below 20 bar, where the flow rates in both compression ratio configurations were quite similar. At higher inlet pressures (>20 bar), the isentropic efficiencies at the two configurations became more similar. At supply pressures above 30 bar, the negative effects of over-compression were reduced to the extent that the lower compression ratio would have unfavourable effects on the isentropic efficiency.

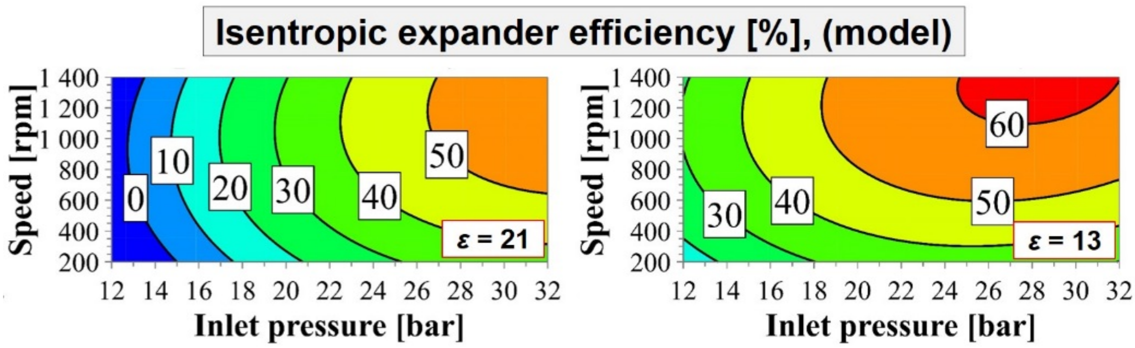

Figure 5-8: Simulated isentropic expander efficiency as a function of the inlet steam pressure and rotational speed for the original (left) and reduced (right) compression ratios

5.2.2 System with expander engaged

The results of the expander simulations presented at the end of chapter ***5.2.1*** and published in ***Paper III*** suggested that lowering the compression ratio of the expansion device should make it possible to achieve similar power outputs at lower expander inlet pressures. Experiments were performed to test this hypothesis. The performance of the expander was therefore evaluated at three different compression ratios (ε=21, ε=13 and ε=9.6).

The experimental hardware was described in chapter ***4.3.1***, in which it was noted that the expander was expected to be over-dimensioned for the heat recovery system investigated in this work. To compensate for this and to create similar EGR boundary conditions for all test cases, the engine was operated at the B100 operating point for all measurements presented in this chapter. The vapour at the expander inlet was superheated at all operation points.

Figure 5-9 shows the mean results (μ) and standard deviations (σ) for steady state samples at various expander speeds with a geometric compression ratio of 21 (the original setting). The plot showing the expander torque also includes the standard deviations for the expander speed in the horizontal direction.

It can be seen that peak power outputs of around 2.5 kW were achieved at inlet pressures close to 30 bar, confirming the model's predictions (***Figure 5-6***). The inlet pressure supplied to the expander decreased with increasing speed of the device, which was expected since the steam throughput increases with speed. A lower speed limit of 400 rpm was therefore imposed under these conditions to avoid reaching inlet pressures in excess of the boiler's 30 bar specification pressure. The EGR heat utilized in the boiler increased slightly as the boiling pressure decreased because the driving force for heat transfer is greater at lower boiling temperatures. However, this effect was less pronounced than might have been expected. The high standard deviations of the expander power output between 400 and 500 rpm were caused by instabilities of the control system for the expander dynamometer in this specific speed range. This was observed in all measurements performed within this speed range and could not be corrected. It should be stated at this point that the dynamometer was not specified to brake devices at the low speed levels used in this work. The high standard deviations observed at speeds above 800 rpm indicated that the stable operating limit of the expander had been exceeded. Based on results from the one-dimensional expander model, the reduction in the mass of trapped live steam per cycle was identified as a major cause of this limitation:

- The inlet pressure of 23 bar (at 900 rpm) was too close to the cylinder pressure at the inlet event, reducing the mass flow through the inlet valve per cycle.

- The amount of mass trapped per cycle declined as the expander speed increased because higher speeds reduce the time available for gas exchange.

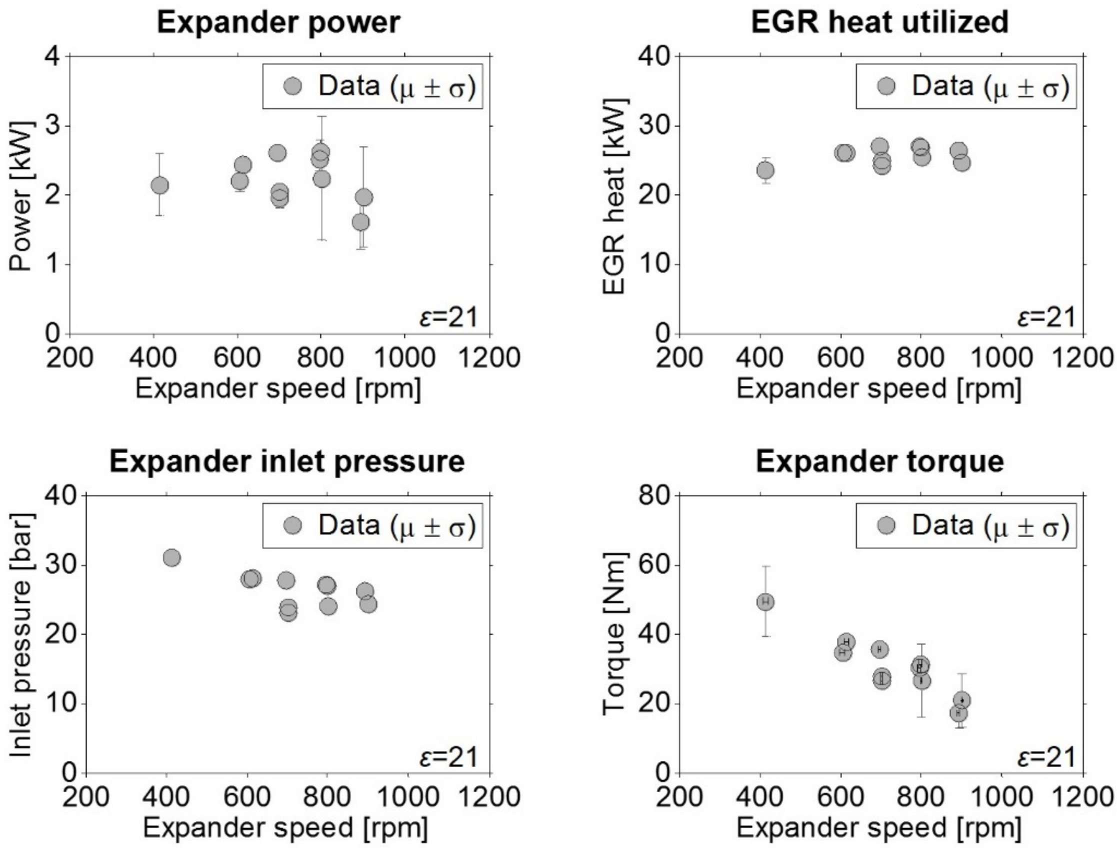

Figure 5-9: Experimental results including standard deviations for the piston expander with the original compression ratio of ε=21 at the engine's B100 operating point

In summary: at the original settings with a high compression ratio (ε=21), the expander produced a peak power of 2.5 kW at the B100 operating point, but it required inlet pressures of up to the boiler's maximum pressure specification to achieve this performance. As the speed of the expander was increased and the inlet pressure was reduced, the device's operating limits were revealed, leading to substantial variation in the steady state power measurements. Besides this particular technical limitation of the current system, the requirement for high inlet pressures also has some more general disadvantages:

- The operating ranges of the expander and heat recovery system are restricted to EGR conditions that can generate the required steam flow rates at such high pressures.
- Increased pump power requirements. For example, 50% more pump power is needed to pressurize the boiler feed water from 1 bar to 30 bar instead of 20 bar.
- Higher stress on components, increased risk of leakages.

- Higher boiling pressures can lead to lower heat utilization at some operating points as a result of the pinch-point limitation, although this effect was rather weak within the tested boiling pressure range.

The geometrical compression ratio could be reduced by installing distance plates of suitable thicknesses between the crankcase and cylinder housing of the expander. The actuation of the inlet valves was adapted to maintain the same valve timings (in degrees CA) in all cases. The outlet port opening and closing were slightly advanced and retarded, respectively, as the compression ratio was reduced because the distance plates lifted the cylinder liners that contain these ports. Other geometrical parameters were not affected by these modifications.

The compression ratio was initially reduced from 21 to 13, yielding the results shown in ***Figure 5-10***. These experiments confirmed the initial hypothesis that the expander power output could be maintained at lower inlet pressures. Peak power outputs of 2.5 kW were measured at inlet pressures of around 20 bar, and a stable torque output could be produced down to steam inlet pressures of 14 bar. High standard deviations for the power output were again evident at the aforementioned critical speed range for the dynamometer (400 - 500 rpm).

Unlike the results presented in ***Figure 5-9***, those shown in ***Figure 5-10*** were collected in three independent measurement campaigns. A variation in the EGR heat utilization can be seen, especially at the operating points with expander speeds of 700-900 rpm and <400 rpm. This was attributed to the raised EGR inlet temperatures (which were 20 °C higher than in the $\varepsilon=21$ case) and the slight increase in the EGR rates. These parameters could not be modified and were controlled by the ECU. This variation in the heat input produced comparatively high variation in the steam inlet pressure and expander power (e.g. at 300 rpm), demonstrating the cycle's sensitivity to the heat supply. At a given mass flow rate within the Rankine cycle, higher EGR temperatures and flows enhance heat transfer, allowing for higher boiling pressures and thus a higher expander inlet pressure. This explains the relatively high variation in the measured expander power output at fixed speeds for operating points where high variation in the expander inlet pressure was observed.

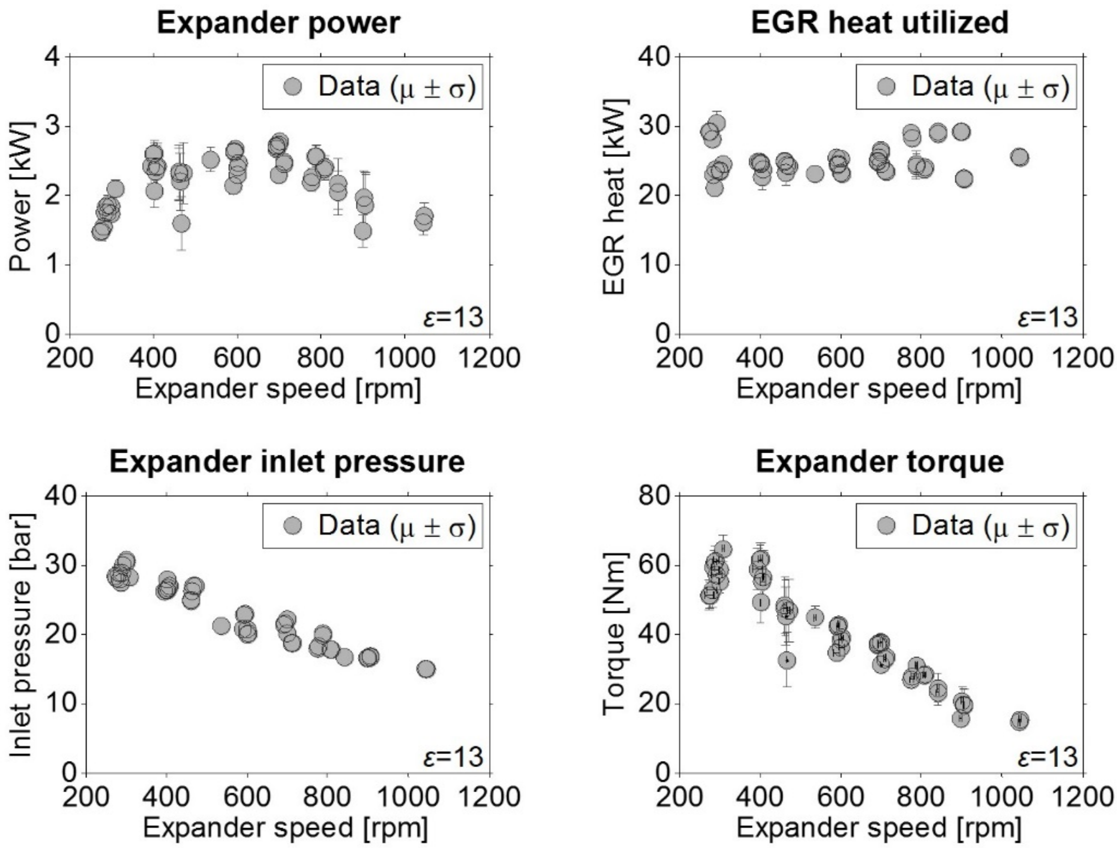

Figure 5-10: Experimental results including standard deviations for the piston expander with the modified compression ratio ε=13 at the B100 engine operating point

Reducing the geometric compression ratio from 21 to 13 made it possible to maintain the device's power output while reducing the inlet pressure by around 30% relative to that for the original compression ratio. Experiments were therefore conducted to determine whether further reducing the compression ratio to 9.6 would enable the use of even lower inlet pressures without reducing the power output. A concern was that the EGR boiler would be unable to deliver a sufficiently high steam mass flow rate under these conditions given the associated increase in the cylinder's dead volume.

Figure 5-11 presents the results of the experiments conducted using a geometric compression ratio of 9.6 for the expander. The results were more similar to those obtained at ε=13 than the ε=13 results were to the ε=21 results because the reduction in the compression ratio was smaller in relative and absolute terms than in the first modification. The expander's power output curve appeared to be slightly flatter, with a rather stable peak power over the entire speed range. A high low-end torque was expected and achieved because of the reduced re-compression in the cylinder. Therefore, high power outputs were achieved even at lower rotational speeds under these conditions. While down-speeding may be advantageous in terms of friction losses, it will usually increase steam leakage and heat transfer because it increases the time available for these processes to occur [91].

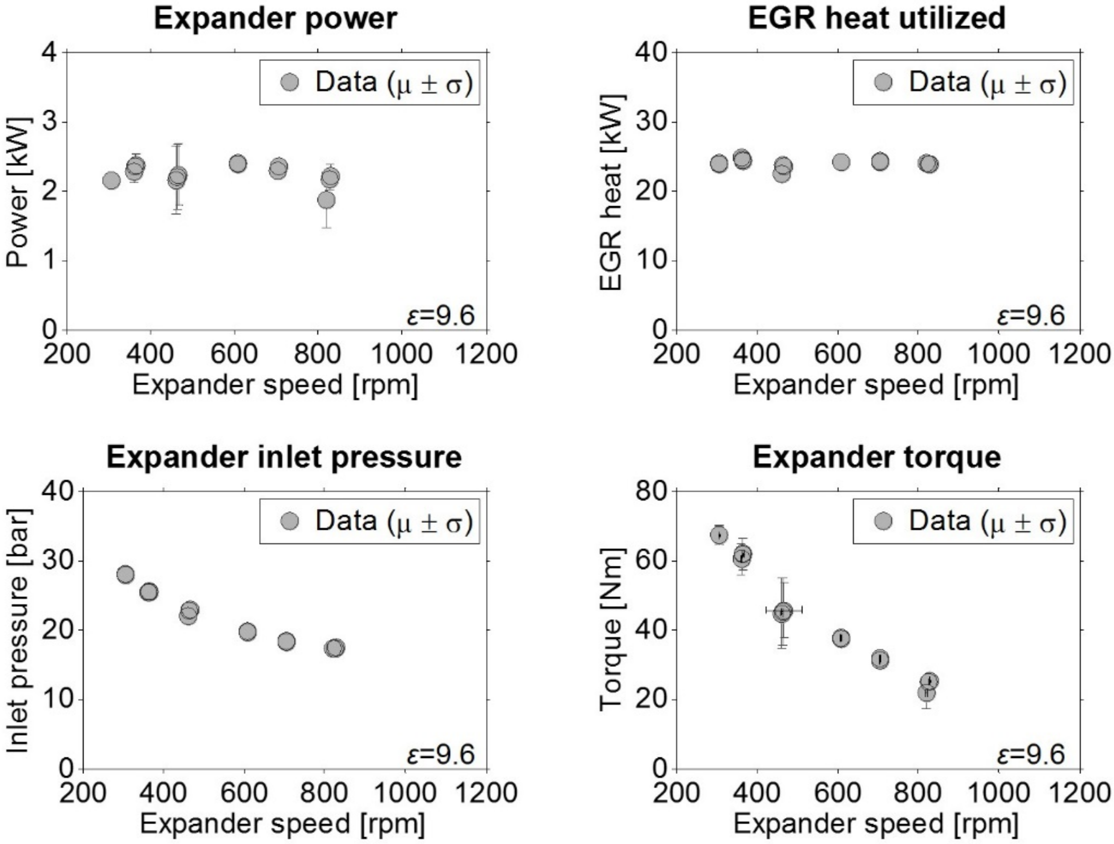

Figure 5-11: Experimental results including standard deviations for the piston expander with the modified compression ratio ε=9.6 at the B100 engine operating point

The optimization path and suggestions concerning the compression ratio are strongly related to the available steam boundary conditions (pressures and flow rates) as well as the particular design of the expansion device. If it had been possible to use higher boiling pressures of 40 or 50 bar together with higher vapour flow rates from the boiler, the original expander design would probably have been more efficient than the modified solutions with lower compression ratios; it is likely that the expander was originally designed to operate under such conditions. The major outcome of these experiments was to emphasize the importance of a properly designed expander solution for the application at hand. The clear and strong relationship between the geometric parameters and steam boundary conditions for reciprocating piston expanders prompted the studies presented in attached ***Paper IV***, which examined the effects of these parameters individually and in combination using the validated expander model developed in this project.

Figure 5-12 shows a p-V diagram computed with GT-SUITE for the three tested expander compression ratios at a constant inlet pressure of 26 bar and atmospheric outlet pressure. The expander speed was held constant at 500 rpm. Valve events for inlet valve opening (IVO), closing (IVC) and outlet port opening/closing (EVO/EVC) are indicated.

The cycle with the highest compression ratio (**cycle 1**) shows a small overshoot of the cylinder pressure at the end of compression. Its cycle area is the smallest of the three alternatives, indicating the lowest work output. The expansion curve of this cycle is low because it has the lowest dead volume in the comparison, reducing the mass of steam that can be admitted and produce expansion work.

Cycles 2 and **3** have higher mean expansion pressures, leading to a higher work output under the chosen boundary conditions. Although the expansion phase of these cycles is shorter and ends with higher steam pressures at the end of the expansion (under-expansion) than in cycle 1, the reduced compression ratios yielded improved isentropic efficiencies. This happened because the increase in cycle work outweighed the higher steam demand at this particular operating point.

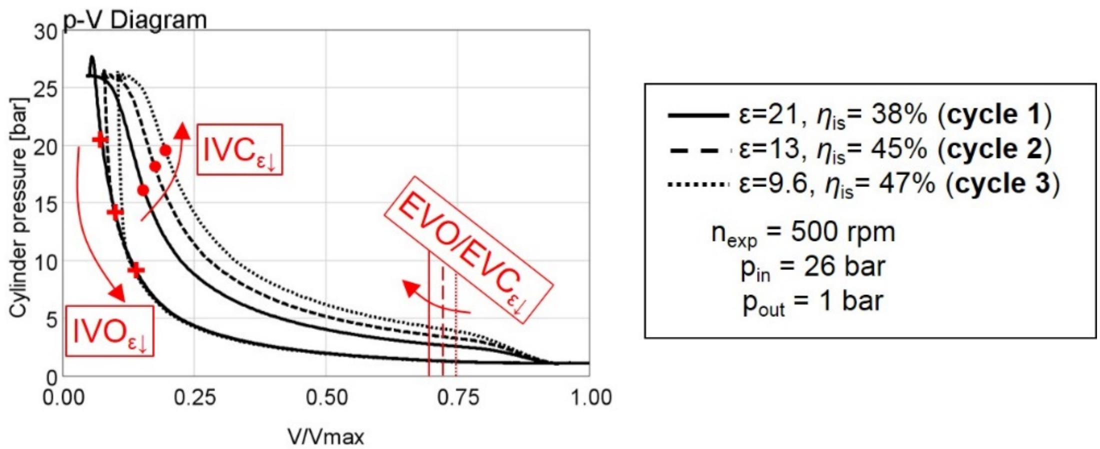

Figure 5-12: p-V diagram for a piston expander at three compression ratios (21, 13 and 9.6), showing the timing of the valve events as functions of the compression ratio

5.3 The design of the experimental setup

The following sections highlight some drawbacks, limitations and issues related to the design of the test rig that were identified during the experimental work. Information of this sort is rarely published and can be valuable for other research groups operating or developing similar systems.

Expander lubrication system

The need for an expander lubrication system increased the test rig's complexity and appeared to be a major weakness of its design. The system's initial flow scheme is shown in ***Figure 5-13***.

Standard engine oil (15W40) was originally used in the circuit, resulting in very poor water separation and problems with low expander oil pressures. It was replaced with a special steam engine oil that maintained viscosity much better in the presence of water and guaranteed fast water separation.

The oil was supplied at a gauge pressure of around 1 bar to the expander, where it lubricated the hydrodynamic bearings of the connecting rods on the crankshaft. From the expander oil sink, the lubricant then flowed back to the external oil tank together with blow-by vapour and working fluid condensate. The tank was heated with an electrical heater to a temperature of 120 °C to constantly evaporate the entrained water in the oil. The initial plan was to feed back the evaporated water from the oil tank to the system downstream of the expander, but this caused excessive oil contamination of the working fluid. The oil could not be removed from the working media by the oil separator and therefore ended up in the EGR boiler. This created a risk of oil deposit formation in the boiler, which would increase its resistance to heat transfer and reduce the overall heat transfer coefficient from the EGR to the Rankine cycle. To avoid excessive oil contamination during the expander's operation, the evaporation line from the oil tank to the Rankine system was removed. The evaporated water from the oil tank was instead transferred into an atmospheric vessel that was not connected to the system.

The high temperatures of the oil in the tank damaged the gaskets of the oil pump in the expander supply line after around 10 hours of operation. To avoid similar problems with the new oil pump, an oil cooler was installed to maintain an oil temperature of around 70 °C upstream of the pump. This cooling also helped to reduce the oil's viscosity, enabling a higher supply pressure to the expander bearings. However, this created a problem in that the oil heater was no longer capable of warming the returning oil from the expander quickly enough to evaporate entrained water, causing the blow-by from the expander to accumulate as a liquid in the oil tank. This limited the expander's running time to around 1 hour, after which the oil in the tank had to be allowed to settle so that the water could be drained. A positive side effect of this procedure was that it became possible to evaluate the expander's blow-by losses by measuring the volume of water separated from the oil. By comparing the volume of water accumulated over a fixed time interval and comparing it to the average mass flow rate for the cycle, it was estimated that around 15-20% of the steam mass entering the expansion cylinders became a blow-by loss.

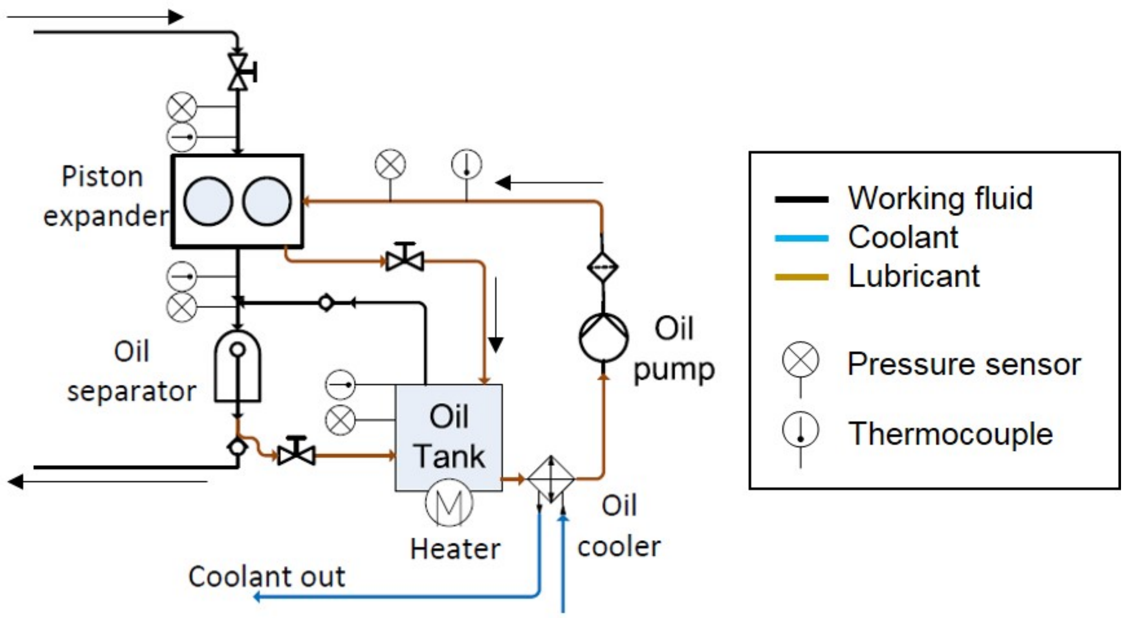

Figure 5-13: The expander subsystem with the oil circuit

Removing the return line for the evaporated water from the oil to the Rankine cycle eliminated the problem of oil contamination in the working fluid. However, it was not clear whether oil from the crankshaft lubrication was still passing through the piston rings and entering the expansion cylinders. After around 5 hours of operation in this configuration, the cylinder head of the expander was removed for maintenance and oil deposits were observed on the piston (***Figure 5-14***). Although no direct oil supply was provided to the cylinder liners and piston rings, some oil from the crankshaft bearings apparently made its way around the piston rings. It was suspected that the (probably small) amount of oil entering the expansion chamber via the cylinder liners started to coke when it encountered superheated steam at temperatures of 200 and 300 °C; this suspicion was later confirmed by the supplier of the oil. The resulting particles were then trapped by the feed-water filter upstream of the pump, so no oil reached the EGR boiler.

Figure 5-14: Piston of an expansion cylinder with oil deposits

EGR Venturi measurement

Chapter ***4.3.2*** describes the introduction of a Venturi tube downstream of the EGR boiler as a sensor for the EGR flow. This pipe was a component of the engine's original EGR loop and EGR control system, so no additional measurement equipment needed to be installed. A comparison of the energy balances over the EGR boiler showed that in more than two thirds of the test cases, the calibrated Venturi tube overestimated the EGR flow by around 30%. Inaccuracies in the flow measurement on the water side could be ruled out as the cause of this inaccuracy, and recalibrating the pipe did not improve the results. During the calibration runs with air, the pipe provided reproducible and exact readings, indicating that there was probably no problem with the tube's differential pressure sensor. The error was largest when the engine was operating under high loads, which are associated with high EGR flow rates and temperatures.

It was suggested that errors in the measured EGR gas outlet temperature may be responsible for the inaccuracy (***Figure 5-15***). The cold working fluid entered the boiler at the lower right end and gradually evaporated on its way to the left hand side, so the heat transfer coefficients were probably quite high in the lower part of the EGR boiler. This hypothesis was supported by the temperature distribution in the EGR boiler (***Figure 5-4***). At the boiler's EGR outlet, the flow in the lower part could have cooled down more than in the upper part, and the thermocouple for the measurement of the EGR outlet temperature was installed quite close to the bottom of the boiler outlet pipe. Insufficient mixing could thus cause the temperature reading at this point to be lower than the average gas temperature, leading to overestimation of the energy balance on the EGR side. To validate this, another thermocouple was installed downstream of the Venturi tube to allow further mixing of the flow. At low load points (e.g. A50 and B50), the readings from this new thermocouple were around 30 °C lower than those from the original. However, at higher EGR flows and temperatures (e.g. the A75, A100 or B100 operating points), the difference between the two thermocouples was close to zero. Therefore, the temperature reading was probably not the source of the error.

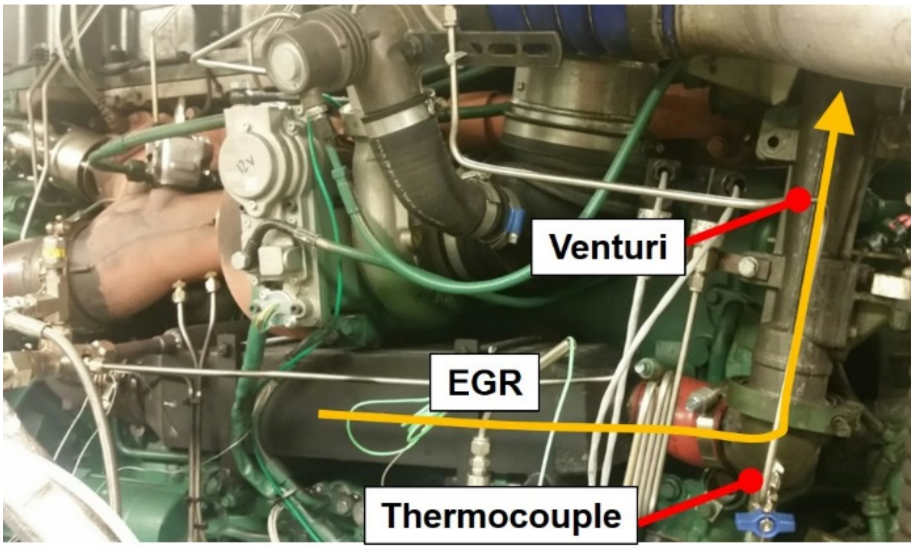

Figure 5-15: EGR boiler with downstream measurement equipment

The problem with the overestimated energy balance on the EGR side was not resolved within the project, so the EGR flow rate was estimated by applying the energy balance to the Rankine cycle side of the EGR boiler.

5.4 The one-dimensional expander and system model

Expander model

The results of the simulations conducted with the one-dimensional expander are compared to the corresponding experimental data in ***Figure 5-16***. The case-sensitive input data to the model were:

- Steam pressures upstream and downstream of the expander.
- The expander speed.
- The inlet steam temperature.

The expander power output predicted by the model shows a good qualitative match with the trends in the experimental data over the speed range. However, the model tended to underpredict the absolute power output by 10 to 20% in some cases, e.g. in the intermediate speed ranges for a compression ratio of 13. For the other two other compression ratios (9.6 and 21), the model's output was generally within the standard deviation of the experimental results, although there were some exceptions.

The predicted and measured mass flow is the gross steam flow rate supplied to the expander, including the mass lost through blow-by and valve leakages. The overall mass flow was not greatly affected by the expander speed because higher speeds caused reductions in the expander inlet pressure. In the model, the blow-by losses are accounted for by an orifice bypass to the expansion cylinders with a constant diameter of 1.2 mm, which approximates a constant gap size. These assumptions yielded reasonable agreement between the flow rates predicted by the model and those observed in the experiments over the tested operating range. The modelled blow-by rates were also consistent with the estimates obtained by measuring the volume of condensate that accumulated in the expander's oil circuit over time.

The expander's shaft power was measured in the experiments but no information on the indicated piston work was available due to the lack of in-cylinder pressure measurements. Therefore, the overall expander efficiency is used in ***Figure 5-16*** rather than the isentropic efficiency to compare the experimental results to the output of the GT-SUITE expander model. Although the qualitative trends in the experimental data agree well with those in the model's output, the efficiency calculated based on the experimental data clearly showed more noise over the considered speed range. Nevertheless, in most cases the quantitative model results were within the standard deviation of the experimental results. The increase in efficiency with speed can be explained as a consequence of the mass flow rate and expander power output being relatively stable as the inlet pressure declines. The latter factor reduces the isentropic enthalpy drop over expansion (at constant outlet pressure) and thus increases the overall expander efficiency.

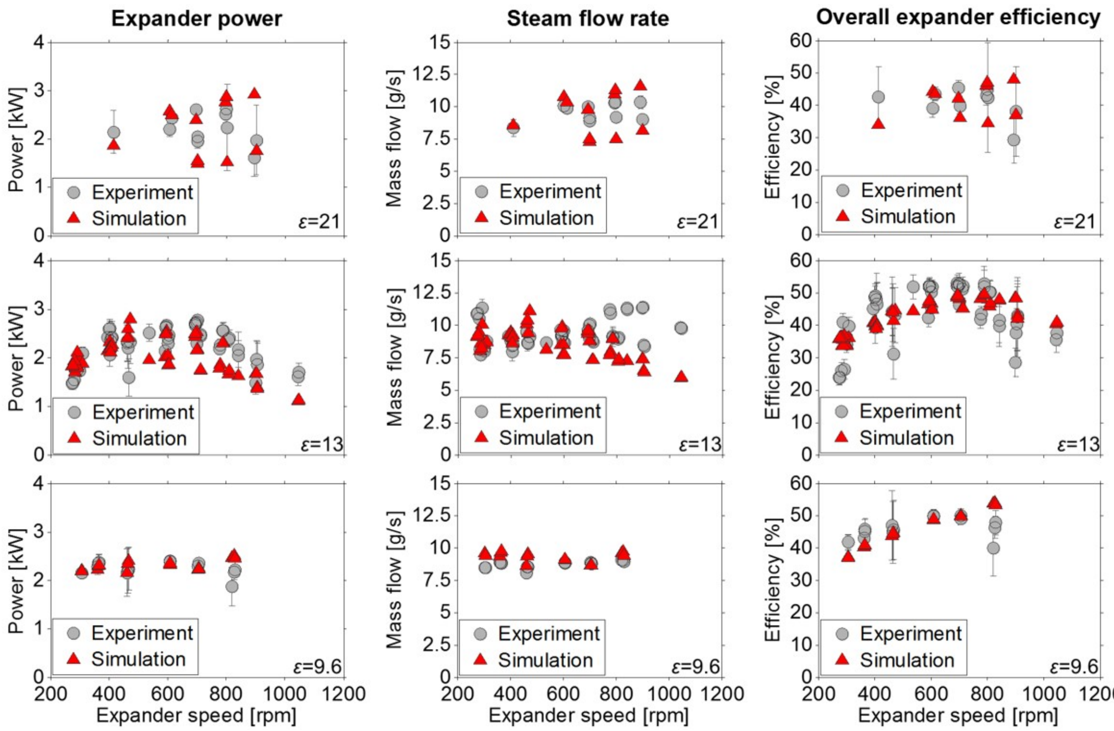

Figure 5-16: Comparison of experimental and simulation results for the expander power, the steam mass flow and the overall expander efficiency for compression ratios of 21, 13 and 9.6

The differences between the experimental and simulation results in some speed ranges may have multiple origins. The standard deviations in the experimental data do not account for some potential error sources such as sensor accuracy values or oil dilution in the expander during long-run tests, which would reduce friction losses by reducing the oil's viscosity.

When implementing the model used in the simulations, it was necessary to make some assumptions that could only be validated to a limited extent due to technical limitations:

- Friction losses were approximated by the Chen-Flynn friction model [87].
- Constant discharge coefficients were used for the inlet valves (0.6) and outlet ports (0.8).
- A "flow" heat transfer correlation developed for IC engines was used [94].

The expander friction model was calibrated at an oil temperature of 70 °C, leading to the correlation presented in ***eq. (5.1)***. High water dilution would reduce the oil's viscosity; under such conditions, this correlation would be expected to overestimate friction losses, which may explain why the expander power output predicted by the model for some operating points is lower than that seen in the experiments.

$$FMEP = 5 \cdot 10^{-3} + 0.005 \cdot p_{cyl,max} + 0.04 \cdot c_{p,m} \quad (5.1)$$

The assumption of the constant discharge coefficients was a simplification made due to the lack of related measurement data. However, incorrect discharge coefficients would have introduced a relatively systematic error into the model, while the actual mismatch appears rather arbitrary.

The heat transfer model used in the model was not developed for steam expanders. Validation and calibration of this correlation was beyond the scope of the present study

Some of the deviation in the modelling results may be due to the way the piston ring blow-by and the leakage of the valves was modelled. In the real expander, inlet valve leakage and blow-by enter the cylinder whereas in the model the blow-by path was implemented as a bypass of the cylinders with a constant orifice size. It is difficult to estimate how much this affects the results. In the real expander, the vapour fraction representing these losses enters the cylinder and can thus still contribute to the cycle work. On the other hand, inlet valve leakages during the compression stroke would reduce the expander cycle work again.

It would be necessary to be able to measure the cylinder pressure to clarify the influence of some of the effects mentioned above. This option was discarded due to technical complications arising from the design of the expander. The measured pressure traces could have been compared to those computed by the simulation model. The magnitudes and locations of the deviations between the pressure traces would have helped to identify the actual causes of the mismatches in the predicted and observed work output.

System model

The implementation of the one dimensional Rankine system model in GT-SUITE was described in chapter ***4.2.3***.

The required input data for the model were:

- Pump speed.
- Expander speed and compression ratio setting.
- The properties of the exhaust gas entering the EGR boiler.
- The properties of the coolant entering the condenser.
- Refrigerant tank temperature.

All the data used in the model's calibration were obtained from experimental results. The effectiveness values for the heat exchangers (EGR boiler and condenser) were calibrated to achieve the best possible match for the corresponding outlet temperatures. For the EGR boiler, a constant effectiveness of 0.85 gave the best results for all cases, while the condenser outlet temperatures showed the best agreement with experiments for an effectiveness value of 0.9.

The predicted performance of the EGR boiler in the system model is shown in ***Figure 5-17***. The case numbers represent the steady state experimental cases that were examined during the tests with the complete system (i.e. with the expander engaged). The evaluated operating points of the IC engine were A100 and B100. The compression ratio of the piston expander was varied during the experiments in five steps (21, 16, 13, 11 and 9.6).

Both the EGR and steam outlet temperature were slightly overestimated by the system model. A higher boiler effectiveness would have enhanced the heat transfer from the EGR in the model, leading to better agreement for the EGR outlet temperature, but the superheating temperature on the Rankine side would have been even higher. Reducing the boiler's effectiveness would have had the opposite effect. The applied case-insensitive value of 0.85 was thus considered to be a good compromise. The boiling pressure and EGR heat utilization predicted by the model were in reasonably good agreement with experiment.

The heat exchangers were simulated as black boxes, which creates the disadvantage that temperature profiles and spatial heat transfer coefficients could not be resolved. However, the lack of corresponding validation data for the heat exchanger from the test rig would have made it impossible to judge the accuracy of any predictions obtained using a more detailed approach to heat exchanger modelling. Further development and research within this area was beyond the scope of the present project. The presented system model with effectiveness-based heat exchangers enabled computation times up to 30 times faster than real time and yielded results of acceptable quality with high numerical robustness.

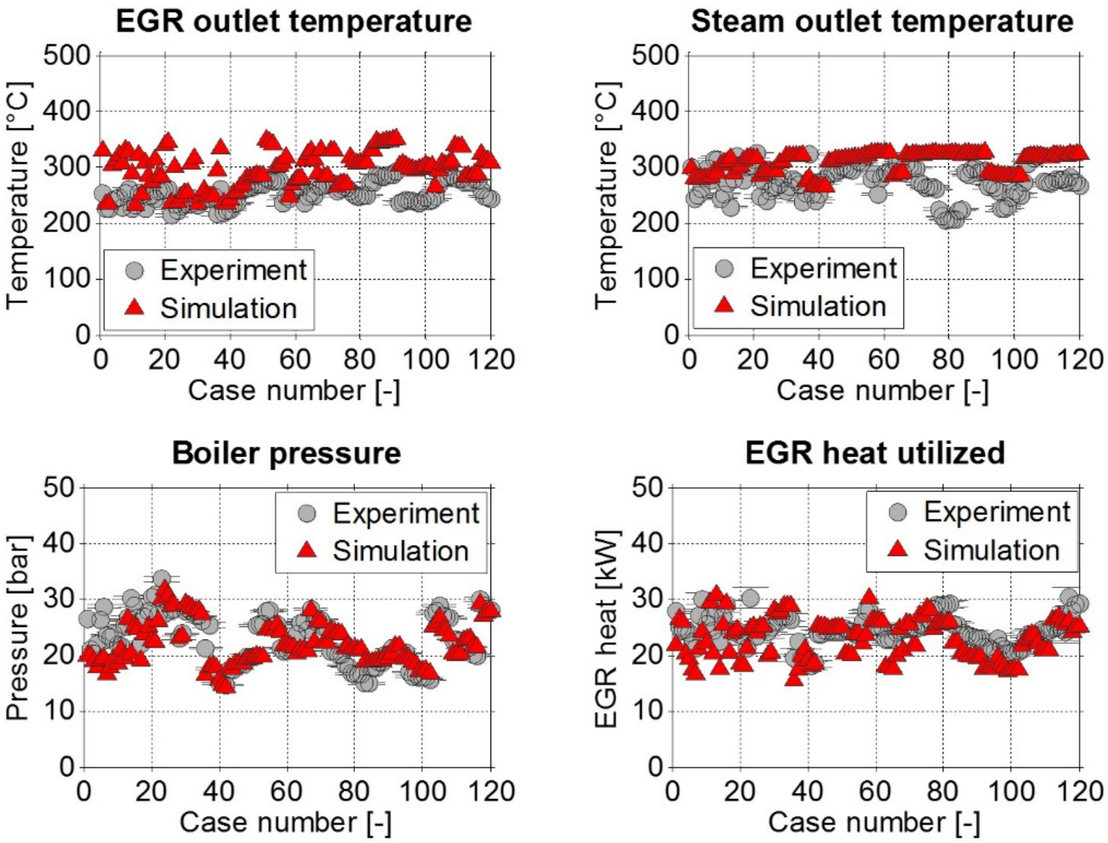

Figure 5-17: EGR boiler performance predicted by the system model compared to the corresponding experimental data

The previously introduced detailed expander model was utilized to compute maps for the overall and volumetric efficiency as functions of the applied expander pressure ratio, superheating temperature level, expander speed and selected compression ratio. Based on these maps and the process boundary data, the expander power output was estimated in the system model. ***Figure 5-18*** presents the results for the expander power and the flow rate of the working fluid in the system model. Both parameters show good agreement with the experimental data. The trends for these results and for the boiling pressure (***Figure 5-17)*** were predicted accurately, indicating that the map-based expander model was a good alternative to the detailed expander model for fast-running system simulations.

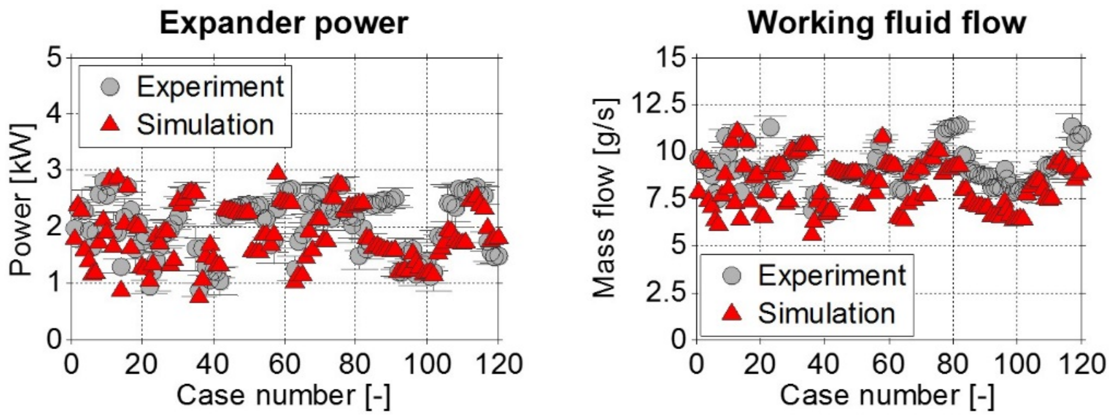

Figure 5-18: Results for the map-based expander implemented in the system model, including comparison to experimental data

5.5 Expander model – Simulation of modification strategies

As discussed in chapter ***5.2.1***, simulations using the one-dimensional expander model indicated that reducing the compression ratio would be one way of adapting the prototype expander's design to achieve a better match with the operating conditions of the heat recovery system used in this project. The high compression of the cylinder charge required by the original expander design made it impossible to achieve a stable expander power output under the initially tested conditions because insufficient steam was admitted at pressures below the system's upper limit of 30 bar. It was practically straightforward to modify the expander's compression ratio at the hardware level, making it possible to obtain sufficient experimental data to validate the one-dimensional model's predictions (chapter ***5.4***).

The validated model was then used to evaluate three alternative expander modifications that could potentially improve its power output and efficiency:

- Extending the steam admission phase.
- Retarding the closure of the steam exhaust to reduce re-compression.
- Increasing the inlet steam pressure and/or reducing the outlet steam pressure.

These strategies were not implemented on the test rig but were tested by simulation.

Figure 5-19 illustrates how each of the simulated modifications affects the p-V diagram of the approximated working cycle in the expander.

<u>Reducing the compression ratio</u> (modification **I**) should theoretically increase the dead volume in the expander's cylinder while reducing the compression-end pressure and increasing the

mean expansion pressure at a fixed inlet valve timing. Extending the steam admission period (**II**) by retarding the closure of the inlet valve was expected to help to maintain a higher steam pressure during expansion and to thereby increase the work output. Retarding the closure of the steam outlet (**III**) should reduce or even eliminate the re-compression work. Finally, altering the expander's inlet and outlet pressures (**IV**) should also improve efficiency and power output, although this could not be tested experimentally because the test rig's technical limitations (the boiler's maximum pressure was 30 bar and the condenser was designed to operate at atmospheric pressure) meant that it was not possible to increase the pressure ratio over the expander.

All four modifications were expected to increase the cycle work output and the required heat input (i.e. the mass of steam entering the expander), and it was anticipated that simulations would show which modification was most effective.

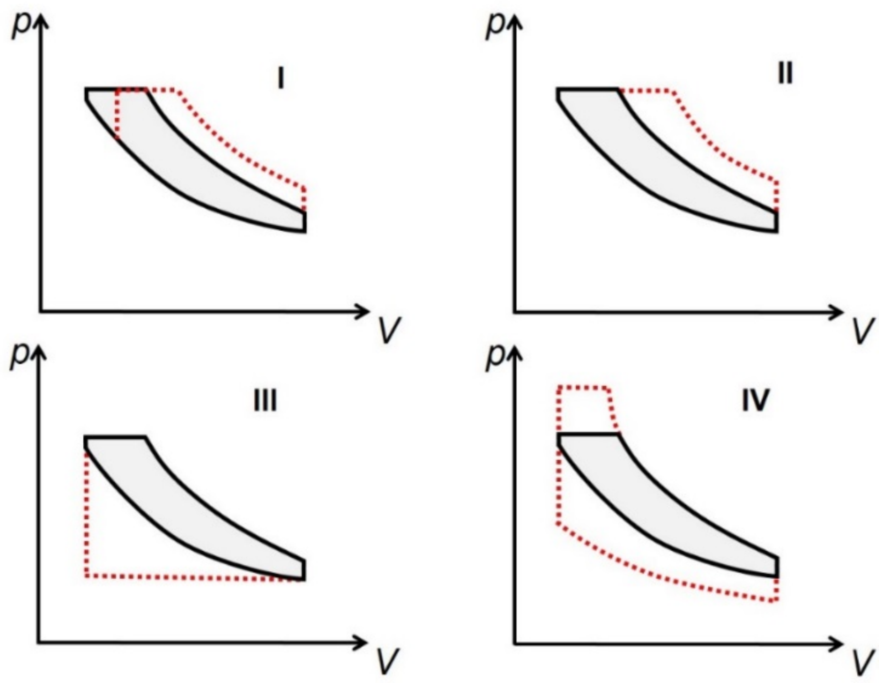

Figure 5-19: Theoretical effects of reducing the compression ratio (I), retarding IVC (II), retarding EVC (III), and increasing the pressure ratio (IV) on the p V diagram of the expander working cycle

Figure 5-20 shows the effects of the geometric modifications (**I-III**) on the expander's brake power, steam flow rate, and isentropic efficiency (for the original settings of the modified parameters, see ***Table 4-2***). The vapour at the inlet was assumed to be superheated (40 ºC above saturation temperature), the outlet pressure was atmospheric, and the expander speed was constant at 600 rpm. The abbreviations IVC_{ret} and EVC_{ret} (shown on the y-axis in cases **II** and **III**) denote the retardation of the inlet and outlet valve closure, respectively, in crank angle degrees.

None of the modifications clearly offered better performance than the others with respect to the simulated expander brake power and steam flow, particularly given that the current system configuration cannot deliver steam flows above roughly 10 g/s. All of the modifications allowed the brake-power (2-3 kW) to be maintained while reducing the steam admission pressure.

The simulated modifications (**I-III**) increased the isentropic efficiency within the displayed inlet pressure range:

- Increasing the dead volume (**I**) or reducing its re-compression (**III**) at inlet pressures of up to 25-30 bar yields an increase in the expander's power output that outweighs the increased steam inlet losses caused by the filling and compression of the dead volume.
- Retarding the IVC (**II**) was somewhat beneficial with respect to expander efficiency, although it is generally known to increase under-expansion and thus reduce expander efficiency (e.g. [18, 92]). In the present case, the original IVC timing of the expander was too far advanced for inlet pressures below 30-35 bar, resulting in poor cycle power output.

The sensitivity of the isentropic expander efficiency to these modifications declined with increasing inlet pressure. At pressures above 30 bar, the modifications started reducing efficiency because the losses they induced outweighed the increased power output.

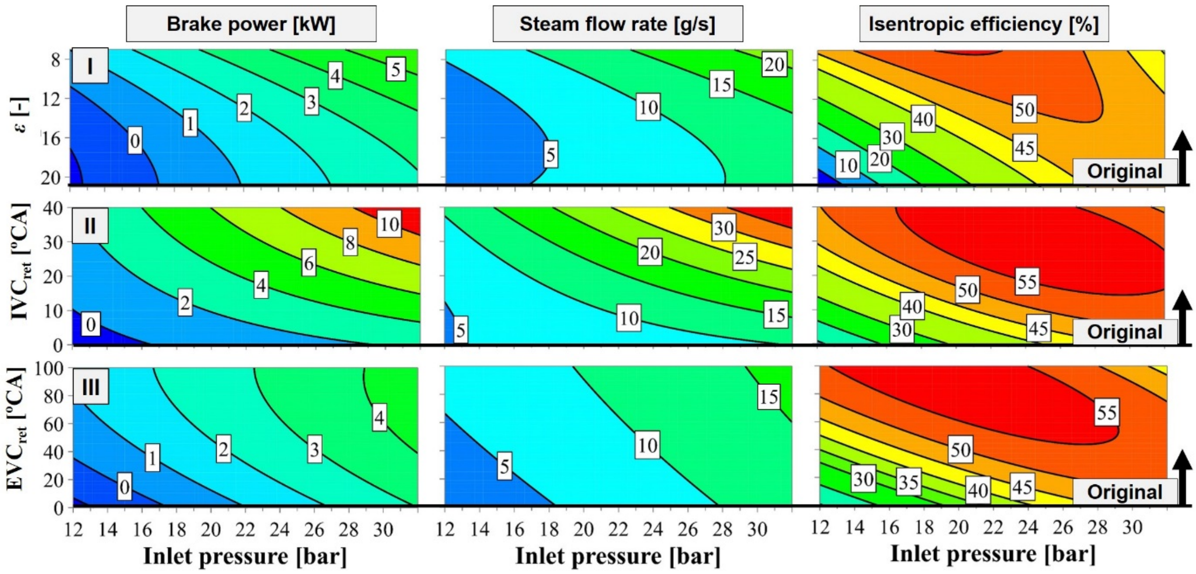

Figure 5-20: Influence of compression ratio ε (I), retarded IVC (II) and retarded EVC (III) on the expander brake power, steam flow rate and isentropic efficiency (speed 600 rpm)

In contrast to the geometry modifications (**I-III**), case **IV** assumed that there were no upper or lower bounds on the pressure levels at any point in the cycle (see ***Figure 5-21***). Like the other modifications, this yielded a simulated power output of 2-3 kW at steam supply rates of up to 10 g/s. The required inlet pressure declined almost linearly with the expander outlet pressure. The optimal efficiency with the original unmodified expander design and an ambient outlet pressure was achieved with an inlet pressure of around 36 bar. These conditions provide the most efficient possible balance between the power output and under-expansion losses. At lower inlet pressures, sub-atmospheric outlet pressures are more efficient. At higher inlet pressures, under-expansion losses predominate and the expander efficiency starts to decrease again.

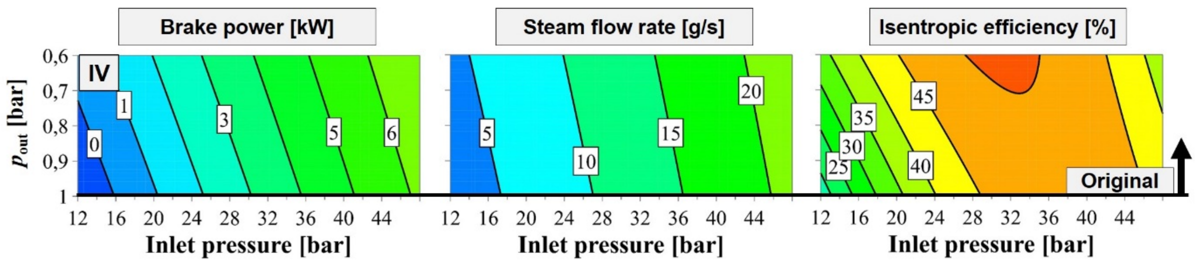

Figure 5-21: Influence of widened constraints of steam pressure boundary (IV) on the expander brake power, steam flow rate and isentropic efficiency (speed 600 rpm)

In summary, simulations with the validated model indicated that the alternative modifications (**II-IV**) should be similarly effective to the experimentally tested approach of reducing the compression ratio (**I**) given the system's current limitations: all of them would permit the expander to be operated at lower inlet pressures without reducing its power output.

5.6 Expander optimization study (*Paper IV*)

The results of the expander optimization study are discussed in detail in ***Paper IV***. The factors with the greatest influence on the reciprocating expander's power output were determined to be the expander inlet pressure, followed by the duration of inlet valve opening and the expander speed. The sensitivity of the expander's performance to changes in the pressure boundary conditions was also confirmed based on the experimental results presented in chapter ***5.2.2***.

In addition to main effects, interactions between the expander geometry and steam boundary conditions were investigated by fitting a response surface model (RSM) to the results matrix from the GT-SUITE simulations of the expander model (see also ***Figure 4-8***). While expander geometry parameters such as the compression ratio and the valve dimensions had relatively weak main effects on the performance, they were involved in most of the model's significant interaction effects. A practical example is the strong correlation of the expander compression ratio and the steam inlet pressure, which is discussed in the previous chapters.

This chapter outlines the differences between the various experimental design approaches used to generate representative simulation cases ("numerical experiments") for the GT-SUITE model. The results obtained in these simulations were then used to fit the RSM model, so it was essential to select a representative set of cases to simulate. Three different approaches were introduced in chapter ***4.2.4*** and are summarized in ***Table 4-4***:

- Full factorial design on three levels (low, medium and high values for each factor).
- Box-Behnken design.
- D-Optimal design.

Figure 5-22 shows the scaled regression coefficients of the RSM model for the isentropic efficiency as a function of the selected steam and expander design parameters. The bar height for a given effect indicates the absolute change in isentropic efficiency when the corresponding parameter is switched from its central to its maximum value. A detailed analysis of the parameter effects on the performance of the expander is provided in ***Paper IV*** and not repeated at this point. ***Figure 5-22*** is intended to visualize some issues that were not discussed in the paper due to space restrictions, namely how the choice of the experimental design affected the overall accuracy of prediction for the main, quadratic and interaction effects. The study primarily focused on interaction effects because the main and quadratic effects (which relate to changing one factor at a time) can be easily estimated directly by performing GT-SUITE simulations using the corresponding parameter settings. However, it was necessary to select a meaningful set of factor combinations to investigate in order to obtain reliable information on the interaction effects.

The required number of simulation cases for each design in this example is specified in ***Figure 5-22*** along with the confidence intervals for each of the predicted effects. For the full-factorial design, several days were required to perform all of the simulations required for the piston expander model. Conversely, the GT-SUITE simulations required under the Box-Behnken and D-Optimal designs could be completed in less than one hour.

The full factorial design on three factor levels is the most expensive in computational terms but provided the highest accuracy for the response predictions as indicated by its narrow confidence intervals. It should thus be the preferred solution when computational resources and time are not a limiting factor. To reduce the number of cases, factors that are known to have no quadratic impact on the response of interest can be varied on only two levels (a maximum and a minimum value). However, some scenarios investigated in ***Paper IV*** included up to 11 parameters, meaning that a full factorial design would have been deeply impractical given the available computational resources.

An alternative that entails much less computational effort was the Box-Behnken design. An important feature of this design is that all of factors are still varied on three levels, but extreme factor combinations are excluded (***Table 4-4***) because they are often physically or practically unrealistic. The design provided accurate results for quadratic effects but was less accurate than the full factorial reference with respect to interaction effects. Importantly, some significant interaction effects were not discovered or underestimated.

The D-Optimal design aims to maximize the spread of the experiments across a given design space for a postulated regression model. As such, it should in principle provide the greatest possible amount of information about the factor interactions for a given number of experiments. A drawback of the approach is that it does not use centre-points for the factors, which made it difficult to assess the curvature of the response. Consequently, the confidence intervals for the quadratic effects were rather wide. However, the absolute estimates for these effects compared quite well to those obtained using the full factorial design. The wide distribution of experiments in this design including extreme factor settings provided some small advantages when it came to the interaction effects, for which the predictions were somewhat closer to those obtained in the full factorial design than those obtained using the Box-Behnken design.

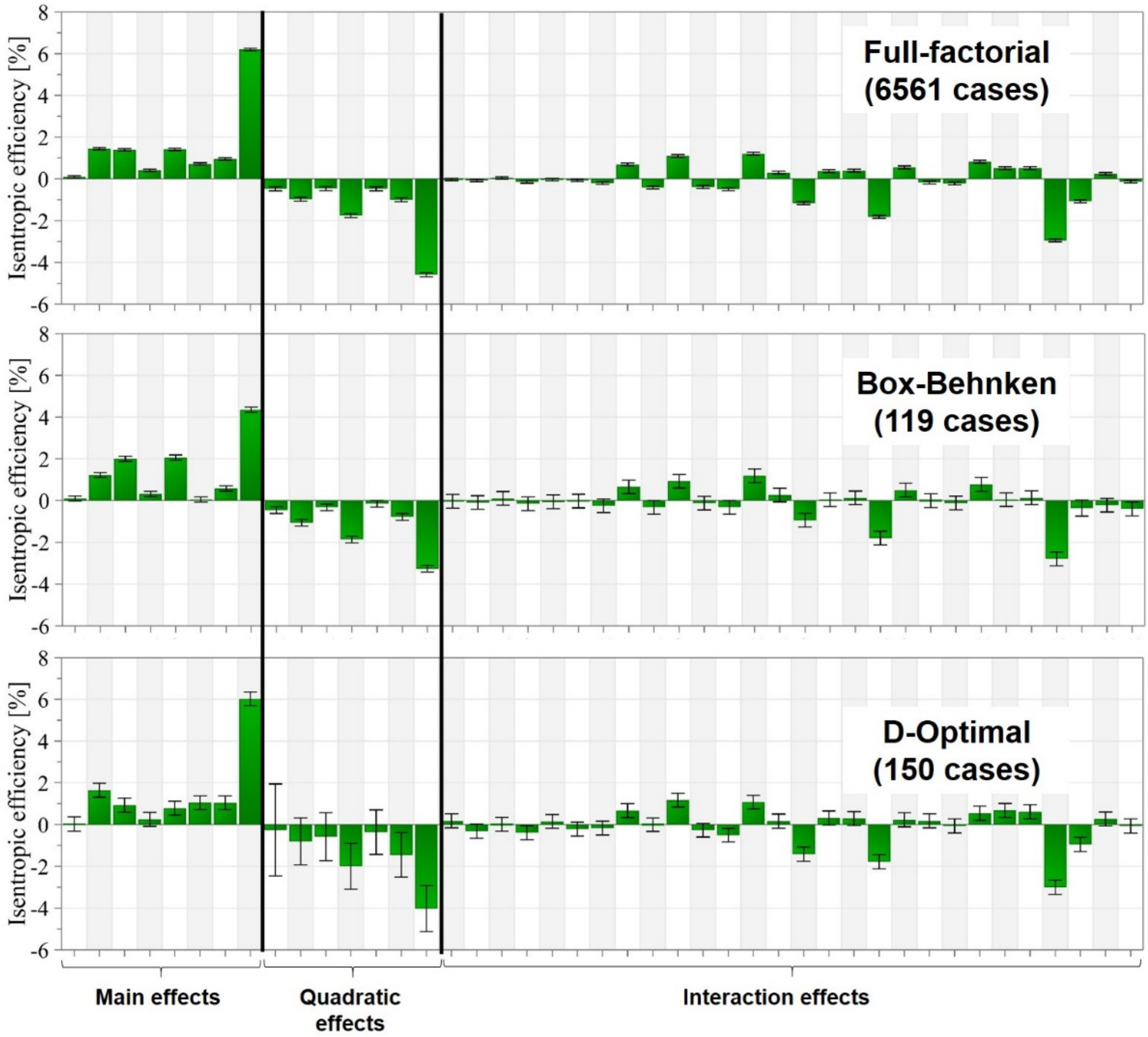

Figure 5-22: Results of the response surface model for the isentropic efficiency as a function of main, quadratic and interaction effects for three different experimental designs

These results indicate that it is advisable to compare multiple experimental designs when studying a nonlinear system such as the reciprocating piston expander, whose performance depends on many factors. This work focused primarily on interaction effects because main and quadratic effects could readily be evaluated using the GT-SUITE model. This prompted the selection of a D-Optimal design to evaluate the interaction effects between expander geometry parameters and steam boundary conditions. The findings obtained using this design were compared to those obtained using the Box-Behnken design, revealing a good agreement between these two approaches.

6 Conclusion

The internal combustion (IC) engine is probably the most important heat engine nowadays but still has a major drawback: most current engine designs reject more than half of the supplied fuel energy in the form of heat losses. There is a pressing need to improve the efficiency of IC engines because of the danger of climate change and the earth's diminishing fossil fuel reserves, making the use of waste heat recovery systems for IC engines increasingly attractive. Systems based on the Rankine cycle are considered to be among the most promising technologies for this purpose because of their heat recovery efficiency.

This thesis addresses several key design challenges associated with the design of a vehicular heat recovery system based on the Rankine cycle, including the selection of a suitable working fluid and evaluation of the interconnections between the fluid choice, the cycle parameters and the expansion device.

Zero-dimensional models were developed to simulate the Rankine cycle. Simulations using these models indicated that water provided higher thermal Rankine cycle efficiencies (up to 18%) than alternative organic working fluids when used with a high temperature (>300 °C) waste heat source such as the exhaust gas from an IC engine. Water also has the advantage of presenting no major safety or environmental issues, although it has the drawback of freezing at low temperatures. This drawback is however readily overcome by using a mixture of water and an anti-freezing agent such as an alcohol. Compared to organic fluids like alcohols and refrigerants, water has a high boiling point, which can reduce the utilization of heat from a sensible source such as the engine exhaust. This factor was accounted for by defining a pinch point in the heat exchange process when extending the Rankine cycle model to determine how different combinations of working fluid, operating parameters and expansion device concepts (displacement and turbine expanders) affected heat recovery. The similarity concept was used to evaluate the impact of the Rankine cycle conditions on the expander concept, suggesting that the conditions arising during water based cycles more closely match the characteristics of displacement expanders, while organic working fluids are more suitable for use with turbines. These conclusions are valid for smaller scale applications such as the recovery of heat from vehicular IC engine exhaust gas.

Most of the existing research on Rankine cycle waste heat recovery systems has been theoretical and computations. It was therefore considered important for the project to include an experimental component that would provide data to evaluate the quality and reliability of the conclusions drawn from the theoretical models. In addition, it was expected that the experiments might reveal operational challenges that could not be discovered using models. A full scale demonstrator test rig using a Rankine cycle was designed based on predicted operating parameters from the simulations. The working fluid used for the experiments was water. Heat was recovered from the exhaust gas recirculation (EGR) system of a Volvo D13 heavy duty Diesel engine. The term “demonstrator test rig” was used because the system was not designed to achieve maximum performance or for packaging in a vehicle. Peak thermal efficiencies of around 10% could be achieved, which is below the predicted potential of such a system given the temperature of the EGR heat source. However, it should be noted that most of the system’s components were prototypes that had not been designed for the boundary conditions that were imposed, which is probably part of the reason that the cycle efficiency was relatively poor. It is important to recall that the purpose of the test rig was to provide a versatile platform for validating the theoretical models created within the project, so a poor efficiency is not surprising or particularly problematic.

Among the challenges discovered during operation was that the original boiler system did not adequately cool the EGR. Gas outlet temperatures of up to 270 °C were measured at full load operating points whereas the original EGR cooler could maintain around an EGR outlet temperature of around 100 °C under similar operating conditions. This has negative effects on IC engine efficiency and emission formation, and also indicated that the heat utilization within the Rankine cycle was sub-optimal. The poor cooling was attributed to the high boiling temperature of water and a previously unrecognized internal flow circulation in the EGR boiler, which reduced its effective heat transfer area.

A reciprocating piston expander operating according to the uniflow concept was used as the expansion device in the system. It was initially designed for a system for recovering heat from tailpipe exhaust and EGR that used ethanol as the working fluid, probably at higher boiling pressures. The pressure in the present system was limited to 30 bar to provide a safety margin for the EGR boiler. Higher boiling pressures would also have exacerbated the EGR cooling problems and would thus have been impractical even if the boiler could have tolerated them. The expander required high levels of steam re-compression in the cylinder, initially necessitating the use of inlet pressures close to 30 bar for stable power generation. Reducing the expander’s geometrical compression ratio from 21 to 13 allowed its power output to be maintained while reducing the steam inlet pressure by 30%. However, it should be noted that this is not necessarily a general solution for such problems; rather, it should be regarded as confirmation of the consequences of using a heat recovery system in which some components are operating outside their design conditions.

The results of the studies on the expander prompted a new investigation to determine how the performance of a reciprocating piston expander depends on its geometry and the applied steam boundary conditions. To this end, a one-dimensional model of the piston expander was odeveloped and validated using data from the expander experiments. Simulations using this model indicated that the parameter with the greatest effect on the device's power output was the inlet pressure, followed by the dwell duration of the inlet valve (cut-off timing), expander speed and outlet pressure. More than 75% of the interaction effects found to have a significant impact on expander performance involved a geometric parameter. This demonstrates the overall importance of using an expansion device that has been tailored to the steam conditions under which it is to be used.

To simulate the behaviour of the complete heat recovery setup, a one-dimensional model was implemented in the commercial software package GT-SUITE. Both the boiler and the condenser were calibrated with a constant effectiveness, giving results that showed a good match with the experimental data. This approach yielded a computationally inexpensive system model that allowed simulations to be performed 30 times faster than real time while maintaining high numerical robustness. The expander in the model was map-based, with the maps being functions of the steam conditions and the expander compression ratio. The output of this system model was compared to 150 sets of steady state experimental data, revealing good matches with respect to pressures, flow rates, temperatures and the power output.

References

1. International Energy Agency (IEA), "Key World Energy Statistics 2015," http://www.iea.org/publications/freepublications/, accessed Nov. 2015.
2. BP Distribution Services, "BP Statistical Review of World Energy June 2015," http://bp.com/statisticalreview, accessed Nov. 2015.
3. Sorrell, S., Speirs, J., Bentley, R., Brandt, A. and Miller, R., "Global oil depletion: A review of the evidence", *Energy Policy* 38(9):5290-5295, 2010, doi:10.1016/j.enpol.2010.04.046.
4. Ghommem, M., Hajj, M. and Puri, I., "Influence of natural and anthropogenic carbon dioxide sequestration on global warming", *Ecological Modelling* 235-236:1-7, 2012, doi:10.1016/j.ecolmodel.2012.04.005.
5. OECD/ITF, "Reducing transport greenhouse gas emissions: Trends & Data 2010", International Transport Forum, 2010.
6. Hansen, J., "Global Warming: Is There Still Time to Avoid Disastrous Human-Made Climate Change?", presented at National Academy of Sciences, USA, April 23rd 2006.
7. Ou, X., Zhang, X. and Chang, S., "Scenario analysis on alternative fuel/vehicle for China's future road transport: Life-cycle energy demand and GHG emissions", *Energy Policy* 38(8):3943-3956, 2010, doi:10.1016/j.enpol.2010.03.018.
8. Sweeting, W. and Winfield, P., "Future transportation: Lifetime considerations and framework for sustainability assessment", *Energy Policy* 51:927-938, 2012, doi:10.1016/j.enpol.2012.09.055.
9. Berggren, C., Magnusson, T. and Sushandoyo, D., "Hybrids, diesel or both? The forgotten technological competition for sustainable solutions in the global automotive industry", IJATM 9(2):148, 2009, doi:10.1504/ijatm.2009.026395.
10. Hawkins, T., Gausen, O. and Strømman, A., "Environmental impacts of hybrid and electric vehicles—a review", *Int J Life Cycle Assess* 17(8):997-1014, 2012, doi:10.1007/s11367-012-0440-9.
11. A. Dufey, "Biofuels production, trade and sustainable development", IIED, London, 2006.
12. Teng, H., Regner, G., and Cowland, C., "Waste Heat Recovery of Heavy-Duty Diesel Engines by Organic Rankine Cycle Part I: Hybrid Energy System of Diesel

and Rankine Engines," SAE Technical Paper 2007-01-0537, 2007, doi:10.4271/2007-01-0537.

13. Edwards, S., "Waste Heat Recovery: The Next Challenge for Truck Engine Development", Behr GmbH & Co. KG, Technical Press Day, 2010.
14. Wang, T., Zhang, Y., Peng, Z. and Shu, G., "A review of researches on thermal exhaust heat recovery with Rankine cycle", *Renewable and Sustainable Energy Reviews* 15(6):2862-2871, 2011, doi:10.1016/j.rser.2011.03.015.
15. Ismail, Y., Durrieu, D., Menegazzi, P., Chesse, P. et al., "Potential of Exhaust Heat Recovery by Turbocompounding," SAE Technical Paper 2012-01-1603, 2012, doi:10.4271/2012-01-1603.
16. Greszler, A., "Diesel Turbo-compound Technology", presented at ICCT/NESCCAF Workshop, USA, February 20th 2008.
17. Rowe, D.M., "CRC Handbook of Thermoelectrics", CRC Press, Florida, USA, ISBN 978-0-8493-0146-9, 1995.
18. Stobart, R., Wijewardane, A., and Allen, C., "The Potential for Thermo-Electric Devices in Passenger Vehicle Applications," SAE Technical Paper 2010-01-0833, 2010, doi:10.4271/2010-01-0833.
19. Baker, C. and Shi, L., "Experimental and Modeling Study of Heat Exchanger Concept for Thermoelectric Waste Heat Recovery from Diesel Exhaust," SAE Technical Paper 2012-01-0411, 2012, doi:10.4271/2012-01-0411.
20. Hussain, Q., Brigham, D., and Maranville, C., "Thermoelectric Exhaust Heat Recovery for Hybrid Vehicles," *SAE Int. J. Engines* 2(1):1132-1142, 2009, doi:10.4271/2009-01-1327.
21. Mori, M., Yamagami, T., Oda, N., Hattori, M. et al., "Current Possibilities of Thermoelectric Technology Relative to Fuel Economy," SAE Technical Paper 2009-01-0170, 2009, doi:10.4271/2009-01-0170.
22. Rankine, W.J.M., "A Manual of the Steam Engine and Other Prime Movers", Richard Griffin and Company, Publisher to the University of Glasgow, Scotland, 1859.
23. Turns, S.R., "Thermodynamics: Concepts and Applications", Cambridge University Press, UK, ISBN 978-0521850421, 2006.

24. Kökeritz, J., "Innovation as business drive → energy efficiency as a drive for sustainable production of power", presented at Green Tec Conference in Hannover, Germany, April 25th 2012.

25. Haraldson, L., "Potentialer för verkningsgradsförbättringar", presented at Stora Marindagen in Gothenburg, Sweden, April 5th 2011.

26. MAN Diesel & Turbo, "Propulsion of 8000-10000 teu Container Vessel", http://marine.man.eu/two-stroke/technical-papers, accessed Nov. 2015.

27. Neunteufl, K., Stevenson, P., Hülser, H. and Theissl, H., "Better Fuel Consumption by Waste Heat Recovery", *MTZ Worldwide* 73(12):12-16, 2012, doi:10.1007/s38313-012-0247-x.

28. Edwards, S., Eitel, J., Pantow, E., Geskes, P. et al., "Waste Heat Recovery: The Next Challenge for Commercial Vehicle Thermomanagement," SAE Int. J. Commer. Veh. 5(1):395-406, 2012, doi:10.4271/2012-01-1205.

29. Seher, D., Lengenfelder, T., Gerhardt, J., Eisenmenger, N., et al., "Waste Heat Recovery for Commercial Vehicles with a Rankine Process", 21st Aachen Colloquium Automobile and Engine Technology, Aachen, Germany, 2012.

30. Bredel, E., Nickl, J. and Bartosch, S., "Waste Heat Recovery in Drive Systems of Today and Tomorrow", *MTZ Worldwide* 72(4):52-56, 2011, doi:10.1365/s38313-011-0042-0.

31. Howell, T., Gibble, J. and Tun, C., "Development of an ORC system to improve HD truck fuel efficiency", presented at Deer Conference 2011, USA, October 5th, 2011.

32. Koeberlein, D., "Cummins SuperTruck Program", presented at Annual Merit Review, USA, June 20th 2014.

33. Endo, T., Kawajiri, S., Kojima, Y., Takahashi, T. and Shinohara, M., "Study on Maximizing Exergy in Automotive Engines", SAE Technical Paper 2007-01-0257, 2007, doi:10.4271/2007-01-0257.

34. Freymann, R., Ringler, J., Seifert, M. and Horst, T., 'The Second Generation Turbosteamer', *MTZ Worldwide* 73(2):18-23, 2012, doi:10.1365/s38313-012-0138-1.

35. Panesar, A., Morgan, R., Miché, N. and Heikal, M., "Working fluid selection for a subcritical bottoming cycle applied to a high exhaust gas recirculation engine", *Energy* 60:388-400, 2013, doi:10.1016/j.energy.2013.08.015.

36. Horst, T., Tegethoff, W., Eilts, P. and Koehler, J., "Prediction of dynamic Rankine Cycle waste heat recovery performance and fuel saving potential in passenger car

applications considering interactions with vehicles' energy management", *Energy Conversion And Management* 78:438-451, 2014, doi:10.1016/j.enconman.2013.10.074.

37. Dolz, V., Novella, R., García, A. and Sánchez, J., "HD Diesel engine equipped with a bottoming Rankine cycle as a waste heat recovery system. Part 1: Study and analysis of the waste heat energy", *Applied Thermal Engineering* 36:269-278, 2012, doi:10.1016/j.applthermaleng.2011.10.025.

38. Stobart, R. and Weerasinghe, R., "Heat Recovery and Bottoming Cycles for SI and CI Engines - A Perspective," SAE Technical Paper 2006-01-0662, 2006, doi:10.4271/2006-01-0662.

39. Teng, H., "Waste Heat Recovery Concept to Reduce Fuel Consumption and Heat Rejection from a Diesel Engine," *SAE Int. J. Commer. Veh.* 3(1):60-68, 2010, doi:10.4271/2010-01-1928

40. Teng, H. and Regner, G., "Improving Fuel Economy for HD Diesel Engines with WHR Rankine Cycle Driven by EGR Cooler Heat Rejection," SAE Technical Paper 2009-01-2913, 2009, doi:10.4271/2009-01-2913.

41. Boretti, A., 'Recovery of exhaust and coolant heat with R245fa organic Rankine cycles in a hybrid passenger car with a naturally aspirated gasoline engine', *Applied Thermal Engineering* 36:73-77, 2012, doi:10.1016/j.applthermaleng.2011.11.060.

42. G. Zyhowski and A. Brown, "Low global warming fluids for replacement of HFC-245fa and HFC-134a in ORC applications", presented at First International Seminar on ORC systems, Delft, Netherlands, September 23th 2011.

43. Badr, O., Probert, S. and O'Callaghan, P., "Selecting a working fluid for a Rankine-cycle engine", Applied Energy 21(1):1-42, 1985, doi:10.1016/0306-2619(85)90072-8.

44. Quoilin, S., Aumann, R., Grill, A., Schuster, A., Lemort, V. and Spliethoff, H., "Dynamic modeling and optimal control strategy of waste heat recovery Organic Rankine Cycles", *Applied Energy* 88(6):2183-2190, 2011, doi:10.1016/j.apenergy.2011.01.015.

45. Cengel, Y., Cimbala, J. and Turner, R., "Fundamentals of Thermal-fluid Sciences", 4th ed., Mcgraw-hill professional, New York, N.Y., 2012.

46. Sprouse, C. and Depcik, C., "Review of organic Rankine cycles for internal combustion engine exhaust waste heat recovery", *Applied Thermal Engineering* 51(1-2):711-722, 2013, doi:10.1016/j.applthermaleng.2012.10.017.

47. Struzyna, R., Eifler, W., and Menne, A., “Suitability of selected working fluids for use in Waste-Heat-Recovery units”, presented at IAV 4th Thermoelectrics Conference in Berlin, Germany, December 10th 2014.

48. Sami, S., “Energy and exergy analysis of an efficient organic Rankine cycle for low temperature power generation”, *International Journal Of Ambient Energy* 29(1):17-26, 2008, doi:10.1080/01430750.2008.9675052.

49. Bao, J. and Zhao, L., “A review of working fluid and expander selections for organic Rankine cycle”, *Renewable And Sustainable Energy Reviews* 24:325-342, 2013, doi:10.1016/j.rser.2013.03.040.

50. Aneja, R., Singh, S. and Sisken, K., “Exhaust Heat Driven Rankine Cycle for a Heavy Duty Diesel Engine”, presented at Deer Conference 2011, USA, October 5th, 2011.

51. Chen, H., Goswami, D. and Stefanakos, E., “A review of thermodynamic cycles and working fluids for the conversion of low-grade heat”, *Renewable And Sustainable Energy Reviews* 14(9):3059-3067, 2010, doi:10.1016/j.rser.2010.07.006.

52. Mohanraj, M., Muraleedharan, C. and Jayaraj, S., “A review on recent developments in new refrigerant mixtures for vapour compression-based refrigeration, air-conditioning and heat pump units”, *International Journal Of Energy Research* 35(8):647-669, 2010, doi:10.1002/er.1736.

53. Katsanos, C., Hountalas, D., Zannis, T., and Yfantis, E., "Potentiality for Optimizing Operational Performance and Thermal Management of Diesel Truck Engine Rankine Cycle by Recovering Heat in EGR Cooler," SAE Technical Paper 2010-01-0315, 2010, doi:10.4271/2010-01-0315.

54. Heywood, J., “Internal combustion engine fundamentals”, McGraw-Hill, New York, 1988.

55. MAN Diesel & Turbo, “Soot Deposits and Fires in Exhaust gas Boilers”, http://marine.man.eu/two-stroke/technical-papers, accessed Nov. 2015.

56. Bae, S., Heo, H., Lee, H., Lee, D. et al., "Performance Characteristics of a Rankine Steam Cycle and Boiler for Engine Waste Heat Recovery," SAE Technical Paper 2011-28-0055, 2011, doi:10.4271/2011-28-0055.

57. Teng, H., Klaver, J., Park, T., Hunter, G. et al., "A Rankine Cycle System for Recovering Waste Heat from HD Diesel Engines - WHR System Development," SAE Technical Paper 2011-01-0311, 2011, doi:10.4271/2011-01-0311.

58. Panesar, A., Morgan, R., Miché, N., and Heikal, M., "An Assessment of the Bottoming Cycle Operating Conditions for a High EGR Rate Engine at Euro VI NOx Emissions," *SAE Int. J. Engines* 6(3):1745-1756, 2013, doi:10.4271/2013-24-0089.

59. El Chammas, R. and Clodic, D., "Combined Cycle for Hybrid Vehicles," SAE Technical Paper 2005-01-1171, 2005, doi:10.4271/2005-01-1171.

60. Larjola, J., "Electricity from industrial waste heat using high-speed organic Rankine cycle (ORC)", *International Journal Of Production Economics* 41(1-3):227-235, 1995, doi:10.1016/0925-5273(94)00098-0.

61. Hung, T., Wang, S., Kuo, C., Pei, B. and Tsai, K., "A study of organic working fluids on system efficiency of an ORC using low-grade energy sources", *Energy* 35(3):1403-1411, 2010, doi:10.1016/j.energy.2009.11.025.

62. Quoilin, S., Declaye, S., Legros, A., Guillaume, L., and Lemort, V., "Working fluid selection and operating maps for Organic Rankine Cycle expansion machines", *Proceedings of the international compressor and engineering conference*, Purdue, 2012.

63. Maraver, D., Royo, J., Lemort, V. and Quoilin, S., "Systematic optimization of subcritical and transcritical organic Rankine cycles (ORCs) constrained by technical parameters in multiple applications", *Applied Energy* 117:11-29, 2014, doi:10.1016/j.apenergy.2013.11.076.

64. Walraven, D., Laenen, B. and D'haeseleer, W., "Comparison of thermodynamic cycles for power production from low-temperature geothermal heat sources", *Energy Conversion And Management* 66:220-233, 2013, doi:10.1016/j.enconman.2012.10.003.

65. Karellas S. and Schuster A., "Supercritical fluid parameters in organic Rankine cycle applications", *International Journal of Thermodynamics*, 11(3):101-108, 2008.

66. Chen, H., Goswami, D., Rahman, M. and Stefanakos, E., "A supercritical Rankine cycle using zeotropic mixture working fluids for the conversion of low-grade heat into power", *Energy* 36(1):549-555, 2011, doi:10.1016/j.energy.2010.10.006.

67. Teng, H., Regner, G., and Cowland, C., "Achieving High Engine Efficiency for Heavy-Duty Diesel Engines by Waste Heat Recovery Using Supercritical Organic-Fluid Rankine Cycle," SAE Technical Paper 2006-01-3522, 2006, doi:10.4271/2006-01-3522.

68. Shengjun, Z., Huaixin, W. and Tao, G., "Performance comparison and parametric optimization of subcritical Organic Rankine Cycle (ORC) and transcritical power

cycle system for low-temperature geothermal power generation", *Applied Energy* 88(8):2740-2754, 2011, doi:10.1016/j.apenergy.2011.02.034.

69. Teng, H., Regner, G., and Cowland, C., "Waste Heat Recovery of Heavy-Duty Diesel Engines by Organic Rankine Cycle Part II: Working Fluids for WHR-ORC," SAE Technical Paper 2007-01-0543, 2007, doi:10.4271/2007-01-0543.

70. Chan, C., Ling-Chin, J. and Roskilly, A., "A review of chemical heat pumps, thermodynamic cycles and thermal energy storage technologies for low grade heat utilisation", *Applied Thermal Engineering* 50(1):1257-1273, 2013, doi:10.1016/j.applthermaleng.2012.06.041.

71. Steffen, M., Löffler, M. and Schaber, K., "Efficiency of a new Triangle Cycle with flash evaporation in a piston engine", *Energy* 57:295-307, 2013, doi:10.1016/j.energy.2012.11.054.

72. Fischer, J., "Comparison of trilateral cycles and organic Rankine cycles", *Energy* 36(10):6208-6219, 2011, doi:10.1016/j.energy.2011.07.041.

73. Gupta, R. and Demirbas, A., "Gasoline, diesel, and ethanol biofuels from grasses and plants", Cambridge University Press, New York, ISBN 9780521763998, 2010.

74. Lemmon, E.W., Huber, M.L. and McLinden, M.O. , "NIST Standard Reference Database 23: Reference Fluid Thermodynamic and Transport Properties-REFPROP", Version 9.1, National Institute of Standards and Technology, Standard Reference Data Program, Gaithersburg, 2013.

75. Klein, S.A., "Engineering Equation Solver", F-Chart Software, 2015.

76. "Regulation (EU) No 517/2014 of the European Parliament and of the Council of 16 April 2014 on fluorinated greenhouse gases and repealing Regulation (EC) No 842/2006 Text with EEA relevance", *Official Journal of the European Union* 57 (L150):195-230, 2014.

77. U.S. Environmental Protection Agency, "Ozone Layer Protection Glossary", http://www3.epa.gov/ozone/defns.html, accessed Nov. 2015.

78. U.S. Environmental Protection Agency , "Montreal Protocol Regulatory Summary", http://www3.epa.gov/ozone/intpol/, accessed Nov. 2015.

79. Baljé, O., "A Study on Design Criteria and Matching of Turbomachines: Part A—Similarity Relations and Design Criteria of Turbines", *J. Eng. Power* 84(1):83, 1962, doi:10.1115/1.3673386.

80. Badr, O., Naik, S., O'Callaghan, P. and Probert, S., “Expansion machine for a low power-output steam Rankine-cycle engine”, *Applied Energy* 39(2):93-116, 1991, doi:10.1016/0306-2619(91)90024-r.

81. Kenneth, E., Nichols, P.E., “How to Select Turbomachinery For Your Application“, http://www.barber-nichols.com/resources, accessed Nov. 2015

82. Rahbar, K., Mahmoud, S. and Al-Dadah, R.K., “Optimized efficiency maps and new correlation for performance prediction of ORC based on radial turbine for small-scale applications”, *Proceedings of the 3rd International Seminar on ORC Power Systems,* University of Liège and Ghent University, Brussels:355-364, 2015.

83. Gamma Technologies Inc., “GT-SUITE Flow Theory Manual”, Version 7.5, http://www.gtisoft.com.

84. Griebel, M., Dornseifer, T. and Neunhoeffer, T., “Numerical simulation in fluid dynamics”, Society for Industrial and Applied Mathematics (SIAM, 3600 Market Street, Floor 6, Philadelphia, PA 19104), Philadelphia, Pa., 1997.

85. Badami, M., Mura, M., Campanile, P. and Anzioso, F., “Design and performance evaluation of an innovative small scale combined cycle cogeneration system”, *Energy* 33(8):1264-1276, 2008, doi:10.1016/j.energy.2008.03.001.

86. McKenna, S., McCullough, G., Douglas, R. and Glover, S., “Mathematical Modelling of a Reciprocating Piston Expander”, presented at VTMS 11 Vehicle Thermal Management Systems, United Kingdom, May 15th 2013.

87. Chen, S. and Flynn, P., "Development of a Single Cylinder Compression Ignition Research Engine," SAE Technical Paper 650733, 1965, doi:10.4271/650733.

88. Gamma Technologies Inc., “GT-SUITE Engine Performance Application Manual”, Version 7.5, http://www.gtisoft.com.

89. Blair, G., Callender, E., and Mackey, D., "MAPS OF DISCHARGE COEFFICIENTS FOR VALVES, PORTS AND THROTTLES," SAE Technical Paper 2001-01-1798, 2001, doi:10.4271/2001-01-1798.

90. Ferrara, G., Manfrida, G. and Pescioni, A., “Model of a small steam engine for renewable domestic CHP (combined heat and power) system”, Energy 58:78-85, 2013, doi:10.1016/j.energy.2013.03.035.

91. Gutermuth, M. and Watzinger, A., "Die Dampfmaschine", Springer, Berlin, 1928.

92. Clemente, S., Micheli, D., Reini, M. and Taccani, R., “Performance analysis and modeling of different volumetric expanders for small-scale organic Rankine cycles”,

presented at 5th International Conference of Energy Sustainability, USA, August 10th 2011.

93. Lemort, V., Quoilin, S., Cuevas, C. and Lebrun, J., "Testing and modeling a scroll expander integrated into an Organic Rankine Cycle", *Applied Thermal Engineering* 29(14-15):3094-3102, 2009, doi:10.1016/j.applthermaleng.2009.04.013.

94. Morel, T. and Keribar, R., "A Model for Predicting Spatially and Time Resolved Convective Heat Transfer in Bowl-in-Piston Combustion Chambers," SAE Technical Paper 850204, 1985, doi: 10.4271/850204.

95. Box, G. and Behnken, D., "Some New Three Level Designs for the Study of Quantitative Variables", *Technometrics* 2(4):455-475, 1960, doi:10.1080/00401706.1960.10489912.

96. Montgomery, D., "Design and analysis of experiments", Wiley, New York, 1991.

97. Reader-Harris, M., "Orifice plates and venturi tubes", Springer International Publishing, Switzerland, ISBN 978-3-319-16879-1, 2015.

98. Quoilin, S. and Lemort, V., "Technological and Economical Survey of Organic Rankine Cycle Systems", presented at 5th European Conference on Economics and Management of Energy in Industry, Portugal, April 2009.

99. Rakesh, A., Sandeep, S., Sisken, K., Dold, R.and Oelschlegel, H., "Exhaust Heat Driven Rankine Cycle for Heavy Duty Diesel Engine", presented at Deer Conference 2011, USA, October 5th 2011.

100. Robinson, F., "A Comparison Between Trochoidal, Rotary Vane and Reciprocating Expanders", *Journal Of Mechanical Design* 103(2):304, 1981, doi:10.1115/1.3254908.

101. Lang, W., Colonna, P. and Almbauer, R., "Assessment of Waste Heat Recovery From a Heavy-Duty Truck Engine by Means of an ORC Turbogenerator", *J. Eng. Gas Turbines Power* 135(4):042313, 2013, doi:10.1115/1.4023123.

102. Dingel, O., Arnold, T. and Ambrosius, V., "Development of Components for a CRP for Vehicle Applications", presented at 4th Thermoelectrics IAV Conference, Germany, December 10th 2014.

103. Stumpf, J., "The Una-Flow Steam-Engine", Second edition, Syracuse, N.Y., USA, ISBN 9781290080019, 1922.